Gulf of Cadiz Expedition
Contribution Number 28

Observations and Hypothesized Generation of a Meddy in the Gulf of Cadiz

by Mark D. Prater

Technical Report
APL-UW TR9210
April 1992

Applied Physics Laboratory University of Washington
1013 NE 40th Street Seattle, Washington 98105-6698

Foreword

This dissertation was submitted in partial fulfillment of the requirements for the degree of Doctor of Philosophy in the School of Oceanography at the University of Washington. Thomas B. Sanford, Principal Oceanographer in the Applied Physics Laboratory and Professor in the School of Oceanography, was chair of the Supervisory Committee. Financial support for this research was provided by the Office of Naval Research, Contract N00014-86-K-0690.

Abstract

The formation of Mediterranean water eddies and the characteristics of the Mediterranean outflow that lead to formation are investigated. In September of 1988, an expedition was made to the Gulf of Cadiz to survey a Meddy soon after formation. The objectives of this study were to i) compare a "young" Meddy with older ones found elsewhere, ii) determine the formation site for the Meddy, iii) determine the generation mechanism for the Meddy, and iv) determine the dynamical relationship between the Meddy and the Mediterranean outflow. A regional survey was done, which mapped the Mediterranean outflow and located a Meddy, which was then mapped in greater detail.

The observed Meddy had a radius to maximum velocity of 9 km, a vertical extent of 650 m, and a central anticyclonic vorticity of $-0.85f$. The Meddy consisted of two vertically aligned cores, both of which were in cyclogeostrophic balance. The Meddy contained a large potential vorticity (Q) anomaly, with levels an order of magnitude lower than ambient. The Meddy had a more negative Rossby number and a higher Burger number than previously observed Meddies. The formation site of the Meddy was found through analysis of Gulf of Cadiz water properties to be near a canyon region south of Portugal. The Meddy was shown not to have been generated solely by geostrophic adjustment, which requires vortex squashing to produce strong negative vorticity. Instead, the most likely candidate mechanism was baroclinic instability of the outflow. This hypothesis is supported by strong vertical shear in the outflow, a radial scale of the Meddy consistent with a baroclinic disturbance, and the existence of a cyclonic partner of the Meddy. Topography, however, may trigger the instability. The Q in the formation region was similar to that in the Meddy. However, the Q anomaly in the Meddy was dominated by negative relative vorticity, while in the outflow the nonlinear effect due to vertical shear dominated. The conversion from the vertical shear to the lateral shear component of the Q anomaly during Meddy formation is consistent with a meandering outflow constrained by potential vorticity conservation. The flux of potential vorticity was markedly less in the formation region than farther upstream, indicating that the outflow Q was recently modified.

Table of Contents

	Page
List of Figures	iii
List of Tables	v
Chapter 1. Introduction	1
Chapter 2. Description of Data	6
2.1 Instrumentation	6
2.2 Measurement Locations	8
Chapter 3. Description of the Cadiz Meddy	20
3.0 Introduction	20
3.1 Translation of the Meddy	20
3.2 Temperature	21
3.3 Salinity	25
3.4 Density and Stratification	27
3.5 Isopycnal Displacement and Available Potential Energy	27
3.6 Velocity Field	29
3.7 Vertical Vorticity and Rate-of-Strain	31
3.8 Gradient-Wind Density Field	32
3.9 Potential Vorticity	33
3.10 Energetics	36
3.11 Discussion	39
Chapter 4. Origin and Generation of the Cadiz Meddy	64
4.0 Introduction	64
4.1 The Mediterranean Outflow in the Gulf of Cadiz	64
4.2 Formation Site of Meddy	65
4.3 Meddy Generation Mechanisms	67
4.3.1 Meanders in the Azores Current	68
4.3.2 Instability of northward current off western Portugal	69
4.3.3 Geostrophic adjustment	69
4.3.4 Transport intermittency	71
4.3.5 Boundary torques	73

4.3.6 Instability of a coastal current 76
4.3.7 Discussion 77
4.4 Potential Vorticity in the Mediterranean Outflow 79
4.4.1 An expression for potential vorticity in the outflow 80
4.4.2 Determination of G 82
4.4.3 Determination of R_i^{-1} 83
4.4.4 Determination of R_o 83
4.4.5 Determination of Q 85
4.4.6 Determination of the flux of Q 85
4.4.7 Viscous modification of X in the outflow 86
4.4.8 Conversion from R_i^{-1} in outflow to R_o in Meddy 88

Chapter 5. Summary and Conclusions 102
5.1 Summary of the Meddy Formation Process 102
5.2 Speculations 103
5.3 Conclusions 104

List of References 106

Appendix A. Referencing the XCP Velocities 113

Appendix B. Estimating Salinity from Sound Velocity and Temperature 122

Appendix C. Diffusion of Heat Radially from a Cylinder 125

Appendix D. Fundamental Frequency of Solid Body Rotating Eddy 128

List of Figures

Number *Page*

1.1 Gulf of Cadiz site map 5

2.1 Location of CTD casts during regional survey 10
2.2 Location of XCP drops during regional survey 11
2.3 Location of XBT drops during regional survey 12
2.4 Location of XSV drops during regional survey 13
2.5 Location of XBT drops during Meddy search survey 14
2.6 Location of XSV drops during Meddy search survey 15
2.7 Location of CTD casts and XCP drops during fine-scale survey 16
2.8 Location of XBT and XSV drops during fine-scale survey 17
2.9 Location of CTD casts during Mediterranean outflow survey 18
2.10 Location of XCP drops during Mediterranean outflow survey 19

3.1 Temperature contours for Meddy translation 42
3.2 Temperature profile through center of the Meddy 43
3.3 Contours of Meddy temperature at 1050 and 1350 dbars 44
3.4 Three-dimensional perspectives of Meddy temperature 45
3.5 Ellipticity of the upper and lower cores of the Meddy 46
3.6 Radial distribution of Meddy temperature at 1050 and 1350 dbars 47
3.7 Contours of Meddy temperature and $\partial T/\partial r$ in the r-z plane 48
3.8 Salinity profile through center of the Meddy 49
3.9 θ_1-S relationship for the Meddy 50
3.10 σ_1 and N profiles for the Meddy 51
3.11 Isopycnal displacement and APE in the center of the Meddy 52
3.12 XCP velocity vectors in the Meddy at 1050 and 1350 dbars 53
3.13 Three-dimensional perspectives of Meddy velocity magnitudes 54
3.14 Contours of Meddy v and $\partial v/\partial z$ in the $r-z$ plane 55
3.15 Contours of Meddy ζ and η in the $r-z$ plane 56
3.16 Radial distribution of v, ζ, and η in the Meddy at 1050 dbars 57
3.17 Contours of Meddy isopycnal displacement and N in the $r-z$ plane 58
3.18 Evaluation of geostrophic and cyclogeostrophic assumptions 59

3.19 Contours of Meddy potential vorticity in the $r-z$ plane 60
3.20 Contours of Meddy APE and KE in the $r-z$ plane 61
3.21 Radial distributions of APE and KE for the Meddy at 1050 dbars 62
3.22 B vs. R_o relationship for historical Meddies 63

4.1 Schematic of boundary layer entrainment 89
4.2 Contours of temperature on isopycnal surfaces 90
4.3 Laboratory experiment of boundary current instability 91
4.4 Contours of the depths of isopycnals in the Gulf of Cadiz 92
4.5 Schematic of frictional boundary layer separation 93
4.6 Results of along-shore momentum equation with frictional drag 94
4.7 Boundary layer over a flat plate 95
4.8 G profiles for Lines F and 04 96
4.9 R_i^{-1} profiles for Lines F and 04 97
4.10 Example of R_o calculation 98
4.11 R_o profiles for Lines F and 04 99
4.12 Q profiles for Lines F and 04 100
4.13 Q contour for Line 04 101

A.1 Results of Meddy model fit to XCP velocity data 117
A.2 XCP velocity vectors at 1050 dbars: layer of constant velocity 118
A.3 Absolute velocity in the near-surface from ADCP and LORAN-C, and estimates of $\overline{v}^*$ 119
A.4 XCP velocity profiles showing vertical shear across the Meddy 120
A.5 XCP velocity vectors showing vertical shear across the Meddy, and the velocity at 1050 dbars 121

B.1 Radial distribution of salinity profiles from XSV/XBT in the Meddy 124

B.2 Comparison of CTD salinities and XBT/XSV salinities 124

C.1 Diffusion of heat radially from a cylinder 127

D.1 Frequency of parcel oscillation vs. Rossby number for an eddy 131

List of Tables

Number *Page*

1.1 Historical Meddy Survey 4

3.1 Results of B_E Model 38
3.2 Summary of Meddy Parameters 40

4.1 McWilliams's (1988) Results for a Cadiz-like Eddy 70

B.1 Sensitivity of Chen & Millero (1978) Inversion 122
B.2 Sensitivity of Standard Salinity Computation 123

Acknowledgments

This dissertation could not have been completed without the steady support of my advisor Tom Sanford, and of Reading Committee members Eric Kunze and Eric D'Asaro. Their constant stream of ideas, advice, help, and encouragement were invaluable, and the lessons they taught me will last the remainder of my scientific career.

Many of the figures in this dissertation were made using "GPL", a General Plotting Language developed by Bill Hess, and John Dunlap put up with an uncountable number of questions dealing with all aspects of computer systems and programming.

Tom Rossby generously allowed me the use of his computer facilities during the last eight months of work on my dissertation.

My advisors made my graduate life productive, my friends made it enjoyable. I want to let the following people know how much I appreciate their friendship. I thank Peter Kaczkowski, Dicky Allison, Jane Verrall, Dave Straub, Peter Spain, Maureen Kennelly, Chuck Lombardo, ... This list is in no particular order and undoubtedly incomplete.

Finally, I thank Susan and Christopher for allowing me all too often to place work ahead of family. Their love made much of this possible.

" . . . . . because when you are a Bear of Very Little Brain, and you Think of Things, you find sometimes that a Thing which seemed very Thingish inside you is quite different when it gets out into the open and has other people looking at it."

The House at Pooh Corner
A.A. Milne

Chapter 1. Introduction

Meddies are small (mesoscale or submesoscale), isolated, subsurface vortices that contain waters of Mediterranean origin (McDowell & Rossby, 1978). They are typically found in the eastern North Atlantic at a nominal depth of 1000 m, with thicknesses of 300-800 m and diameters of 30-100 km. Meddies are pressure "highs" due to having less stratification in their cores than the surrounding waters at the same depth. Thus, their waters have anticyclonic rotation. Meddies are very noticeable in hydrographic surveys because of their anomalously high temperature and salinity. Depending on the individual Meddy and the nature of the ambient waters, the Meddy can contain waters several °C warmer and up to 1 psu saltier than its environment.

Even though they were probably first reported by Piip (1969), the name "Meddy" was coined by McDowell and Rossby (1978) in describing what they considered to be a *M*editerranean *eddy* in the western Sargasso Sea. The discovery that an isolated eddy could travel thousands of kilometers over a period of several years and still maintain the identity of its source water surprised oceanographers. It suggested that lateral mixing of water types might not occur solely by molecular or eddy-like diffusion. In certain regions, discrete eddies might transport their source waters far from their origin, then inject those waters into the ocean interior by some decay process. The decay process could be either gradual by lateral intrusions or double diffusive processes (Ruddick & Hebert, 1988; Hebert et al., 1990) or catastrophic by interaction with topography (Richardson et al., 1989).

Meddies have been found by many investigators in the basin to the south and east of the Azores in the eastern North Atlantic (Table 1.1). Most Meddies have been found by hydrographic surveys of varying resolution. Two experiments featured direct velocity measurements of Meddies and also followed the Meddies over a period of time (Armi et al., 1989; Richardson et al., 1989; Berestov et al., 1986; Yegorikhin et al., 1987). From 1984 to 1986, a Meddy was tracked with SOFAR floats, starting in the Canary Basin and moving southward (Armi et al., 1989). That Meddy, named "Sharon" after the winner of a shipboard lottery, was thought to have a typical structure for Meddies, with a radius of maximum velocity of near 20 km and a central relative vorticity of $-0.35f$. Though an impressive volume of literature dealing with Meddies has been

generated in the past ten years, there are still basic questions remaining that have not been answered. It is not known for certain how Meddies propagate, and many aspects of the Meddies' stability and interaction with their surroundings remain unclear. It is beyond the scope of this work to address all of the unresolved issues, however a seemingly simple question remains on which this dissertation will focus.

Where do Meddies originate, and how are they formed?

The obvious answer as to the source of their temperature and salinity anomalies is "the Mediterranean". However, even though that is the source of the Meddy's hydrographic signature, the more precise location of the origin of the vortex itself is more difficult, and is intimately connected to the question of formation.

An observational study was needed that would examine a Meddy in the process of forming, or soon after, and gather detailed information on both the Meddy and its generation environment. To this end, in September of 1988, an expedition was made to the Gulf of Cadiz (Figure 1.1) to survey a Meddy soon after formation. The objectives of this study were to

i) compare a "young" Meddy with older ones found elsewhere,

ii) determine the formation site for the Meddy,

iii) determine the generation mechanism for the Meddy, and

iv) determine the dynamical relationship between the Meddy and the Mediterranean outflow.

A regional survey was done, which mapped the Mediterranean outflow and located a Meddy, which was then mapped in detail. Details of the expedition and the data acquired are presented in a series of cruise reports (Kennelly et al., 1989a,b,c,d).

The purpose of this work is to address the Gulf of Cadiz expedition objectives, and to extend the understanding of the formation of Meddies. Chapter 2 gives a brief discussion of the expedition and data acquired. The first objective of the study is addressed in Chapter 3, where a detailed description of the observed Gulf of Cadiz Meddy is given, along with a comparison with historical Meddies. In Chapter 4, the remaining three objectives are addressed. First, a formation site for the Meddy is suggested. Next, Meddy generation mechanisms that have been mentioned in the literature are evaluated,

and a likely candidate mechanism is chosen. The remainder of Chapter 4 examines the relation between the potential vorticity in the Meddy and in Mediterranean outflow. Chapter 5 concludes with a summary of the study.

Table 1.1 Historical Meddy Survey

Reference	*Date and Location*	*Measurements*
McDowell & Rossby (1978)	1976: 25.0 N, 70.0 W	XBTs, CTDs, and SOFAR floats
Armi & Stommel (1983)	1980: 26.5 N, 29.1 W	single CTD cast
Armi & Zenk (1984)	1981: lens 1, 31.0 N, 26.8 W	CTD survey
Armi & Zenk (1984)	1981: lens 2, 31.1 N, 22.7 W	CTD survey
Armi & Zenk (1984)	1981: lens 3, 33.1 N, 21.6 W	CTD survey
Berestov et al. (1986) Yegorikhin et al. (1987)	1985: from 20.0 N, 38.0 W to 20.0 N, 38.0 W	CTD survey, towed CTD, buoys with deep current meters
Käse & Zenk (1987)	1982: lens A, 36.0 N, 20.7 W	regional scale CTD survey
Käse & Zenk (1987)	1982: lens B, 33.0 N, 23.2 W	regional scale CTD survey
Käse & Zenk (1987)	1982: lens C, 31.0 N, 22.5 W	regional scale CTD survey
Vorob'yev et al. (1988)	1987: 32.5 N, 12.1 W	CTD survey
Zubin & Ozmidov (1988)	1985: 36.0 N, 13.7 W	two CTD transects
Käse et al. (1989)	1988: lens A, 37.5 N, 12.0 W	regional scale CTD survey
Käse et al. (1989)	1988: lens B, 40.5 N, 11.7 W	regional scale CTD survey
Käse et al. (1989)	1988: lens C, 39.5 N, 15.0 W	regional scale CTD survey
Käse et al. (1989)	1988: lens D, 35.5 N, 17.0 W	regional scale CTD survey
Armi et al. (1989) Hebert et al. (1990) Schultz Tokos & Rossby (1991)	1984-1986: Meddy 1 from 32.0 N, 22.0 W to 22.0 N, 22.0 W	multiple CTD surveys, SOFAR floats, Pegasus and XCP survey
Richardson et al. (1989)	1985-1986: Meddy 2 from 33.3 N, 24.0 W to 31.5 N, 28.0 W	CTD survey, SOFAR floats
Richardson et al. (1989)	1985-1987: Meddy 3 from 24.0 N, 23.4 W to 20.0 N, 25.5 W	CTD survey, SOFAR floats

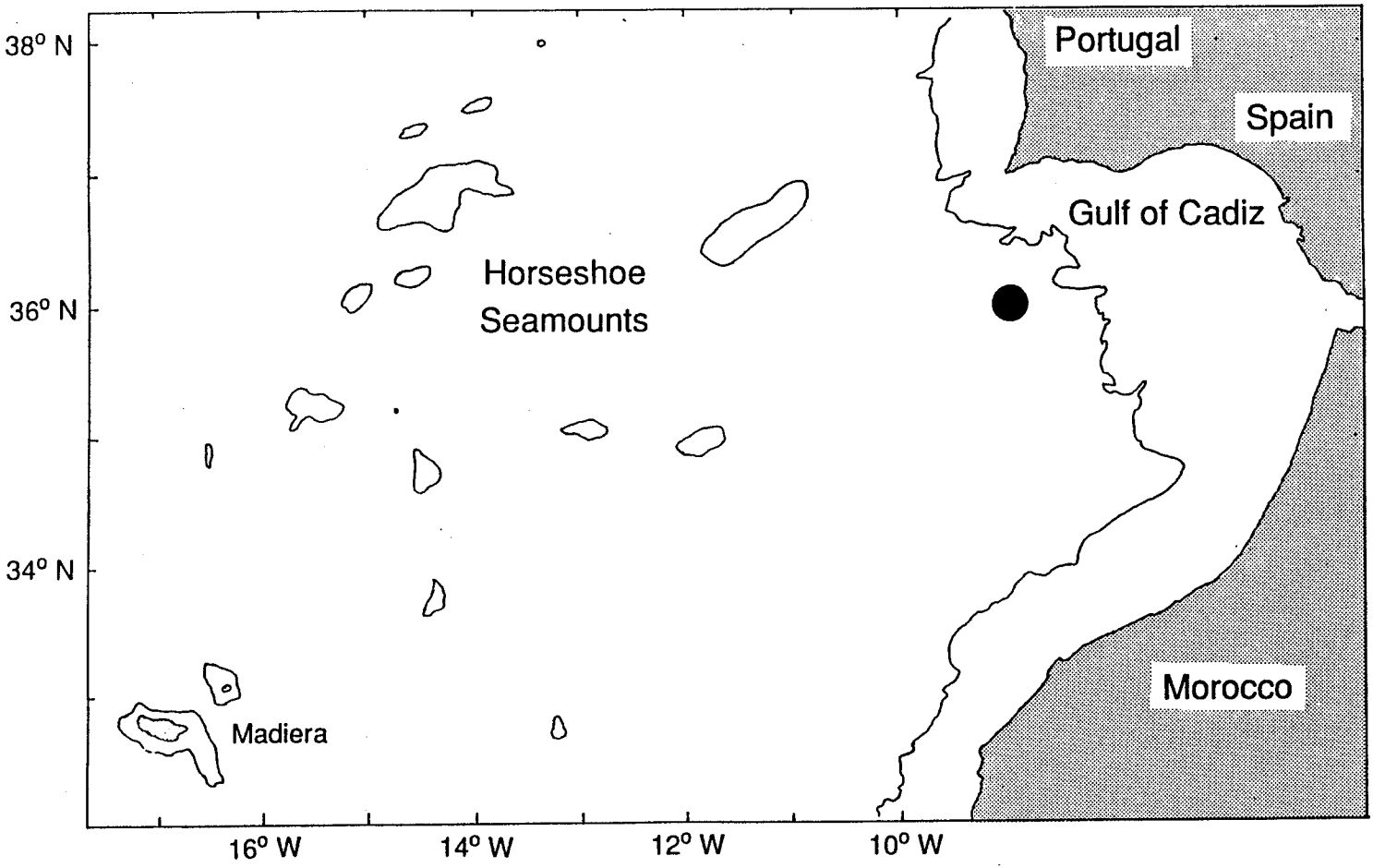

Figure 1.1.Site map of the Gulf of Cadiz, showing the 1000 fathom (≈1830 m) bathymetry line. Numerous seamounts and islands west of the Gulf are also shown. The dark circle at 36° N and 9° W indicates the location of the Cadiz Meddy observations. The circle has a 30 km diameter.

Chapter 2. Description of Data

2.1 Instrumentation

Three expendable vertical profilers were used throughout the course of the experiment: the XBT, the XSV, and the XCP, all manufactured by Sippican Ocean Systems Inc. The three probe types are launched from the side or stern of the ship while the ship is underway and return the data signal either by a thin copper wire or radio transmission. The depth for the expendable probes is empirically computed from the time-of-fall of the probe and is not measured directly.

The XBT (eXpendable BathyThermograph) contains a thermistor and returns a voltage proportional to the ambient temperature (T) as a function of time. Three models of XBT were used; the T-6 (with a maximum depth of 460 m), the T-7 (760 m), and the T-5 (1830 m). Sippican Inc. reports the accuracy of the XBT as 0.15°C (Sippican, 1983). The XCP (eXpendable Current Profiler) measures the voltage induced by the moving water passing through Earth's magnetic field. This voltage can be interpreted as the horizontal velocity within a depth invariant (barotropic) component. Thus, a relative velocity is measured, not an absolute velocity. The accuracy of the XCP velocity is about 0.01 m s^{-1} (Sanford, 1982) with a maximum depth of about 1600 m. The XCP also contains a thermistor similar to that in the XBT. The XSV (eXpendable Sound Velocimeter) returns a frequency proportional to the ambient sound velocity, with an accuracy of 0.25 m s^{-1} (Sippican, 1983). Two models of XSV were used, the SV-03 (850 m) and primarily the SV-02 (2000 m).

High quality T and conductivity were obtained from a Sea-Bird Electronics Model 9 CTD (Conductivity, Temperature, and Depth). The CTD contained a Paroscientific pressure sensor (accurate to 0.02%), two temperature sensors (0.01°C), and two pumped conductivity cells (0.001 S m^{-1}). The temperature sensors and conductivity cells were calibrated before and after the cruise. A 1.5-liter Niskin bottle was used to collect a water sample during each CTD cast to further calibrate the calculation of salinity (S).

During the course of the experiment, the shipboard RD Instruments 150-kHz acoustic Doppler current profiler (ADCP) collected 5 minute average vertical profiles of water velocity relative to the ship's motion ($v_{w/s}$). Also, a two-chain, range-range Loran-C system was used for positioning and for estimating the absolute ship's velocity

relative to ground (v_{abs} or $v_{s/g}$) (Dunlap, 1989).

Since the depth of an expendable probe is an empirical quadratic function of fall time, a method to obtain a better estimate of depth was needed (Prater, 1991). The method uses the band-passed temperature signals from an XCP and a nearby CTD, and piece-wise shifts the profiles in depth until their correlation is maximized. The temperature difference at the shifted depth is also found. Comparisons between 65 XCP / CTD pairs and 29 XSV-02 / XBT-05 pairs were made. The XCP depth and temperature were modified, as was the XSV-02 depth. Details of the method and results are found in Prater (1991).

In order to compare the corrected expendable data with CTD data, the expendable probes' depths were converted to pressure. A method given by Saunders and Fofonoff (1976) and Saunders (1981) was used, and its application to the Cadiz data is described in Kennelly et al. (1989a). The method consists of integrating the hydrostatic equation downward from the surface using densities derived from CTD data, resulting in a relation between pressure and depth. The vertical reference of the XBT and the XSV was converted to pressure, and the data were averaged in 2-dbar bins, while the data from the XCP were averaged in 6-dbar bins, incremented by 2 dbars. The primary vertical coordinate system used here will be pressure in dbars, positive downward from the sea surface. However, there will be occasional use of depth in meters, positive upward from the surface.

The data from the XBT and XSV were combined, and an equation for sound speed as a function of T, S (salinity), and P (pressure) (Chen & Millero, 1977) inverted for S. This gave us the ability to estimate salinity from expendable probes. However, the sensitivity of the inversion was such that only a qualitative estimate of salinity was possible. Details of the salinity computations from expendable probes are given in Appendix B.

The XCP data, as stated above, are processed to produce a relative velocity profile. Several methods were attempted to estimate an absolute velocity profile, using other instrument systems and/or knowledge of the circulation in the Gulf of Cadiz. Details of the XCP referencing methods are given in Appendix A.

For a detailed description of these and other instrument systems used during the experiment, the reader is referred to the series of Cadiz Cruise reports (Kennelly et al., 1989a,b,c,d).

2.2 Measurement Locations

A regional survey of the waters south and west of Portugal and Spain was performed in search of a Meddy in the act of or soon after formation. During this survey, 157 XBT profiles, 34 XCP profiles, 18 XSV profiles, and 34 CTD casts were made. This portion of the Cadiz Cruise is called the "regional survey". The data locations from the above survey are shown in Figures 2.1-2.4. A primary difficulty in locating a Meddy in the region is that its temperature and salinity signatures are indistinguishable from those of the Mediterranean outflow.

After almost six days of searching, several anomalous temperature and salinity features were observed. None was clearly a Meddy, but the most likely candidate was thought to be a feature observed in the southernmost part of the regional survey, near CTD 025 (Figure 2.1). In relocating the feature, 16 XBT profiles and 8 XSV profiles were made, and their positions are shown in Figures 2.5 and 2.6. This portion of the Cadiz Cruise is called the "relocation survey".

Once the supposed Meddy was relocated, and an estimate of its center was made, a fine-scale survey of the feature was conducted, which showed that the feature was indeed a Meddy. This survey was performed with 29 XBT profiles, 29 XSV profiles, 31 XCP profiles, and 7 CTD casts. The data locations for the above profiles are shown in Figures 2.7 and 2.8. This portion of the Cadiz Cruise is called the "fine-scale survey". By using mainly expendables, the entire survey was performed in one day, with the expendable part taking only 14 hours.

After the Meddy survey, the first leg of the cruise ended in Cadiz, Spain. The objective of the second leg of the Cadiz experiment was to survey the Mediterranean outflow, in order to study its structure and plume dynamics. During this survey, 64 XCP profiles and 98 CTD casts were made. The data locations for the Mediterranean Outflow survey are shown in Figures 2.9 and 2.10. This portion of the Cadiz Cruise is called the "outflow survey".

The majority of the data from the Cadiz expedition was collected in "Lines" roughly orthogonal to the Mediterranean outflow. The Lines from the first leg are labeled by number (01, 02, ...), while those from the second leg are labeled by letter (A, B, ...). Later, in Chapter 4, I will explicitly use data from Lines F and 04.

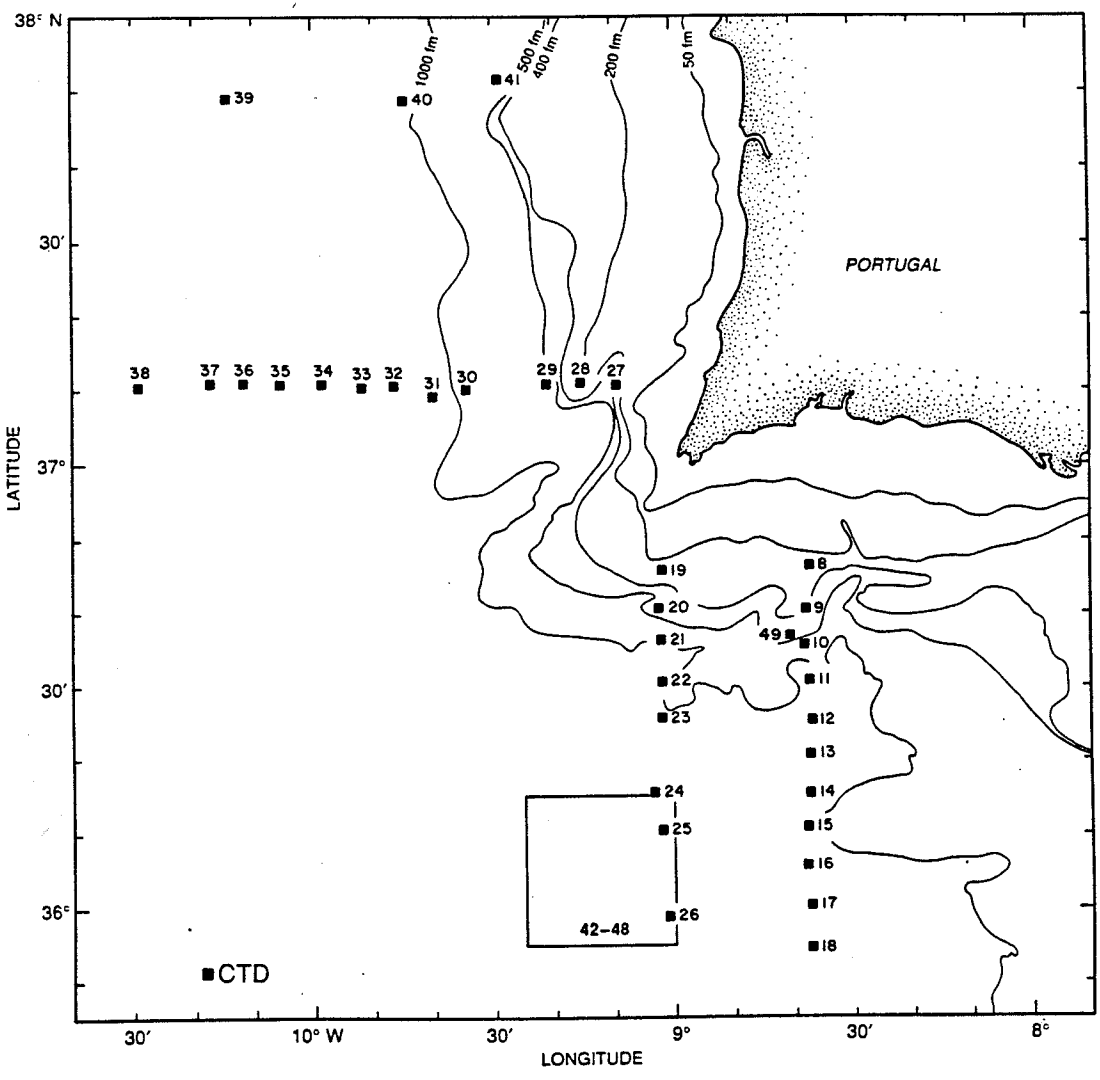

Figure 2.1. Location of CTD casts during the regional survey. The boxed area is the site of the fine-scale Meddy survey.

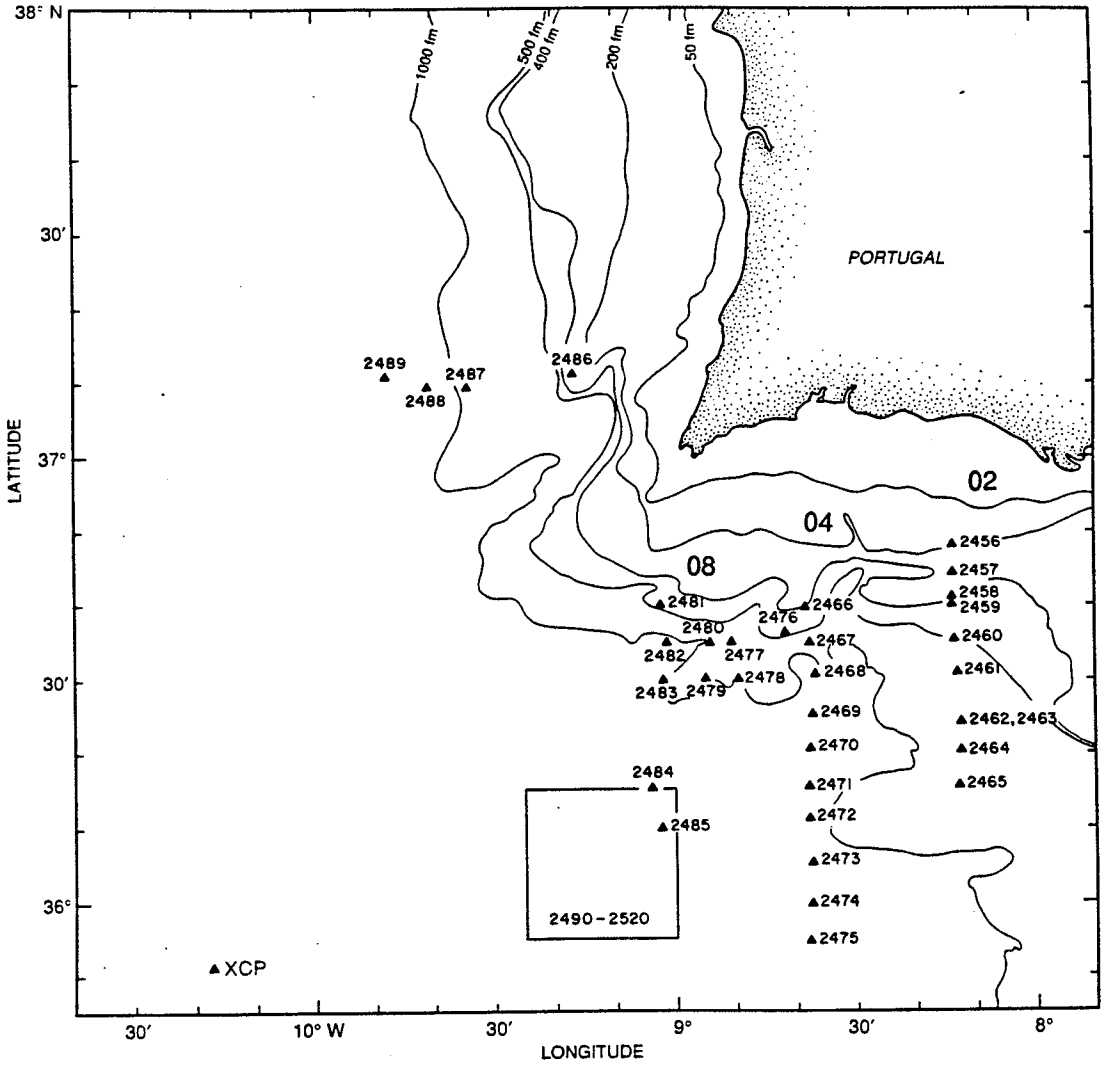

Figure 2.2. Location of XCP drops during the regional survey. The boxed area is the site of the fine-scale Meddy survey.

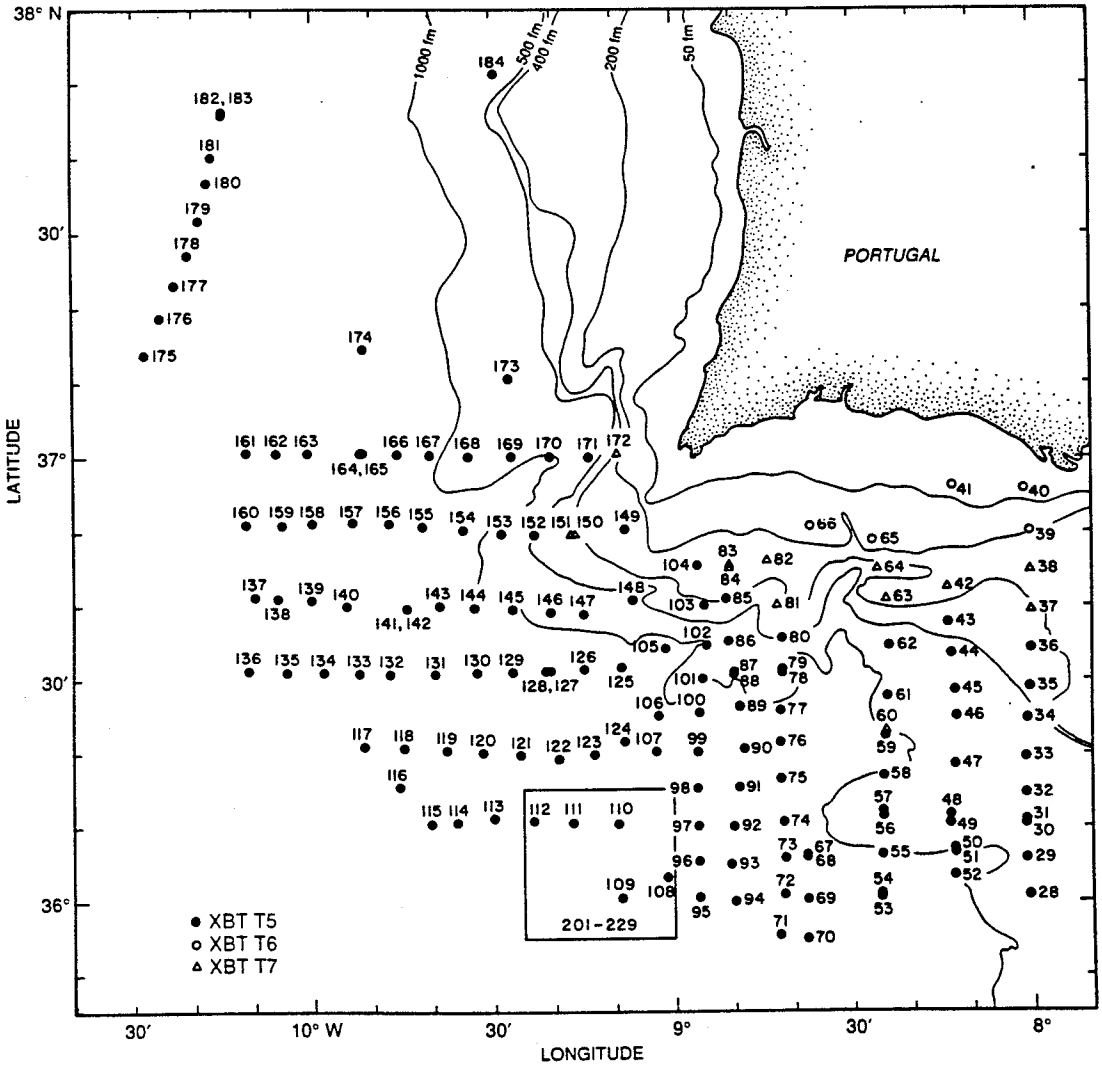

Figure 2.3. Location of XBT drops during the regional survey. The boxed area is the site of the fine-scale Meddy survey.

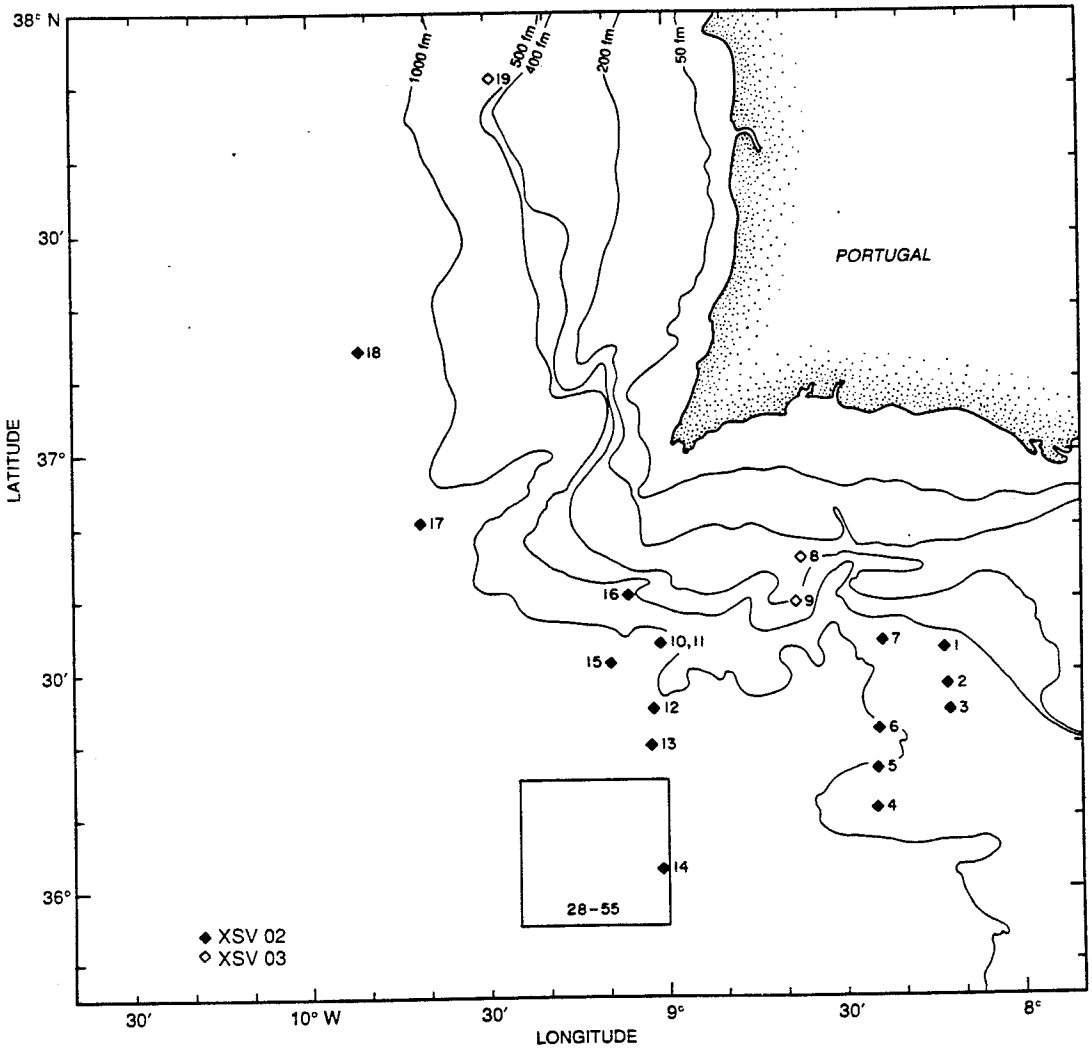

Figure 2.4. Location of XSV drops during the regional survey. The boxed area is the site of the fine-scale Meddy survey.

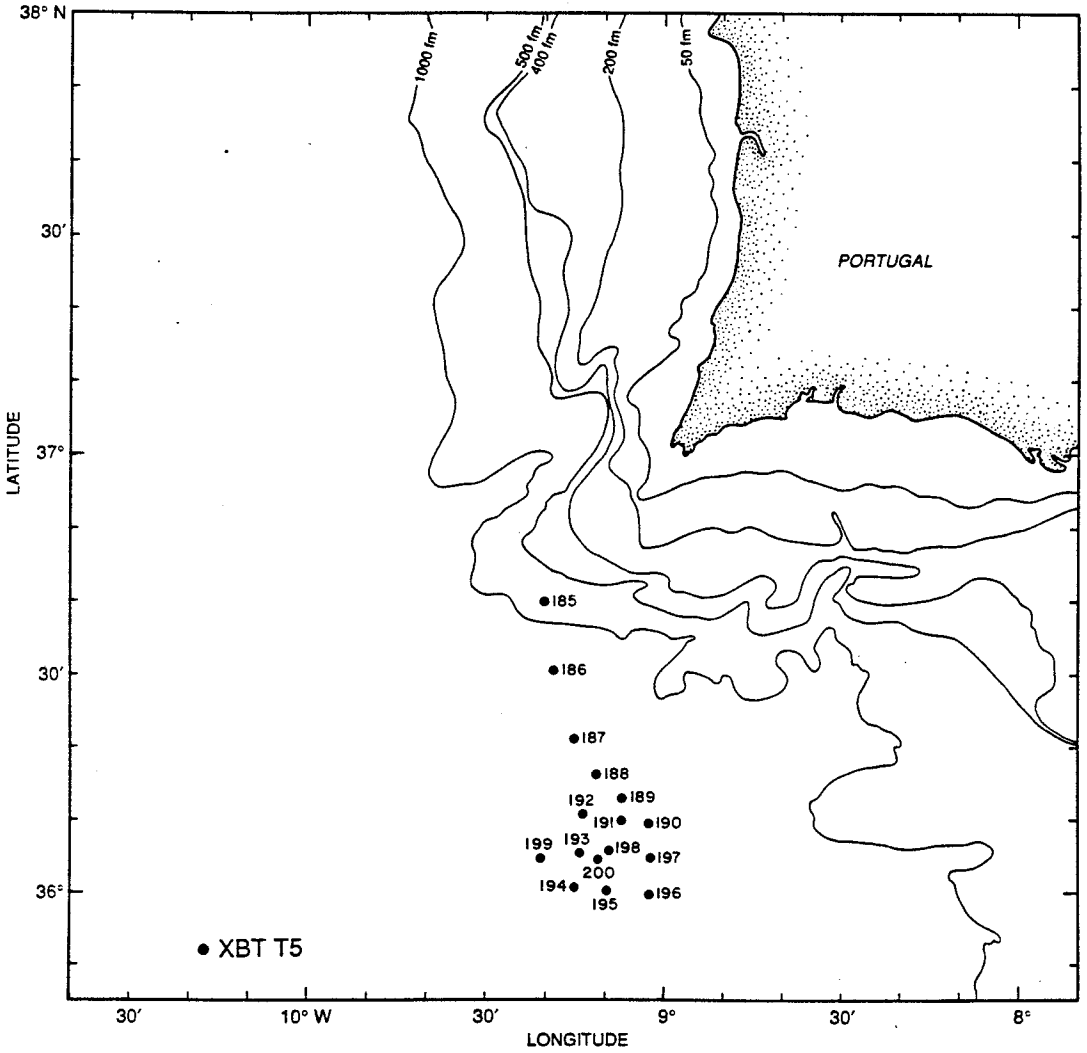

Figure 2.5. Location of XBT drops during the relocation survey.

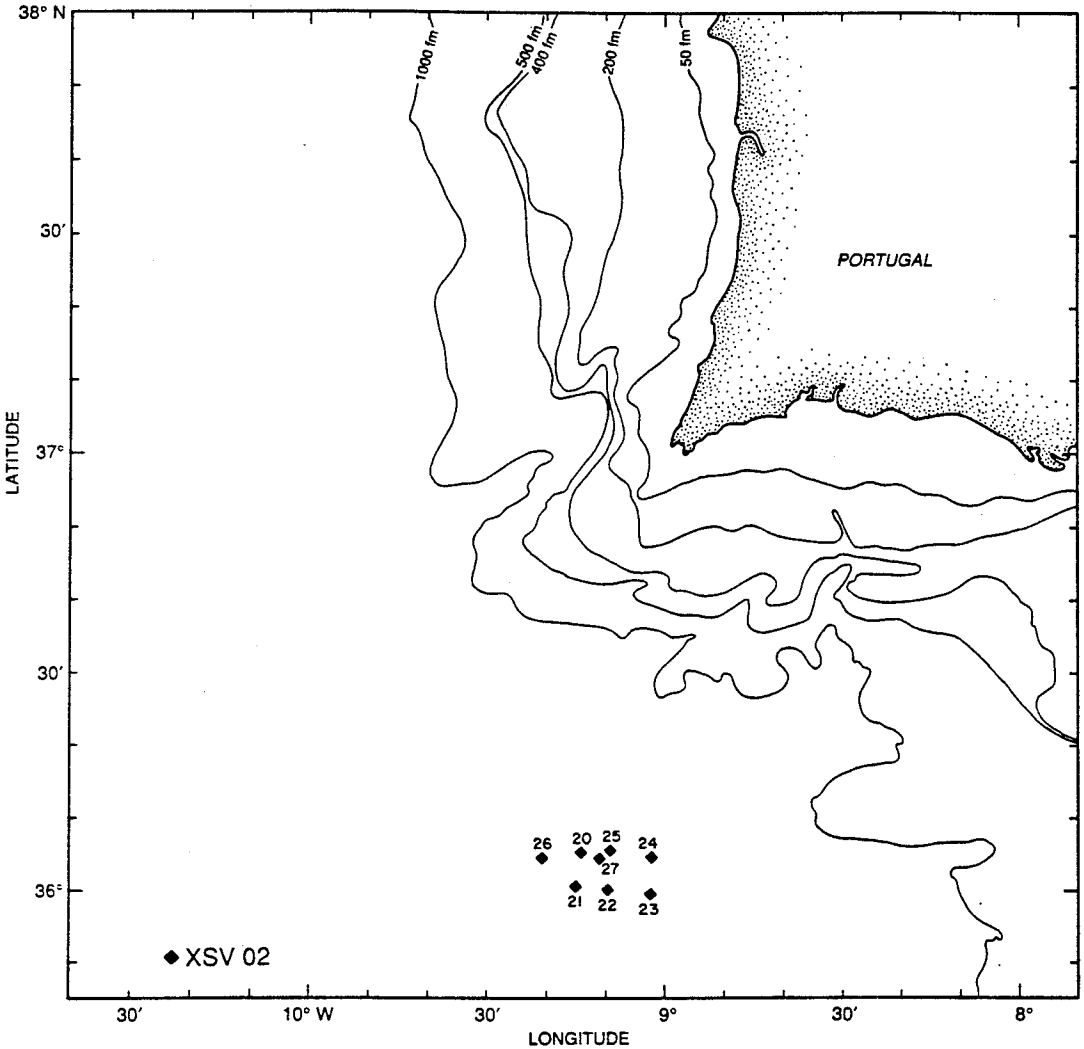

Figure 2.6. Location of XSV drops during the relocation survey.

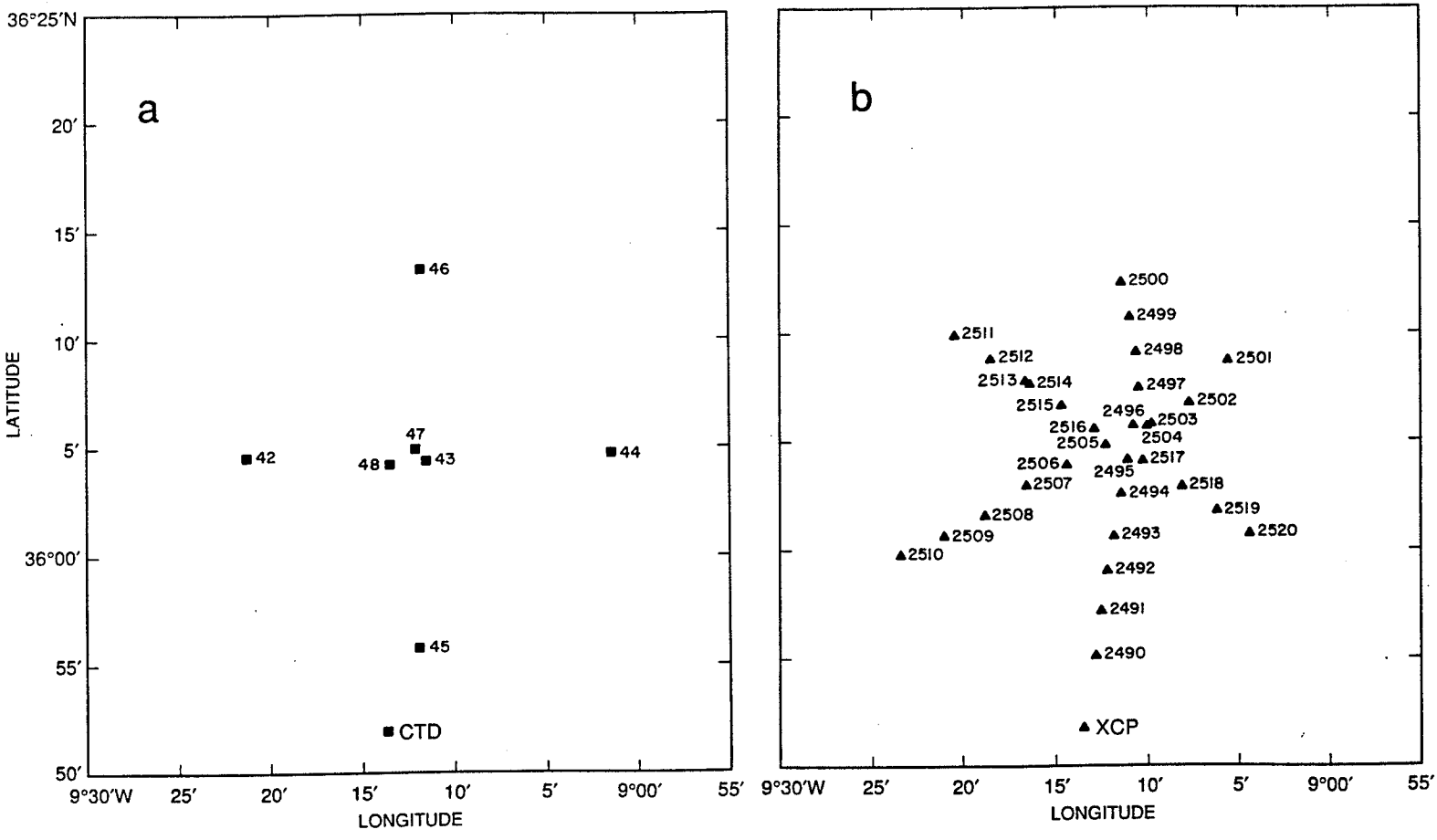

Figure 2.7. Location of drops during the fine-scale Meddy survey. *a*) CTD positions. *b*) XCP positions.

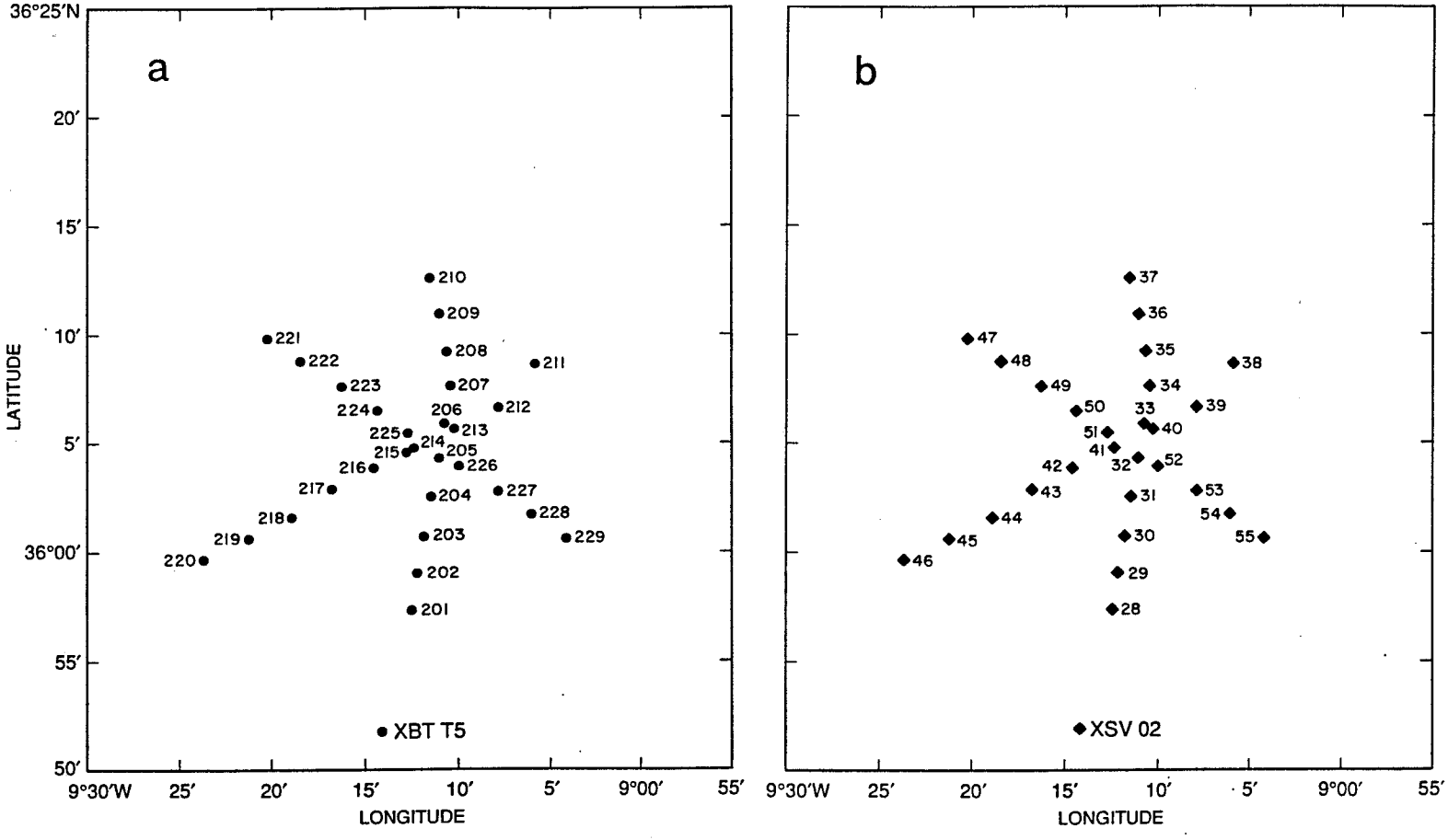

Figure 2.8. Location of drops during the fine-scale Meddy survey. *a*) XBT positions. *b*) XSV positions.

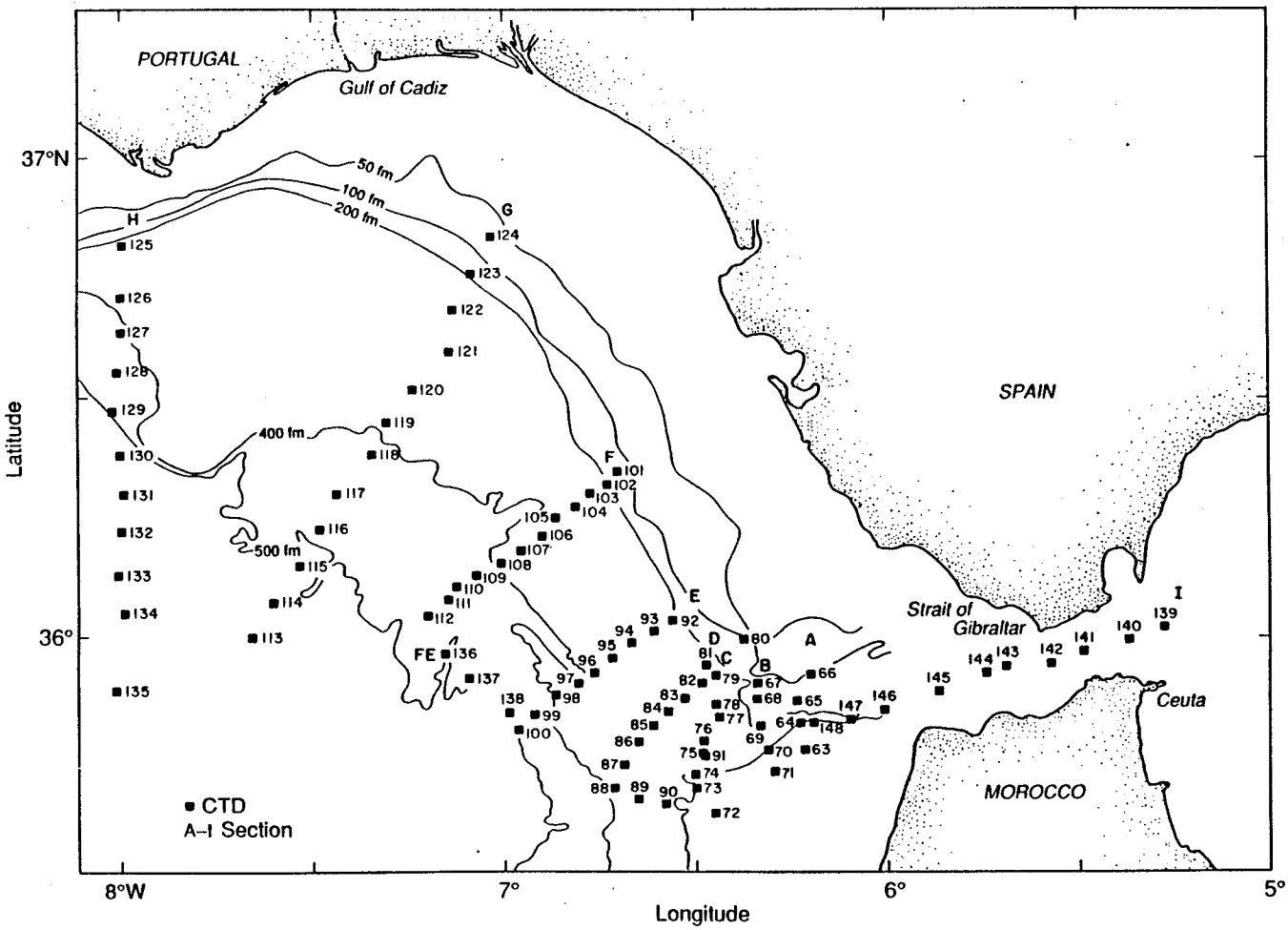

Figure 2.9. Location of CTD casts during the Mediterranean outflow survey.

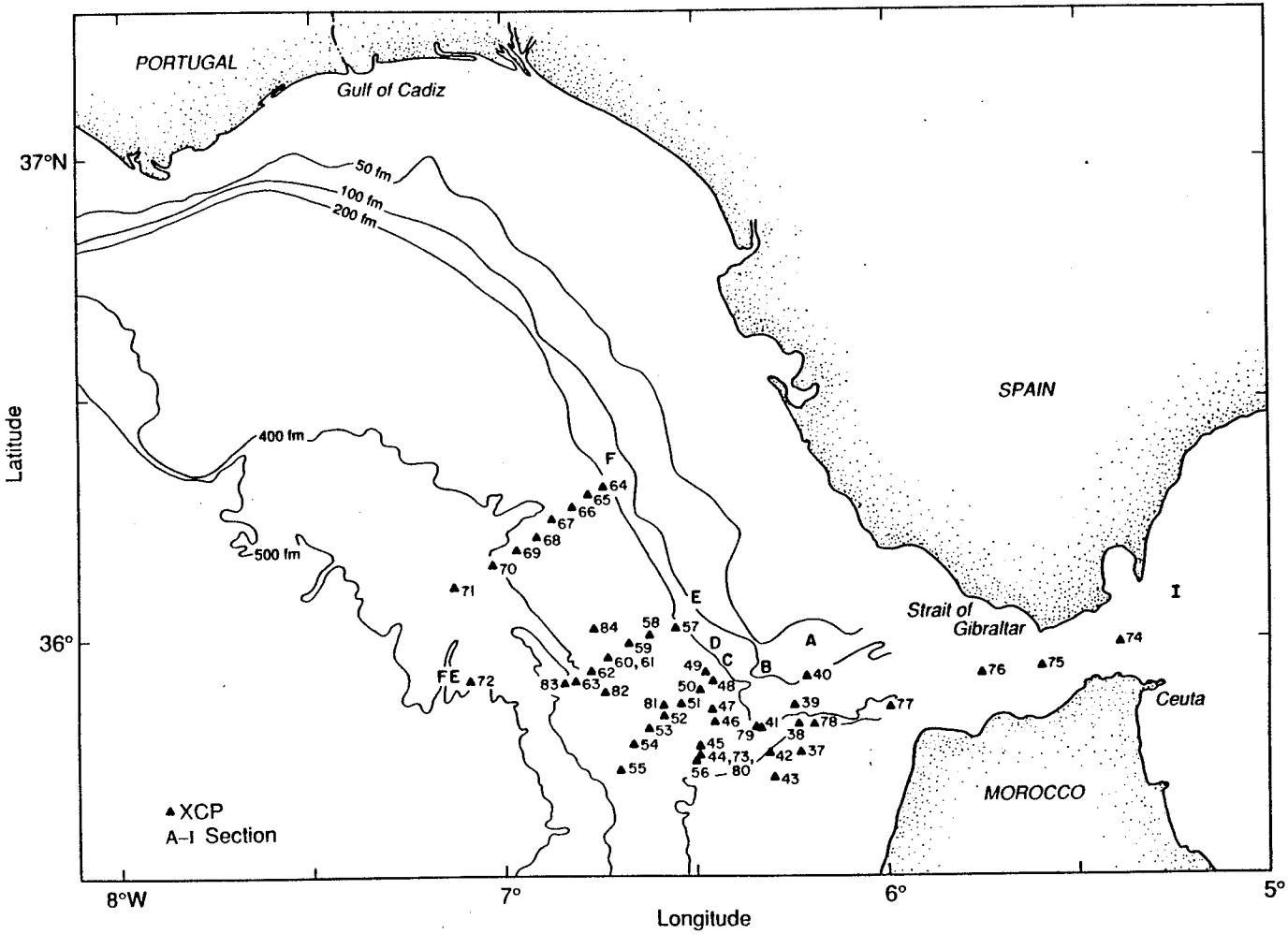

Figure 2.10. Location of XCP drops during the Mediterranean outflow survey.

Chapter 3. Description of the Cadiz Meddy

3.0 Introduction

A description of the Cadiz Meddy is given in this chapter. The data collected are described, and dynamical assumptions about the Meddy are tested.

Data from XCPs, XBTs, and CTDs give a detailed picture of the Meddy's temperature and velocity field. In this section, the Meddy will be treated as an isolated feature. Later, in Chapter 4, the relationship between the Meddy and its surroundings will be discussed.

3.1 Translation of the Meddy

Translation of the Meddy is particularly important because of the distortion caused by sampling in fixed space a feature moving through that space.

The method for determining the Meddy's translation uses two observations of the Meddy separated by about 4 days. The 11°C and 12°C temperature contours* at 1050 dbar from the regional and fine-scale surveys of the Meddy are shown in Figure 3.1. A reference time was chosen as the center time of the fine-scale Meddy survey. The drop positions in both the fine-scale and regional surveys were then translated by a given velocity to the specified reference time. The correlation between the two temperature fields was then computed, and the process repeated using different translation velocities until a maximum correlation between the two temperature fields was obtained. This process gave a translation velocity of the Meddy of 2.0 cm s^{-1} to the west and 1.4 cm s^{-1} to the south, with a correlation between the two fields of over 0.93. The error on the translations velocities is on the order of 0.5 cm s^{-1}.

*Unless otherwise specified, all horizontal contour plots were developed by fitting two-dimensional cubic smoothing splines to the data. The spline acts as a filter that removes spatial variations in the data at less than a specified horizontal scale. The specified "smoothing" scale that was used depended on the spacing of the original data and the scales of the features that were to be analyzed.

The translation speed of the Meddy, at 2.4 cm s^{-1} to the southwest, indicates that during the fine-scale survey the Meddy moved only 1.2 km. The Meddy translation also agrees in magnitude and direction with the Meddy "Sharon" (Armi et al., 1989), although this might be coincidental given how close the Cadiz Meddy is to both land and strong currents. Theoretical (Nof, 1982; Killworth, 1983) and modeling (Beckmann & Käse, 1989) estimates of Meddy motion give somewhat slower velocities to the west or southwest, and are dependent on β-plane effects. Since long-term tracking of the Cadiz Meddy was not done, and the absolute velocities in the waters surrounding the Meddy are not known, further comparisons with theoretical movements will not be pursued.

3.2 Temperature

A vertical temperature profile through the center of the Meddy (Figure 3.2) reveals two temperature maxima. The upper maximum is near 12.25°C at 1030 dbars, while the lower maximum is 12.1°C at 1350 dbars. The Meddy's temperature signal extends from 850 dbars to near 1500 dbars, giving a thickness of 650 dbars.

A horizontal slice through the Meddy at 1050 dbars, corresponding to the upper maximum (Figure 3.3a), reveals that the temperature field is generally circular, with a well-defined isothermal region. A slice at 1350 dbars showing the temperature field through the lower maximum is presented in Figure 3.3b. These isothermal regions of homogeneous temperature, bounded by increasing temperature gradients, will be called the "cores" of the Meddy. There are several differences between the upper and lower Meddy cores. First, the lower core is not as axially symmetric, but stretched along a northeast to southwest line. The lower core's temperature contours do not close to the northeast, giving the lower core the appearance of a blister on a warm tongue, rather than an isolated eddy. Finally, the temperature gradients to the south and west of the lower core are much higher than in the upper core.

The ellipticity of the lower core of the Meddy might be due to an attachment back to the Mediterranean outflow. Thus, the lower Meddy might not be a completely isolated feature, but still connected to the outflow. Another hypothesis is that the Meddy might be interacting with nearby eddies. Evidence of a cyclonic neighbor to the southeast is given in Chapter 4 (Fig. 4.6). An additional neighbor to the northwest, as

yet unidentified, would create the needed strain field to distort the Meddy in the observed manner. However, only the lower core of the Meddy is deformed, and the velocity structure of the neighboring eddy is not defined well enough to support this hypothesis.

Often it is difficult to visualize a three-dimensional feature with a series of two-dimensional slices. To alleviate this, software was developed to plot three-dimensional perspectives of data fields. Temperature profiles were low-pass filtered with a 3-dB point filter at 50 m, and subsampled at 10-m intervals. Then, each horizontal surface from -700 to -1600 m at 10-m intervals was fit with a two-dimensional smoothing-spline and sampled on a 1000-m by 1000-m grid. Out of the resulting "data cube", a temperature is selected, and the corresponding isothermal surface is found. Figure 3.4 presents the 12°C and the 11.8°C isothermal surfaces of the Meddy, as viewed from the southeast. The data cube is approximately 35 km by 35 km by 900 m. The horizontal-to-vertical aspect ratio (1/39) of the data cube is similar to the ambient f/N ratio (1/33). Warmer temperatures exist within the shaded region. The upper core of the Meddy has a distinctly different characteristic shape than the lower core. The upper core is (with the present aspect scaling) a slightly oblate spheroid, while the lower core is much more flattened and elliptical.

The center of the Meddy's temperature field is obtained, in a manner similar to that of the velocity field discussed in Appendix A, by a nonlinear least-squares fit to an axially symmetric model. The model has six parameters; the center coordinates of the Meddy (Lat_o, Lon_o), the Meddy core and background temperatures (T_c, T_b), and the radii of the transition region between the core and the background (R_c, R_b). An error of 0.2°C was assigned to each data point, incorporating both error in temperature as well as error is position. Although the model itself may not be meaningful for the less circular lower core, a consistent estimate of the Meddy center was obtained (36.097°N, -9.194°E). Thus, although the temperature model places the Meddy center approximately 1 km south of the velocity model center, the error bounds on the center of velocity and on the center of temperature (± 500 m) are large enough that a distinction between the two estimates is difficult to defend.

The visually apparent ellipticity of the Meddy can make interpretation of the radial distribution of temperature difficult. To "correct" for this ellipticity, an "equivalent" radius to each data point is computed and used, rather than the actual measured radius. The equivalent radius is the radius of a circle that has the same area as the ellipse. The radial distance of data points on the major axis of the ellipse is thereby reduced, while the opposite is true for points on the minor axis.

A measure of the ellipticity of the Meddy is given by its *eccentricity* ε, which is computed by

$$\varepsilon = \frac{\sqrt{a^2 - b^2}}{a} \tag{3.1}$$

where a and b are the major and minor axes of the ellipse, respectively. The orientation of the ellipse is the angle α that the major axis makes with the x-axis.

To compute the equivalent radius, first the major axis of the ellipse on which a data position is found is rotated back to the x-axis (east). Next, the x-coordinate is kept the same, but the y-coordinate of the data position is expanded by a factor of λ^2, so that $y' = \lambda^2 y$, where

$$\lambda = \left[1 - \varepsilon^2\right]^{-1/4} = \left[\frac{a}{b}\right]^{1/2} \tag{3.2}$$

Finally, the resulting distance is scaled such that

$$r' = \frac{\sqrt{x^2 + y'^2}}{\lambda} \tag{3.3}$$

The area of a circle encompassed by a radius of r' is the same as the area of the ellipse defined by the data point, ε, and α. The above method was based on that given in Hebert (1988a).

The ellipse parameters for the upper and lower cores of the Meddy were determined by estimating the major and minor axes lengths from contour plots of temperature, and measuring the angle α with a protractor. The upper core had an eccentricity of 0.5 and an orientation of 40°, while the lower core had an eccentricity of 0.75 and an orientation of 55°. These estimates were not optimal in a least-square sense, but provide a zeroth-order correction to the data. Figure 3.5 shows the ellipses for the two cores.

With the ellipticity of the Meddy quantified, the radial distribution of temperature is examined. Here, all the temperature data are considered, regardless of azimuthal location of the data position.

The radial temperature structure of the Meddy, using the uncorrected data radii, is shown in Figures 3.6a and 3.6c. Each data point is averaged over a 50-dbar window centered at 1050 dbars for 3.6a and 1350 dbars for 3.6c. The radial temperature structure using the equivalent data radii is shown in Figures 3.6b and 3.6d. The solid line in Figure 3.6 is derived by solving the diffusion equation governing a warm cylinder of water in a cooler environment. The details and limitations of the model are given in Appendix C. The model has four parameters: the initial temperature of the warm cylinder T_{max}, the initial temperature of the environment T_{min}, the initial radius of the cylinder r_o, and the nondimensional time $t_o = \kappa t / r_o^2$ where κ is the thermal eddy-diffusivity. The use of this model serves as a method to generate a smooth curve through the data.

For Figures 3.6a and 3.6b, $T_{max} = 12.25°C$, $T_{min} = 10.80°C$, $r_o = 10.7$ km, and $t_o = 0.017$. There is virtually no horizontal temperature gradient out to 6 km, followed by a sharp temperature gradient. The temperatures in the outer regions of the Meddy are not uniform due to the proximity of the Mediterranean outflow and consequent spatially varying background temperature field.

The radial structure at 1350 dbars (Figures 3.6c and 3.6d) shows a core of gradually decreasing temperature out to 10 km. The transition region at 1350 dbars is irregular compared with that at 1050 dbars, due to the asymmetry of the Meddy. The solid curve is defined by $T_{max} = 12.05°C$, $T_{min} = 10.50°C$, $r_o = 18$ km, and $t_o = 0.05$. The larger value of t_o in the lower core corresponds to the reduced radial gradients of temperature compared with those in the upper core, as if the lower core had undergone thermal diffusion for a longer time.

A small but noticeable reduction in scatter is observed in the upper core (Figure 3.6b) when the ellipticity of the Meddy is treated. In the lower core (Figure 3.6d), correction for the ellipticity reduces the scatter of the temperature field dramatically, due to the large ε there. Thus, the ellipticity of the Meddy can be corrected, and the axially symmetric aspects of the Meddy's description can be discussed.

The temperature field of the Meddy in z,r-space is contoured in Figure 3.7a. Again, adjustment to the radial distances for the ellipticity of the Meddy is made, but, being constrained by the software used to generate the smoothed data field, compromise values of $\varepsilon = 0.66$ and $\alpha = 47.5^{\circ}$ were used for the entire vertical extent of the Meddy. Differentiation between the upper and the lower cores is seen, with a cooler water layer between them. The volume of relatively warm water (over 11.5°C) is much larger in the lower core of the Meddy, although the upper core is warmer. The lower core temperature maximum can be traced outward to the ambient Gulf of Cadiz waters of 11°C at 1200 dbars. The upper core, however, appears distinct from the surrounding waters. Isotherms above the Meddy at 700 dbars show little displacement with respect to the background. The Meddy is within the thick, nearly isothermal Gulf of Cadiz water, which varies by less than 1 °C from 600 to 1300 dbars. High gradients of temperature (on the order of 0.03 °C m^{-1}) are found immediately beneath the Meddy. The isotherms at 1600 dbars are still depressed, indicating that the Meddy influenced its surroundings at a depth beyond what we measured. The radial temperature gradient (Figure 3.7b) reaches a maximum in the upper core at a radius of 10 km, in agreement with the radial distribution of Figure 3.6. The lower core shows a different structure of radial gradient, due primarily to the depression of the isotherms under the Meddy.

3.3 Salinity

The fine-scale Meddy survey did not provide high quality estimates of salinity at the same horizontal spatial resolution as the temperature data. High quality salinity profiles were taken at the Meddy center (three CTD casts) and at the boundaries of the fine-scale survey region (four CTD casts). It was anticipated prior to the cruise that sound velocity data from the XSVs and the temperature data from XBTs could be combined to obtain an estimate of salinity. However, the method was too inaccurate to be useful for anything but the most qualitative comparisons. Refer to Appendix B for details on the salinity method. One result from the XSV-XBT combination is that the extent of the homogeneous salinity core appears to be the same as that of temperature (Figure B.1).

A salinity profile from a CTD cast in the Meddy center is shown in Figure 3.8. As with the temperature, the Meddy core has two salinity maxima separated by a minimum. The upper maximum is 36.5 psu near 1150 dbars, while the lower maximum is 36.65 psu at 1400 dbars.

The T-S characteristics of the Meddy are shown in Figure 3.9a, using data at 2-dbar intervals from the three CTD casts near the center of the Meddy. The Meddy is seen as an intrusion (in T-S space) of Mediterranean water into the background North Atlantic Central Water. The signal of the Meddy in the Gulf of Cadiz is not as pronounced as the figure might indicate. The ambient waters in the Gulf of Cadiz, outside of the Mediterranean outflow and any Meddy, have a strong Mediterranean water signature. As the Meddy continues to advect out of the region along density surfaces, its $T-S$ anomaly, compared with the background state, will increase.

Increasing the resolution of the $T-S$ plot (Figure 3.9b), we see not only the $T-S$ minimum between the upper and lower cores, but also smaller $T-S$ minima within each core. The center three CTD casts were within 3 km and 1 day of each other. Since CTD data were not available throughout the Meddy, the horizontal scales of this layering are not known. However, the vertical profiles of temperature were smooth, and did not show the perturbations typical of thermohaline intrusions (Hebert et al., 1990). The layering within the Meddy, both the upper and lower core "layers" as well as the finestructure layering, resembles the layering in the Mediterranean outflow, and thus is probably a remnant of the source waters (e.g., Fig. 4.9). An alternative hypothesis is that a dynamic process formed the $T-S$ minima. Vastano & Hagan (1977) found evidence of a secondary circulation within a cyclonic Gulf Stream ring consisting of two counter-rotating cells, with horizontal inflow at the top and bottom of the ring and an outflow at mid-depth. Flierl & Mied (1985) examined the secondary circulation in a warm-core ring under the influence of nonunit Prandtl (P_r) numbers (momentum diffusion / mass diffusion $\neq 1$) for low-Rossby number conditions and found that an inflow at mid-depth is possible if mass diffuses faster than momentum. An analysis of XCP velocity vectors shows no inward veering between the upper and lower cores. However, if the induced inflow is less than a few cm s^{-1}, the velocity fluctuations from internal waves would obscure the signal. Also, the Meddy has nearly order one Rossby number dynamics (refer to Sections 3.7 & 3.8), and the value of P_r is not known. Thus, I assume that the fine-scale layering arose from the outflow waters, and the hypothesis of a dynamical

source for the layering will be postponed for further study.

3.4 Density and Stratification

As with the salinity, high-quality estimates of density were made only with CTD data. Thus, only a comparison between the core and the background can be made. (Later, in Section 3.8, the gradient-wind approximation will be used to estimate the density field from XCP velocity data.) Profiles of density and buoyancy frequency of the core and the background are shown in Figure 3.10. The density was computed as if the waters were moved adiabatically to 1000 dbars, and is denoted as σ_1. The buoyancy frequency was computed as

$$N^2 = -\frac{g}{\rho}\frac{\partial \rho}{\partial z} \tag{3.4}$$

where the partial derivative was approximated by linear fits to σ_1 over 100-m intervals. The buoyancy frequency profile in the center of the Meddy shows a stratification minimum at the center of the upper and lower cores, with a pronounced maximum between them. The buoyancy frequency in the cores ($\approx 1.5\times10^{-3}$rad s^{-1}) is half the value above, between, and below the two cores. The stratification minima are due to isopycnal separation in the Meddy cores, and are an indication of anticyclonic flow around the center.

3.5 Isopycnal Displacement and Available Potential Energy

The displacement of isopycnals Π (in dbars) from the background state to the center of the Meddy is given by

$$\Pi(\sigma_i) = p_{center}(\sigma_i) - p_{background}(\sigma_i) \tag{3.5}$$

The background density profile is assumed to be the average density from three of the four outside CTDs (the northernmost CTD, closest to the Mediterranean outflow, was deemed not representative of the far-field conditions). The isopycnal displacement in the center of the Meddy is shown in Figure 3.11a. Since three of the seven CTDs in the Meddy survey stopped near 1600 dbars, and none went below 1800 dbars, the deep structure of the Meddy was not mapped. Similar to the isotherms discussed earlier (Figure 3.7a) that showed downward displacement beneath the Meddy, the isopycnal

displacements are not shown returning to zero below the lower core of the Meddy. It is assumed that the displacements do indeed approach zero, but the depth at which that occurs is unknown.

The total available potential energy APE contained in an isolated feature has been determined by Hebert (1988b) to be

$$APE_{tot} = \int_{Vol} \left\{ \frac{1}{2} \rho N_{ref}^2 \left[1 - \frac{\partial \Pi}{\partial p} - \frac{\Pi}{3N_{ref}^2} \frac{\partial N_{ref}^2}{\partial p} \right] + O(\Pi^4) \right\} dVol \tag{3.6}$$

Isopycnal displacement in meters and in dbars is considered here to be equivalent within a difference in sign. The Boussinesq approximation, given by Reid et al. (1981) and shown to be accurate to within 10% for most oceanic applications, is

$$APE_{total} = \int_{Vol} \frac{1}{2} \rho N_{ref}^2 \Pi^2 \, dVol \tag{3.7}$$

Hebert (1988b) derived two obvious constraints on the validity of (3.7):

$$\left[\frac{\partial \Pi}{\partial p} \right] \ll 1 \tag{3.8}$$

and

$$\left[\frac{\Pi}{3N_{ref}^2} \frac{\partial N_{ref}^2}{\partial p} \right] \ll 1 \tag{3.9}$$

For (3.7) to be valid, just the volume integral of the constraints must be small. However, when examining the magnitude of the integrand, the original constraints are in effect. The value of (3.9) never exceeds 0.15, and is usually closer to 0.05. However, values of (3.8) often occur in the range 0.5 to 1.2 (Figure 3.11b). This does not necessarily invalidate the approximation. In (3.6), the isopycnal displacement and the vertical gradient of displacement are 90° out-of-phase. Thus, when the gradient is large, the displacement is small, and therefore the product of the two terms (as well as its contribution to the APE) is likewise small .

The integrand of (3.7) is plotted in Figure 3.11c. The majority (over 70%) of the *APE* in the Meddy center is in the region above the upper core, from 780 to 1070 dbars. The maximum APE density is 33 J m^{-3}. A secondary source of *APE* occurs below the lower core, for the remaining 30% of the total. It is presumed that the isopycnal displacements below 1600 dbars do not substantially contribute to the total *APE*. Estimates of the isopycnal displacement Π and of available potential energy *APE* for the entire Meddy will be estimated from XCP velocity data later in this chapter.

3.6 Velocity Field

The horizontal velocity field of the Meddy was obtained from XCPs. The XCP measures velocity to within a depth-invariant offset. The methods used to reference the XCP velocities to the Meddy coordinate system are described in Appendix A. To illustrate the horizontal velocity structure of the Meddy, the XCP data were averaged in 100-dbar bins, sampled at 1050 and 1350 dbars, and plotted in Figure 3.12. Superimposed on the velocity data is the temperature field at that depth. An anticyclonic circulation is evident in both cores, and the velocities in both cores follow the isotherms, even in the lower core where the temperature field is stretched to the north. The Meddy velocity field shows some asymmetry, with higher velocities in the southeast quadrant. The cause of the asymmetry is unknown, but several hypotheses are suggested. If the asymmetry is due to long-term (many f^{-1} periods) dynamics, the measured velocity field indeed forms a "snapshot" of the Meddy. If the asymmetry is due to short-term (f^{-1} or less) dynamics, the picture of the Meddy was distorted by temporal variability during the survey. Another possibility is that the apparent asymmetry is due to the XCP velocities not being correctly referenced, and the asymmetry is merely an artifact of the referencing process. In any case, the asymmetry in velocity is not supported by a similar asymmetry in the temperature field.

As with the temperature data, an attempt was made to visualize the Meddy velocity structure. The XCP velocity data were filtered and splined, and a data-cube of velocity magnitude was created. Shown in Figure 3.13 are perspectives of the 0.18 m s^{-1} and the 0.13 m s^{-1} surfaces of constant velocity magnitude. Inside the surfaces, the velocity magnitude is greater, outside it is less. Only the upper core has velocities exceeding 0.18 m s^{-1}, and although a varicose structure is observed modulating the

torus-like feature, the upper core's velocities seem fairly uniform. When the 0.13 m s^{-1} velocity surface is examined, the upper core's torus is now "puffier", and larger in volume. Surfaces of velocity magnitude are now observed in the lower core, although not with a torus-like structure. Regions of high velocity are seen on the east and west sides of the lower core, which is consistent with the ellipticity noted earlier in the temperature field. An elliptic pressure distribution will create higher velocities at the minor axis, and slower velocities at the major axis of the ellipse.

Due to the difficulty in interpreting the azimuthal structure in any greater detail, the majority of the remaining discussion of the Meddy's dynamics will focus on the azimuthally averaged velocity data. This averaging eliminates the asymmetric aspect of the Meddy and assumes that most of the first-order dynamics is contained in the axially symmetric portion of the Meddy. In reducing the complexity of the Meddy through this averaging, information about higher-order dynamics is lost, and the assumption of negligible radial velocity and horizontal divergence is made.

As with the radial distribution of temperature, the XCP drop locations were adjusted to account for the ellipticity of the Meddy. In addition, two other corrections for the XCP velocity data were done. First, the azimuthal velocity was taken to be along the curve of the ellipse centered about the Meddy, rather than along a circle. This procedure did not modify the azimuthal component much, but did reduce the radial velocity component. Second, the magnitude of the azimuthal velocity was modified to account for the velocity vectors sweeping out equal areas in equal time, analogous to Kepler's law of planetary motion (A.D. Kirwin, personal communication, 1991). This is just a restatement of the conservation of angular momentum as a water parcel moves azimuthally with varying radius from the center of the Meddy, and was at most a 7% correction of the velocity.

The results of the corrected radial distribution of velocity and functions of velocity for the Meddy are presented in the r,z-coordinate system, and are obtained by averaging in the vertical and applying smoothing-splines in the radial directions. An advantage of smoothing-splines is that derivatives are easily obtained. Unless otherwise stated, the variable v will denote the anticlockwise (cyclonically) positive azimuthal velocity. Figure 3.14 shows vertical slices of the Meddy's azimuthal velocity and vertical shear ($\partial v / \partial z$) fields. The strong upper-core flows ($v \approx -0.23$ m s^{-1}) are centered near a radius of 9 km. The lower core velocities are reduced and smeared radially. The

vertical shear reaches a maximum of 1.2×10^{-3} rad s^{-1} above the upper core, with local maxima between the cores and below the lower core. Minima in shear are found at the mid-depths of the two cores.

3.7 Vertical Vorticity and Rate-of-Strain

The vertical vorticity is obtained from

$$\zeta = \frac{\partial v}{\partial r} + \frac{v}{r} \tag{3.10}$$

and rate-of-strain is from

$$\eta = \frac{\partial v}{\partial r} - \frac{v}{r} \tag{3.11}$$

If the core of a vortex is in solid body rotation, the two terms in the above equations will be of equal size (and sign), and will thus double the contribution for vorticity, while canceling for rate-of strain. Thus, rate-of-strain is expected to be relatively low in the Meddy core. Beyond the radius of maximum velocity, the derivative term changes sign, and the rate-of-strain will be maximized. These two quantities are contoured in Figure 3.15. The vorticity reaches a maximum magnitude of $-0.85f$ in the center, which approaches the limit of inertial stability of $-f$. The rate-of-strain is nearly zero in the center of the Meddy, and reaches a maximum of $0.5f$ at 11.5 km, at 1.3 R_{max}. High rate-of-strain indicates that parcels of water displaced a small amount radially rapidly separate azimuthally. The lower core reaches the same vorticity level as the upper core, but the extreme vorticity region is of lesser radial extent. The rate-of-strain of the lower core does not show any pronounced maxima. The radial distribution of v, ζ, and η at the depth of the upper core is plotted in Figure 3.16. Both ζ and η are nearly constant out to a radius of 6 km. Superimposed on Figure 3.16 is the model Meddy structure

$$v = -0.27 \text{ m s}^{-1} \left(\frac{r}{r_{max}}\right) \qquad r \le r_{max} \tag{3.12}$$

and

$$v = -0.27 \text{ m s}^{-1} \left(\frac{r_{max}}{r}\right)^2 \qquad r \ge r_{max}$$

The model is unphysical near r_{max} due to the large gradients in ζ and η, but otherwise it

compares well. Schultz Tokos (1989) also found this model to agree well with the Meddy "Sharon" data, although with a different velocity coefficient. The above model has the interesting characteristic that the integral of vertical vorticity over the entire horizontal domain ($r \rightarrow \infty$) is zero.

3.8 Gradient-Wind Density Field

Because independent density data throughout the Meddy were lacking, the radial distribution of density was estimated by means of the gradient-wind equation. For two-dimensional, axially symmetric flows, the relationship derived from the radial momentum equation assuming cyclogeostrophic balance is

$$\frac{v^2}{r} + v f = \frac{1}{\rho_o} \frac{\partial p}{\partial r} \tag{3.13}$$

Differentiating with respect to z and assuming hydrostatics, we have

$$\left[\frac{2v}{r} + f \right] \frac{\partial v}{\partial z} = \frac{1}{\rho_o} \frac{\partial}{\partial r} \frac{\partial p}{\partial z} - \frac{g}{\rho_o} \frac{\partial \rho}{\partial r} \tag{3.14}$$

Thus, the horizontal density gradient in the core of the Meddy depends on the vertical shear and a measure of absolute vorticity. With the assumption that the far-field density is known, the equation can be integrated from r_∞ inwards toward the center, so that

$$\rho(r) = \rho(\infty) \left[\frac{2v}{r} + f \right] \frac{\partial v}{\partial z} dr \tag{3.15}$$

For the Meddy, the reference density field at infinity was taken from the mean density profile from three CTD stations, averaging 17 km from the center. The above reference is the same as was used in Section 3.4. The computation of density performed using the splined velocity data and the resulting contours of isopycnal displacements (from the reference) are plotted in Figure 3.17a. The isopycnals are separated in the center of the Meddy, pushed upward above and downward below. An estimate of the buoyancy frequency was also computed, using (3.4). Figure 3.17b shows contours of N. The upper and lower cores of the Meddy show decreased values of N; between the cores and below the lower core, the buoyancy frequency is increased due to compression of the isopycnals.

To judge the validity of the above procedures, comparisons were made between the density computations made from CTD data and those made integrating XCP velocity data and assuming geostrophy and cyclogeostrophy. In all the comparison figures, the light line is the CTD data, the dark dashed line the geostrophic assumption, and the dark solid line the cyclogeostrophic assumption. Figure 3.18a shows a comparison of isopycnal displacement, 3.18b shows the density difference between the center and the reference on pressure surfaces, and 3.18c shows the computed buoyancy frequency. In all three comparisons, the cyclogeostrophic model matches the CTD data results better than the geostrophic. Without the cyclogeostrophic term creating an additional outward force in the radial momentum balance, the geostrophic assumption requires a larger radial pressure gradient to maintain the observed azimuthal velocities. The differences between the cyclogeostrophic results and the CTD data are small in the upper core of the Meddy, but in the lower core the computed displacements and the radial differences in density are more than 50% larger than CTD data show. It is not likely that the errors are from the cyclogeostrophic assumption. The fit was not improved by simple modifications to the vertical shear or the azimuthal velocity, as would occur if the XCPs were referenced differently. The differences are probably due to the presence of near-inertial waves, which are not in thermal wind balance; if present in or below the lower core, near-inertial waves would contribute vertical shear without a compensating radial density gradient. The agreement between the fit and data is close enough to provide justification that the Meddy is in cyclogeostrophic balance, and so the density field and especially the buoyancy frequency computed by gradient-wind are valid representations of what would have been observed.

3.9 Potential Vorticity

Potential vorticity in an inviscid fluid is conserved by each fluid parcel (Pedlosky, 1979) and is given (e.g., Gill, 1982) as

$$Q = -(f\hat{\mathbf{k}} + \zeta) \tag{3.16}$$

The sign of the above equation has been modified such that Q is positive, so negative values of Q imply inertial instability. For an axially symmetric eddy with no radial or vertical velocities, the potential vorticity in cylindrical coordinates is

$$Q = -\frac{1}{\rho}\left[f + \frac{\partial v}{\partial r} + \frac{v}{r}\right]\frac{\partial \rho}{\partial z}\frac{1}{\rho}\frac{\partial v}{\partial z}\frac{\partial \rho}{\partial r} \tag{3.17}$$

Assuming, as was shown in Section 3.8, that the Meddy is in gradient wind balance, and using (3.14), we have

$$Q = -\frac{1}{\rho}\left[f + \frac{\partial v}{\partial r} + \frac{v}{r}\right]\frac{\partial \rho}{\partial z}\frac{1}{g}\left[f + \frac{2v}{r}\right]\left[\frac{\partial v}{\partial z}\right]^2 \tag{3.18}$$

Now, let

$$\rho = \bar{\rho}(z) + \rho'(x, y, z) \tag{3.19}$$

where $\bar{\rho}$ is the mean vertical structure of density, and ρ' is the density anomaly associated with the Meddy. Equation 3.18 can thus be expressed as

$$Q = \frac{1}{g}\left\{(f + \zeta)(\bar{N}^2 + N'^2)(f + \frac{2v}{r})\left[\frac{\partial v}{\partial z}\right]^2\right\} \tag{3.20}$$

Kunze (personal communication, 1991) has simplified (3.20) in terms of nondimensional parameters, so

$$Q = \frac{f\,\bar{N}^2}{g}\left[(1 + \frac{\zeta}{f})(1 + \frac{N'^2}{\bar{N}^2}) - (1 + \frac{2v/r}{f})\right. \tag{3.21}$$

or

$$= \frac{f\,\bar{N}^2}{g}\left[(1 + R_o)(1 + G) - (1 + R_v)R_i^{-1}\right]$$

or finally

$$Q = \bar{Q}\left[1 + R_o + G + R_o G - R_i^{-1} - R_v R_i^{-1}\right] \tag{3.22}$$

where the ambient potential vorticity $\bar{Q}$ is $f\,\bar{N}^2/g$, the two forms of the Rossby number are $R_o = \zeta/f$ and $R_v = 2v/rf$, the inverse Richardson number R_i^{-1} is $S_z^2/\bar{N}^2$ where $S_z^2 = (\partial v/\partial z)^2$, and the normalized buoyancy gradient anomaly G is $N'^2/\bar{N}^2$. The above expression for Q can be further simplified as

$$Q = \bar{Q}\left[1 + X\right] = \bar{Q} + Q' \tag{3.23}$$

where

$$X = R_o + G + R_o G - R_i^{-1} - R_v R_i^{-1} \tag{3.24}$$

and the potential vorticity anomaly is

$$Q' = \overline{Q} X$$

Thus, the ambient potential vorticity $\overline{Q}$ in the Meddy is modified by X, a sum of nondimensional terms.

The potential vorticity of the Meddy is decreased compared with the reference state by the local decrease in N^2 (Figures 3.10, 3.17, and 3.18) which would result in a negative G, and an increase in negative relative vorticity (Figure 3.15) which results in a negative R_o. The reduction of Q by the vertical shear of the Meddy is moderated by a negative R_v. At the center of the upper core of the Meddy, the sum of the modifying terms is –0.95, with $R_o = -0.87$, $G = -0.61$, the product $R_o G = 0.53$, and the remaining terms contributing little due to the low vertical shear in the core. Note the importance of the nonlinear term $R_o G$ in the core. The two vertical shear terms contribute little anywhere in the Meddy, with a combined maximum value in the Meddy of 0.13 in the high shear region above the upper core (Figure 3.14b).

Contours of Q for the Meddy are shown in Figure 3.19a, while the radial distribution at 1050 dbars is shown in Figure 3.19b. The upper and lower cores are distinguished by reduced Q compared with the far-field. The value of Q at the center of the Meddy's upper core is 4×10^{-12} $(\mathrm{m\,s})^{-1}$, 17 times less than the background value at the same pressure. This is substantially lower than was found in Meddy Sharon, where minimum values of 3×10^{-11} $(\mathrm{m\,s})^{-1}$ were computed (Schultz Tokos & Rossby, 1991). The Cadiz Meddy's lower Q was from both lower stratification and more negative relative vorticity. The change in potential vorticity occurs over a 6-km range, from the nearly homogeneous core at 6 km to the background state at 12 km. The transition region is well resolved, with 20 XCP drops between 3 and 15 km. The conservation of Q with water parcels (assuming an inviscid environment) indicates that parcels at the levels of the Meddy cores, and particularly the upper core, are inhibited from moving radially into regions of different Q.

As was found in other isolated eddies (Elliott & Sanford, 1986a,b; Kunze, 1986; D'Asaro, 1988a) the ambient Q is governed by the mean stratification $\overline{N}$, while the interior Q is a strong function of the relative vorticity and vortex stretching. The value

of Q in the upper core is well represented by

$$Q = \overline{Q}\,[\,1 + R_o + G + R_o\,G\,] \tag{3.25}$$

when the upper core values of $\zeta \approx -0.75f$ and $N' \approx 1.7 \times 10^{-3}$ rad s^{-1} are used. Likewise, using the background values of $\zeta \approx 0$ and $N = \overline{N} \approx 2.8 \times 10^{-3}$ rad s^{-1}, the background Q is obtained.

The vertical shears along the equatorial plane of the upper core are nearly zero, thus (3.25) is a good approximation of (3.22) for Q, regardless of the radial distance. There, the potential vorticity can be expressed somewhat differently, as

$$Q(r) = \frac{f + \zeta(r)}{h(r)} \tag{3.26}$$

where $h(r)$ is the radially varying isopycnal separation. Solving for $\zeta(r)$ and integrating over the horizontal domain,

$$\int_A \zeta(r)\,rdr = \int_A Q(r)\,h(r)\,rdr - fA \tag{3.27}$$

If the area integrated relative vorticity is zero, as suggested in Section 3.7, then the volume integral of potential vorticity reduces to the background level fA. Thus, although the relative vorticity is important locally, it is not important in an integral sense. This is suggested in the work of Haynes & McIntyre (1987). They show that in the generation of isolated features, the transport of potential vorticity is lateral along isopycnals, and that the negative potential vorticity anomaly in the core would be balanced by a positive anomaly surrounding the core. Thus the integrated anomaly is zero.

3.10 Energetics

In Section 3.5, the *APE* density in the center of the Meddy was discussed. Using the isopycnal displacements computed in the previous section and (3.8) from Section 3.5, the *APE* density for the r,z-plane was computed. *APE* densities at pressures greater than 1250 dbars were divided by $(1.5)^2$ to correct for the over-estimate in the isopycnal displacements due perhaps to near-inertial waves below the lower core, as mentioned in Section 3.8. The resulting contours are shown in Figure 3.20a.

Likewise, the total kinetic energy of the Meddy can be computed from

$$KE = \int_{Vol} \frac{1}{2} \rho_o v^2 \, dVol \tag{3.28}$$

where the integrand is the KE density, plotted in Figure 3.20b. High values of APE are concentrated at the center of the upper core, mimicking the maximum isopycnal displacements. The KE levels are maximal at the location of maximum velocity.

The contours of APE and KE densities in the r-z frame are somewhat misleading, since the total energy is the volume integral of the densities, and the differential volume increases linearly with radial distance. Computing the total energies in radial bins (Figure 3.21a), and cumulative total energies (Figure 3.21b), we see that the KE exceeds the APE from 8.5 km outward. When the radial accumulation extends to 17 km (the reference radius) the total APE is 1.7×10^{12} J and total KE is 4.3×10^{12} J.

The ratio of $KE / APE = 2.5$ is a form of the Burger number B_E (D'Asaro, 1988a). The amounts of APE and KE in the Meddy are somewhat uncertain, given the proximity of the reference CTDs to the Meddy, the referencing of the XCPs, and the error associated with the isopycnal displacements. However, varying the position of the reference station and the smoothing of the vertical shears affected the ratio by less than 50%. Thus we can conclude that the Meddy has considerably more KE than APE. A numerical study by McWilliams & Gent (1986) suggests that an eddy with a "large" Burger number is barotropically unstable, and that it would segment vertically and form two or more new eddies with more moderate values of B. Their formulation for B requires a value greater than 1.2 for instability, thus the Cadiz Meddy might be susceptible to vertical segmentation. However, the relationship between the McWilliams & Gent expression for B and the B_E used here is not clear.

To investigate the meaning of the large B_E, a Meddy was modeled with an azimuthal velocity of

$$v(r,z) = \alpha r V_o \exp[-(\alpha r)^2] \exp[-(\beta z)^2] \tag{3.29}$$

where

$$\alpha = \frac{1}{\sqrt{2}\, r_{max}}, \quad \beta = \frac{1}{\sqrt{2}\, Z_o}, \quad \text{and} \quad V_o = 2.33\, v_{max}$$

Z_o is defined as the distance from the center of the Meddy (where the vertical shear is zero) to the level of maximum vertical shear. Analogously, r_{max} is defined as the distance from the center of the Meddy (where the azimuthal velocity is zero) to the radius of maximum velocity. KE was computed by (3.28), and APE was computed by assuming cyclogeostrophy and using (3.13) and (3.7).

The model is not an exact representation of the Cadiz Meddy. However, the form of the model allows us to vary the shape of the Meddy through three parameters (r_{max}, Z_o, and v_{max}) to explore the subsequent variation of B_E. The parameters were constrained by two stability requirements: first, nowhere could the Rossby number (R_o) defined as ζ/f be below -1; second, with the assumption of a uniformly stratified background density field, the total buoyancy frequency must be real-valued. Table 3.1 lists the results of the model, keeping r_{max} constant at 9000 m and increasing Z_o. The maximum magnitude of v_{max} that met the stability criteria was used, until the value of the Cadiz Meddy (–0.23 m s^{-1}) was reached.

For small Z_o, v_{max} is constrained by the stratification stability criterion to be small. Otherwise, the large vertical shears obtained through the gradient-wind-derived density equation (3.15) would result in an unstable vertical density profile. As Z_o increases, the vertical shear decreases for a given v_{max}, decreasing the density anomaly in the center of the Meddy and decreasing the isopycnal displacement on which the APE depends. But, the volume of the Meddy containing a specified velocity magnitude increases, thus increasing the integrated KE. Thus for a given r_{max} and v_{max}, increasing the vertical

Table 3.1 Results of B_E Model

Z_o (m)	v_{max} (m s^{-1})	B_E
100	0.045	0.21
150	0.150	0.54
200	0.230	0.94
300	0.230	2.11

scale of the Meddy increases B_E. The connection between B_E and the more typical definition of the Burger number B_L is shown by scaling and the use of the gradient wind relation, so that

$$\frac{\partial v}{\partial z} \approx \frac{v}{H} = \frac{g}{(f+\zeta_v)\rho}\frac{\partial \rho}{\partial r} \approx \frac{N^2 H}{(f+\zeta_v)L} \tag{3.30}$$

where ζ_v here refers to $2v/r$. Letting ζ_a denote the absolute vorticity, the above reduces to

$$v \approx \frac{N^2 H^2}{\zeta_a L}$$

and

$$B_E \approx \frac{v^2}{N^2 H^2} \approx \frac{(N^4 H^4)/(\zeta_a^2 L^2)}{N^2 H^2} = \frac{N^2 H^2}{\zeta_a^2 L^2} \tag{3.31}$$

In the absence of relative vorticity, B_E and B_L have equivalent scaling definitions, but B_L is a scaled quantity, while B_E is an integral quantity. A large B_E ratio, in the absence of relative vorticity, indicates that the Meddy is tall and thin with respect to the ambient N/f scaling. If significant negative relative vorticity exists and the other scales remain the same, the value of B_E increases (the kinetic energy was increased, but not the available potential energy).

3.11 Discussion

The Meddy observed in the Gulf of Cadiz has been described in detail. A description on its own, however, does not convey as much information as does comparison with other, similar features. That comparison is what we will do now. To aid in a quantitative comparison, the Cadiz Meddy is parameterized and the parameters are given in Table 3.2.

The height of the Meddy was estimated two ways. The first (H_s) was a measure of the thickness of the temperature and salinity anomaly. The second estimate (H_d) was the distance between the isopycnal surface that had the maximum upward displacement and the surface with the maximum downward displacement, and is a more dynamic

Table 3.2 Summary of Meddy Parameters

Parameter	Definition	Value
r_{max}		8.5 km
v_{max}		0.23 m s^{-1}
T_{max}		12.25°C, 12.05°C
S_{max}		36.5 psu, 36.65 psu
N_{min}		1.8, 1.2×10^{-3} rad s^{-1}
H_s	scalar	650 m
H_d	isopycnal	575 m
R_o	ζ / f	-0.85
R_v	$2v_{max} / f\ r_{max}$	-0.60
R_v / R_o		0.71
B_L	$(N_{ref}^2 H^2) / (4f^2 r_{max}^2)$	1.08
KE		4.3×10^{12} J
PE		1.7×10^{12} J
B_E	KE / PE	2.5

measure of the Meddy's vertical extent. The ratio of R_v / R_o is a measure of the horizontal structure of the Meddy (D'Asaro, 1988a). The Cadiz Meddy has a value of 0.71. If the Meddy were driven by a Gaussian pressure anomaly, the maximum R_v / R_o would be less than 0.6.

Of the Meddies mentioned in any detail in the literature (Table 1.1), most were surveyed coarsely with CTDs and little information on the Meddy dynamics was given. To make a consistent comparison including these poorly sampled Meddies, a modified definition of the Burger number (B_M) was used. B_M uses H_s, a Garrett-Munk like (Munk, 1981) buoyancy frequency profile for N, and 1.5 times the homogeneous scalar core radius as an estimate of r_{max}. For Meddies for which velocity measurements were made, either indirectly by geostrophic assumptions or directly by floats, moorings, or profilers, estimates of R_v were made. Figure 3.22 presents a summary of observed Meddies in R_v-B_M space. The values of R, B for the Meddies occur between $B = R/2$ and $B = 2R$, with the majority having R or B below 0.4. The Cadiz Meddy (denoted by 'o') and Meddy Sharon (x, the first survey) are on nearly opposite ends of the scale.

The Cadiz Meddy has a high aspect ratio (tall and thin) and a high core vorticity, while Sharon has a lower aspect ratio and a lower core vorticity. Two possible reasons for the difference between the Cadiz Meddy and Sharon are (i) difference in age and evolution, and (ii) difference in generation. The first, taken to its extreme, supposes that all Meddies are nearly the same initially, and the age of the Meddy determines its R and B. The second supposes that there is more than one generation mechanism, and the origin of the Meddy dominates the selection of R and B. A discussion of the place of origin for the Cadiz Meddy and possible generation mechanisms is given in the next chapter.

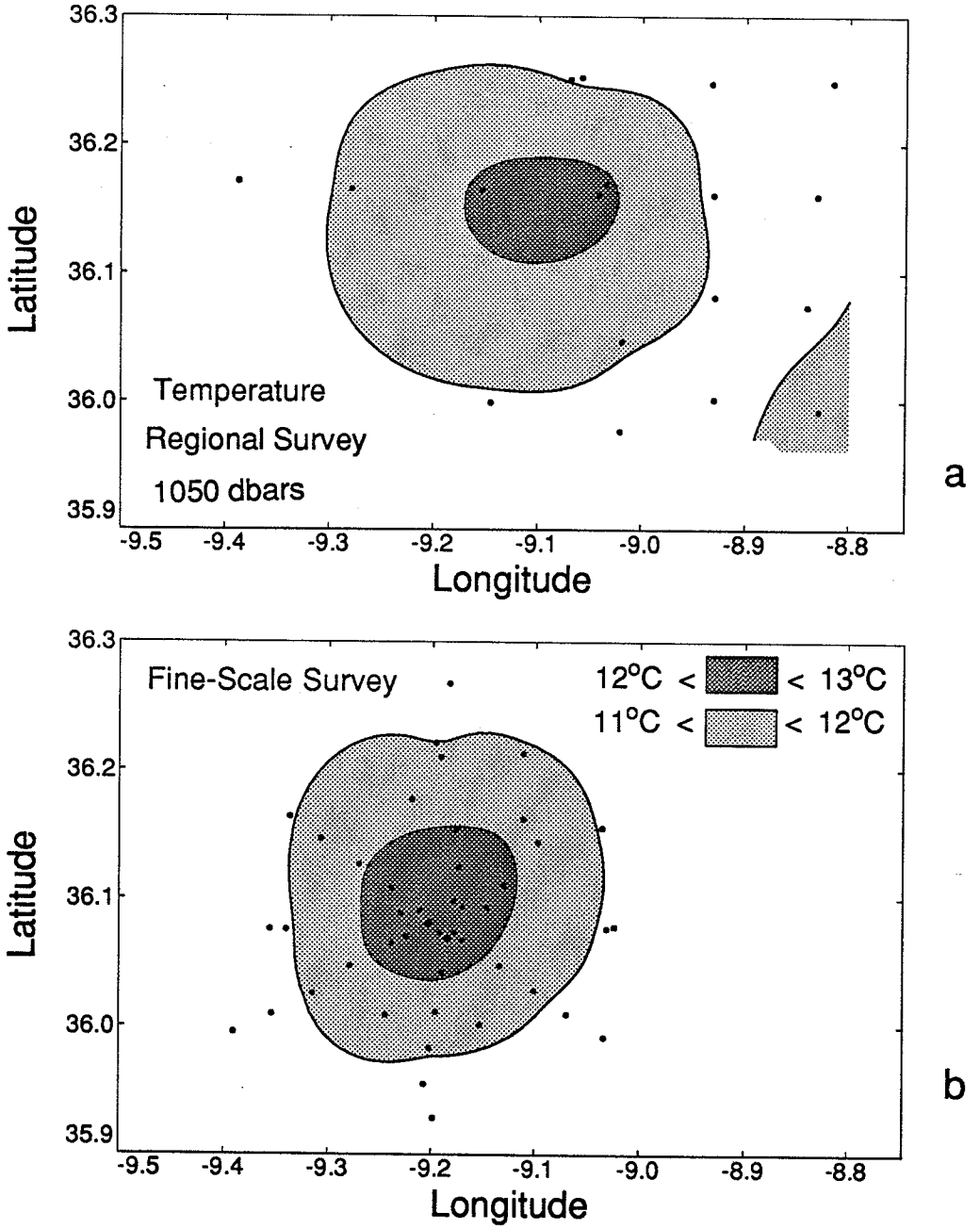

Figure 3.1. Temperature contours of the Meddy at 1050 dbars for *a*) the regional survey and *b*) the fine-scale survey. In four days, the Meddy moved 8.3 km to the southeast (2.4 cm s^{-1}). The dots are data locations.

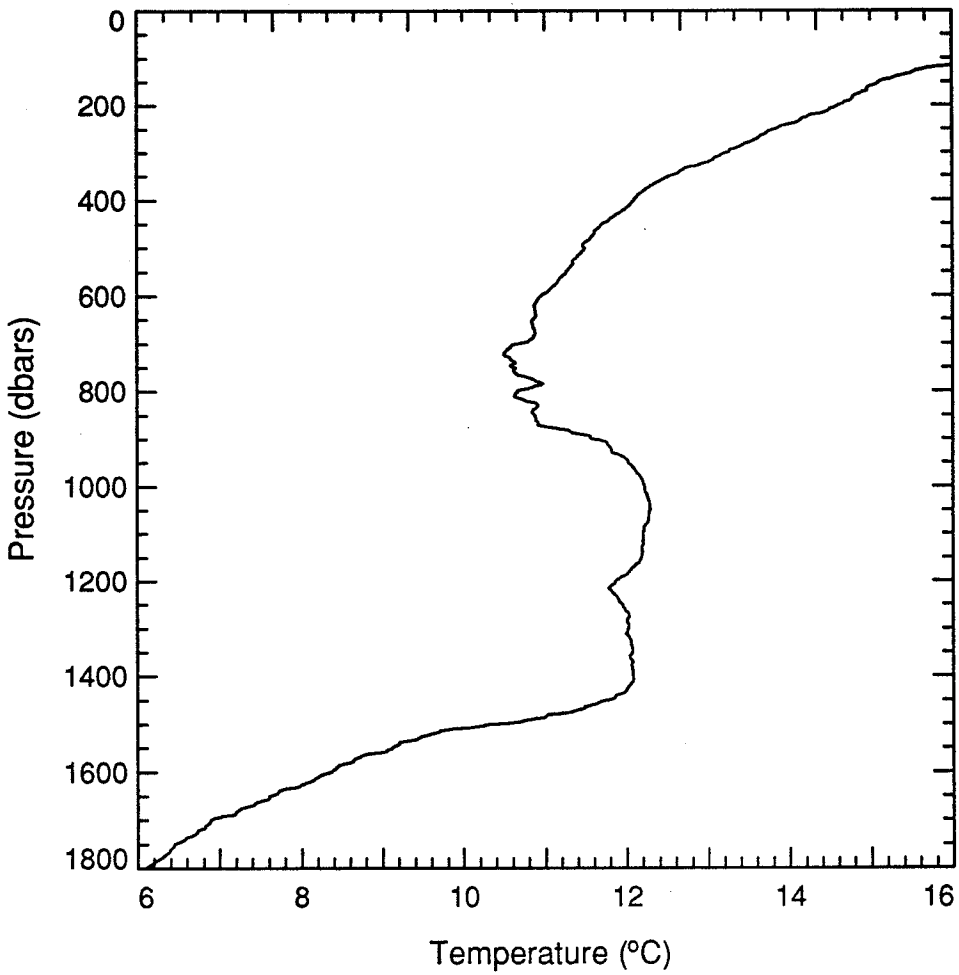

Figure 3.2. Temperature profile from a CTD cast through the center of the Meddy.

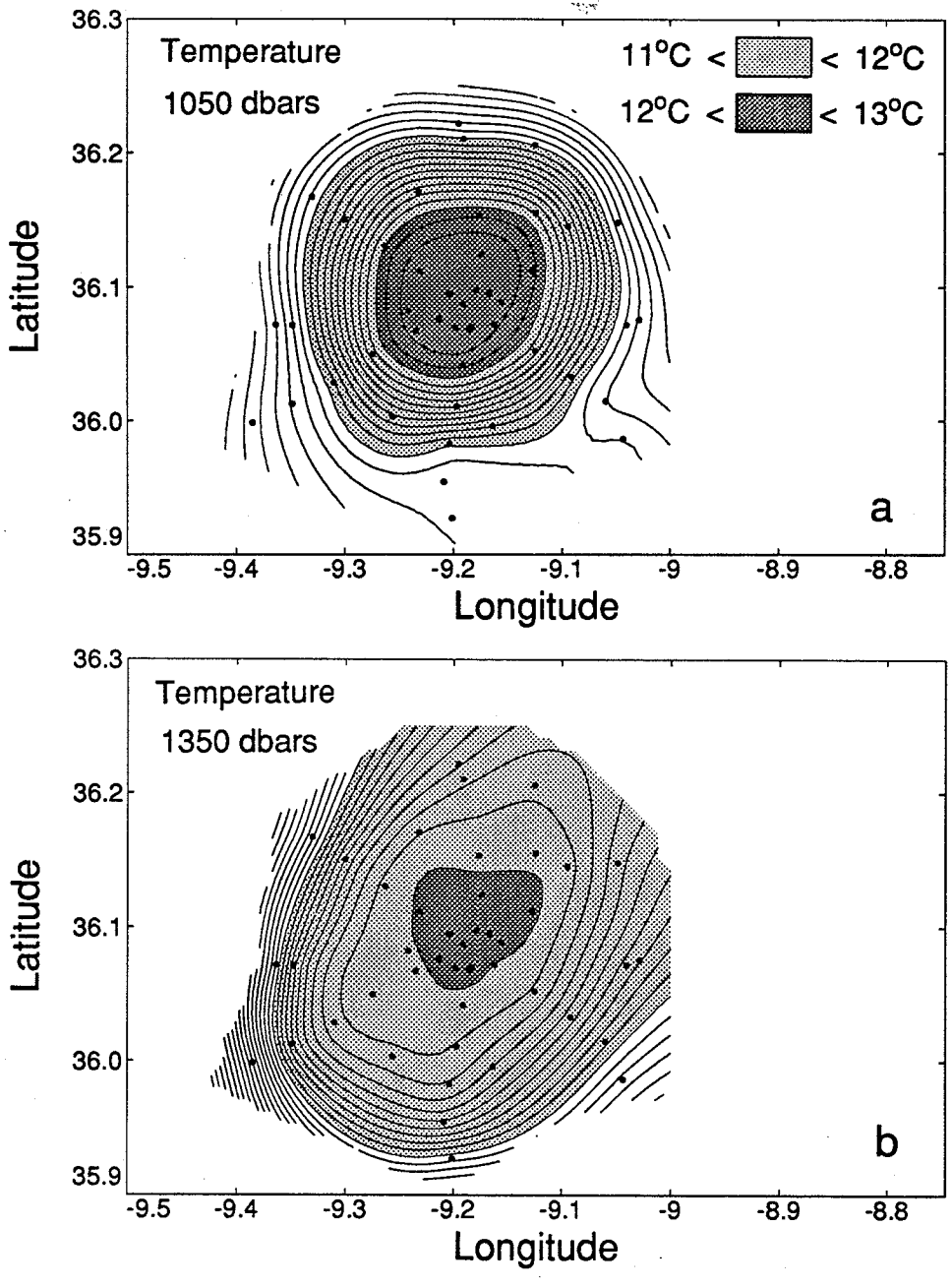

Figure 3.3. Contours of temperature on horizontal layers through the Meddy. The contour interval is 0.1°C. Dots show the data locations. *a*) 1050 dbar level. *b*) 1350 dbar level.

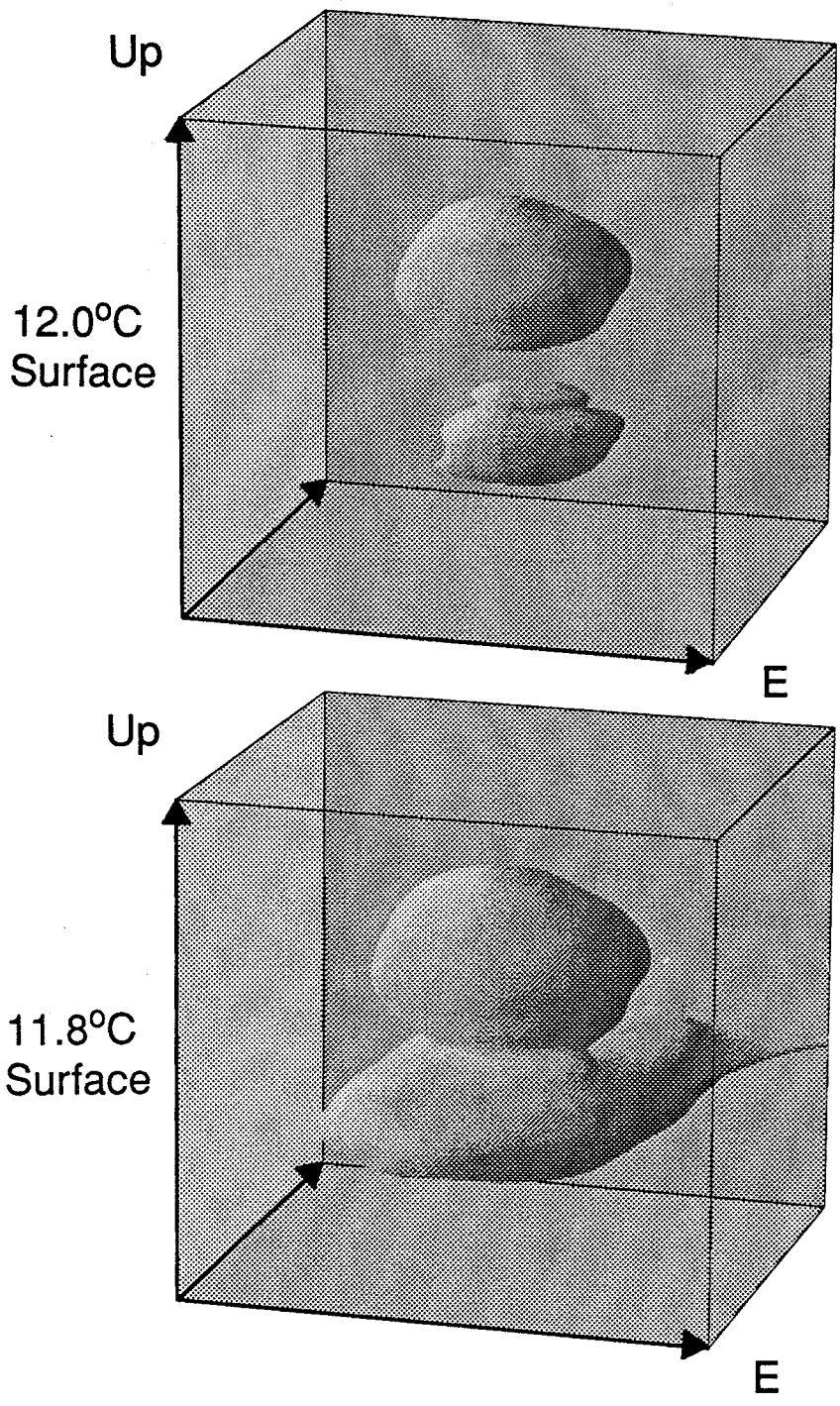

Figure 3.4. Three-dimensional perspective of Meddy temperature structure. The box is approximately 35 km by 35 km by 900 m.

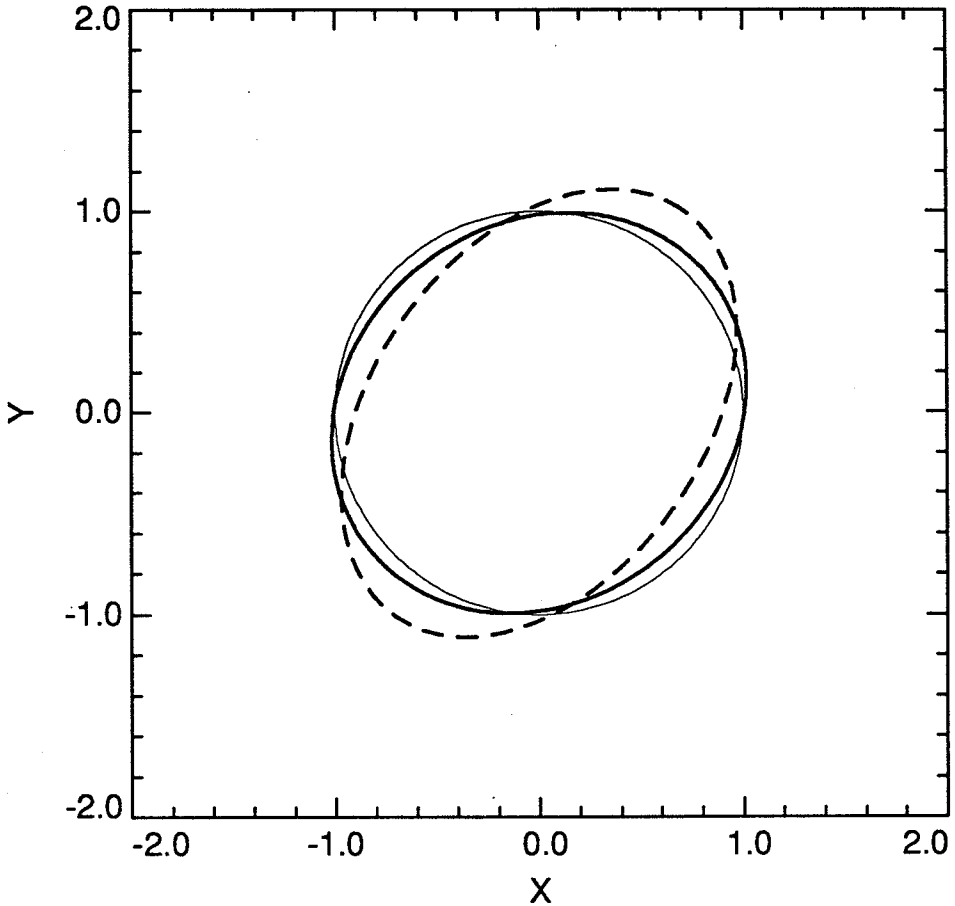

Figure 3.5. Ellipticity of the Meddy. The light line is a circle. The dark solid line has the eccentricity ε (0.5) and the orientation α (40°) of the upper core. The dark dashed line has ε (0.75) and α (55°) of the lower core.

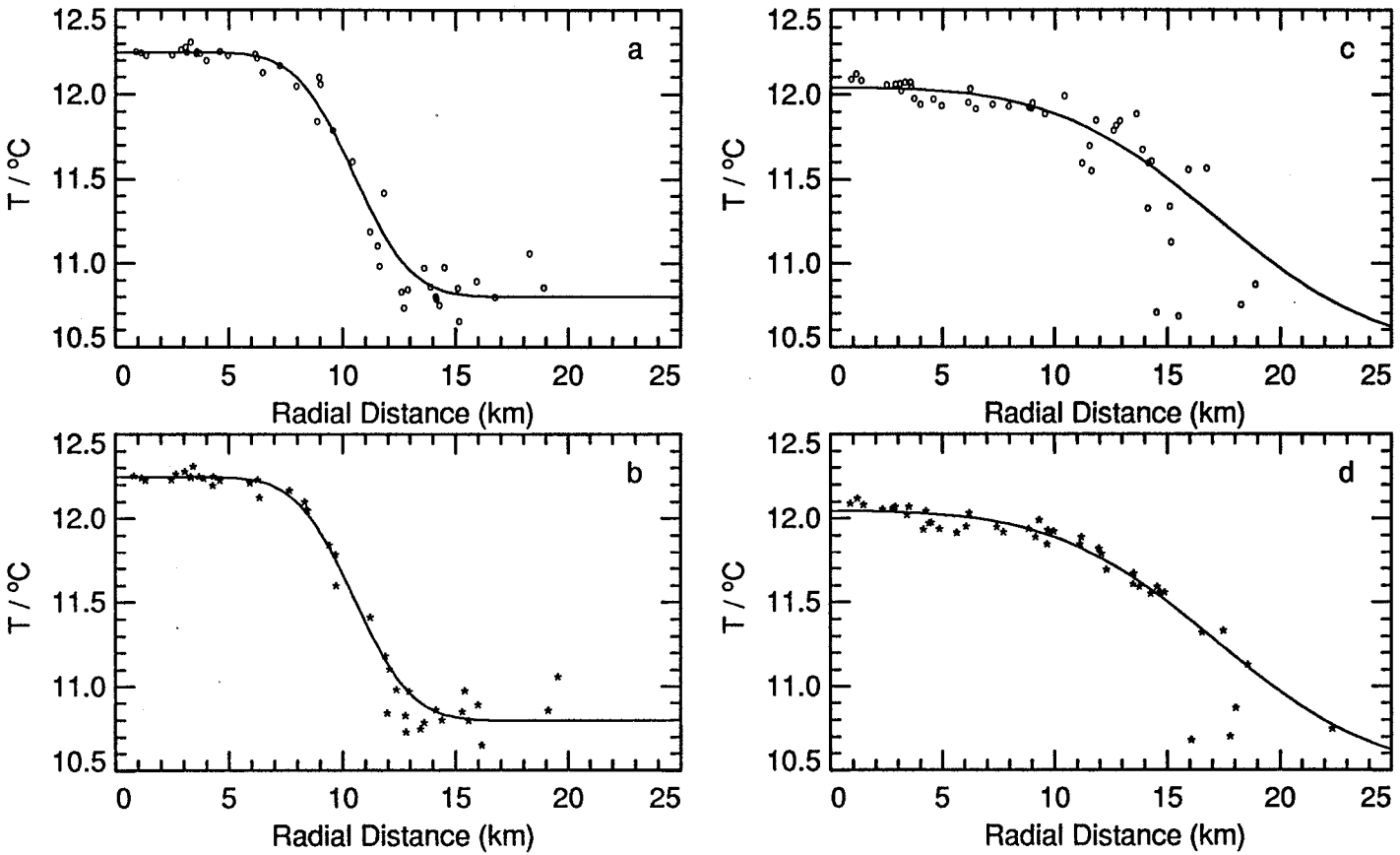

Figure 3.6. Radial distribution of temperature in Meddy. Panels ***a***) and ***b***) are for the upper core, while ***c***) and ***d***) are for the lower core. The open circles in panels ***a***) and ***c***) denote the *in situ* radial distances, while stars in panels ***b***) and ***d***) denote the equivalent elliptic radial distances. The solid lines are from the temperature model described in the text.

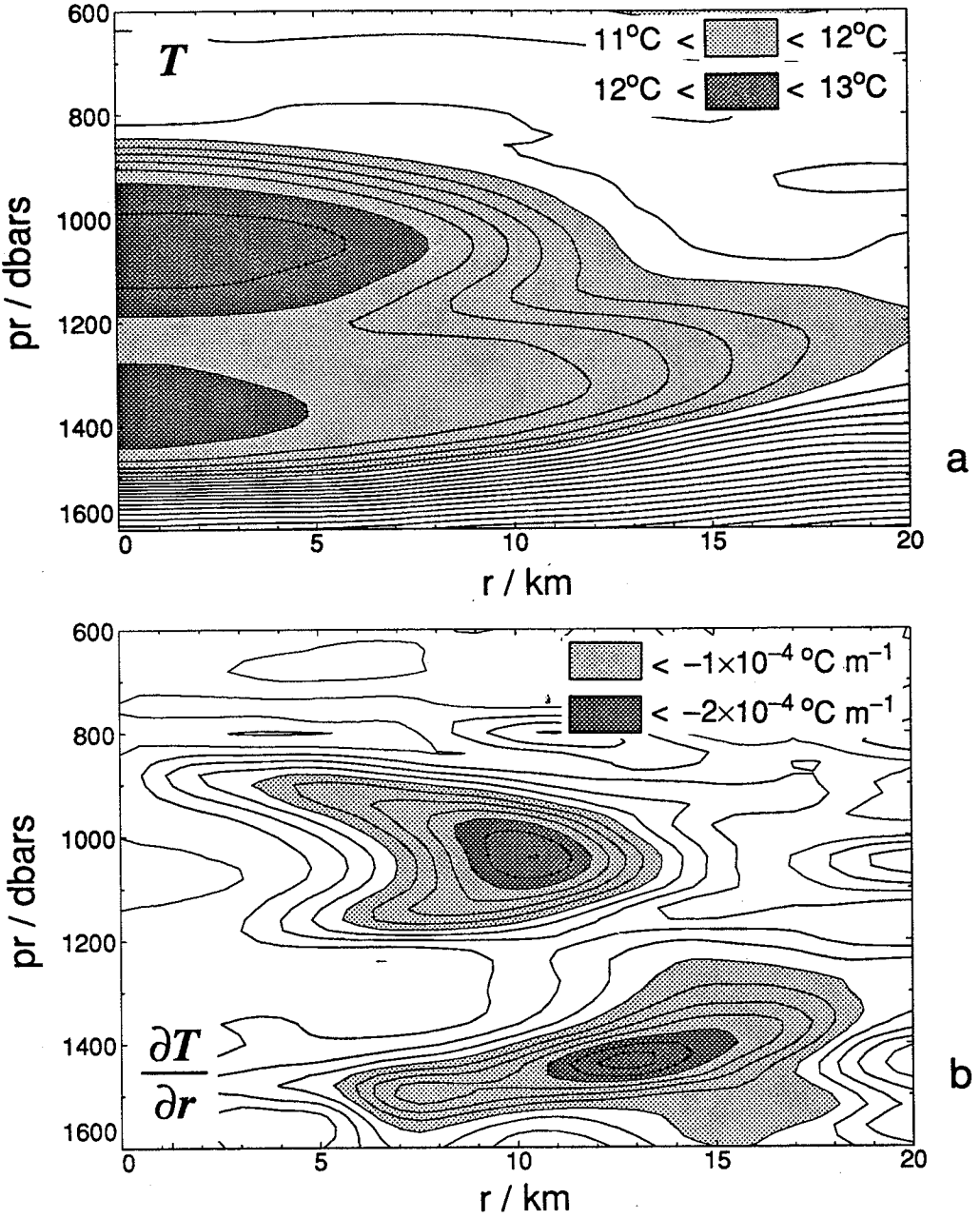

Figure 3.7. *a*) Contours of temperature in the r-z plane. The contour interval is 0.2°C. *b*) Contours of $\partial T/\partial r$ in the r-z plane. The contour interval is 0.25×10^{-4} °C m^{-1}.

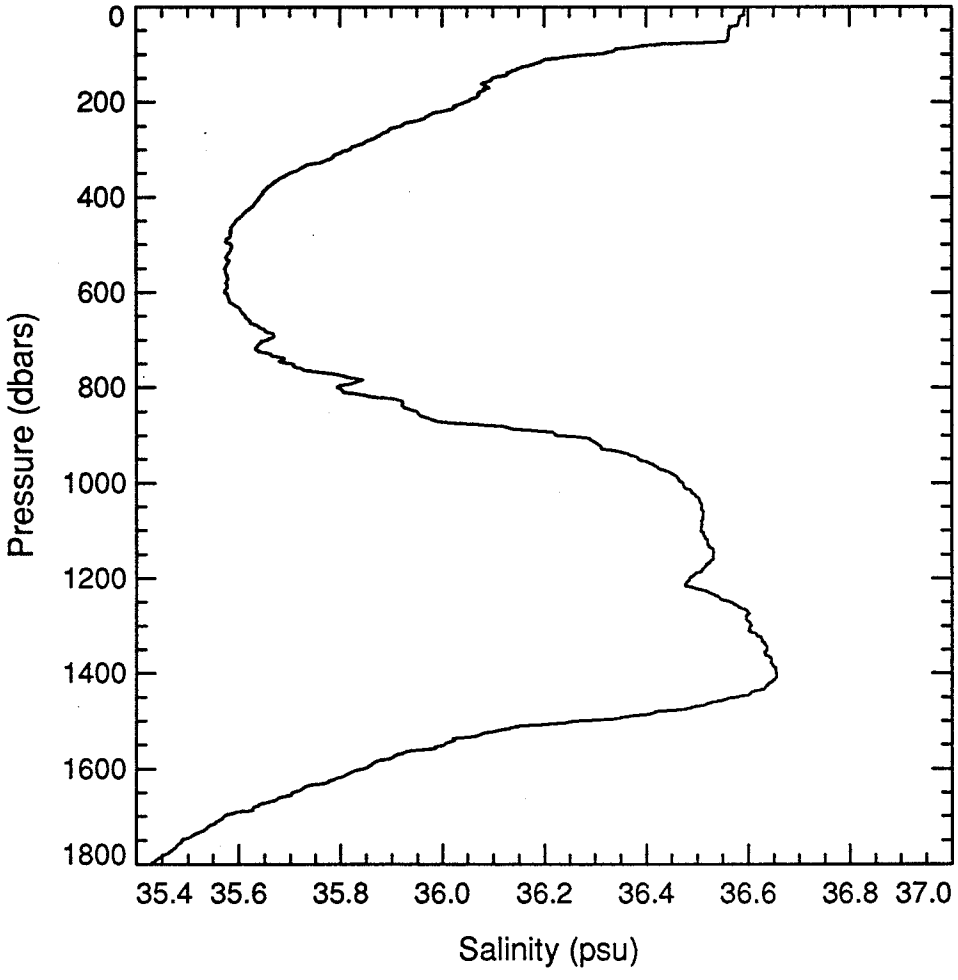

Figure 3.8. Salinity profile from a
CTD cast through the center of the Meddy.

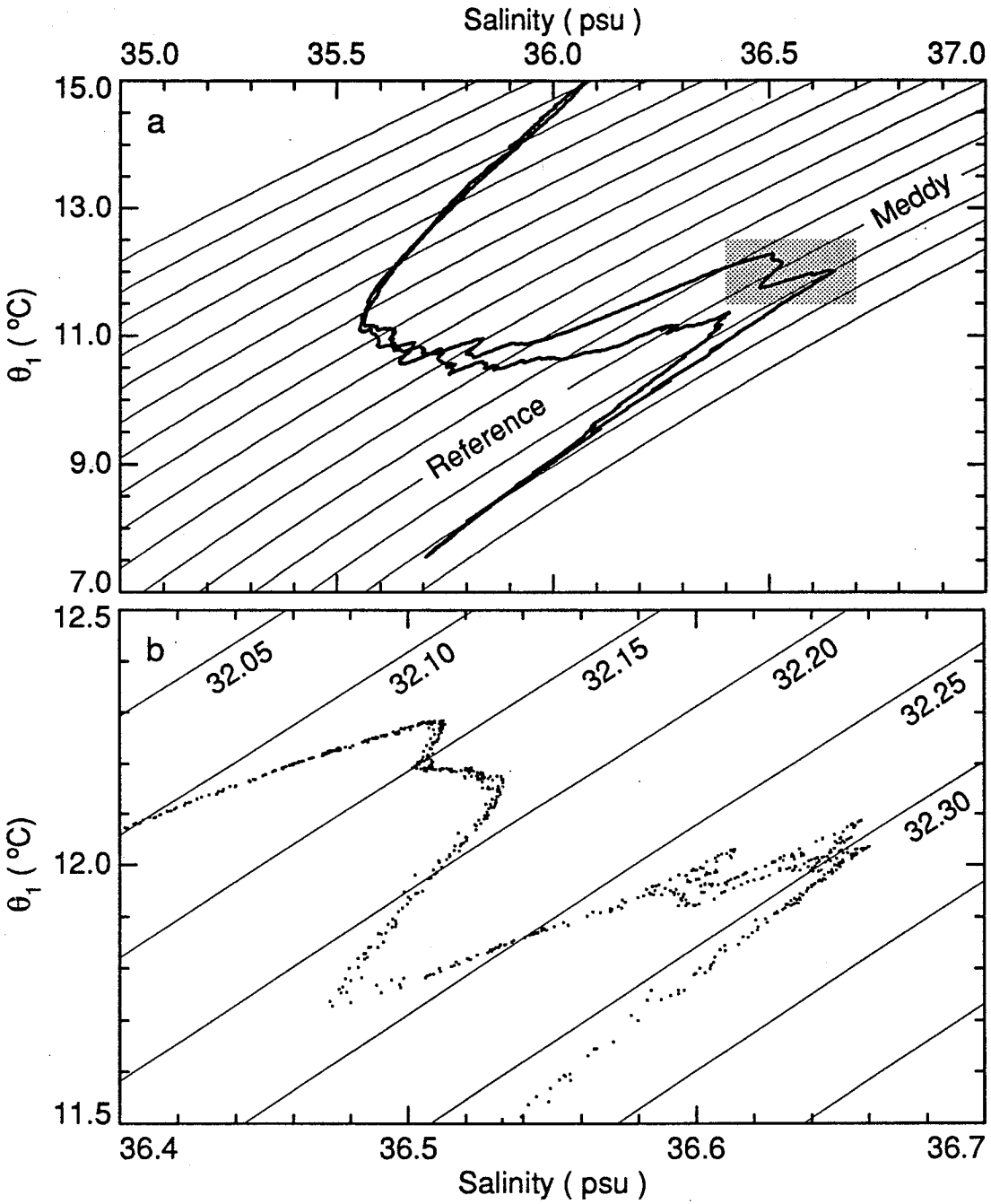

Figure 3.9.*a*) θ_1-S relation in the center of the Meddy and for the average reference station, 17 km away. The light lines are constant σ_1, extending from 31.0 to 32.5, incremented by 0.1. *b*) Enlargement of the high salinity region. Each dot is 2-dbar data from each of the three center CTD casts.

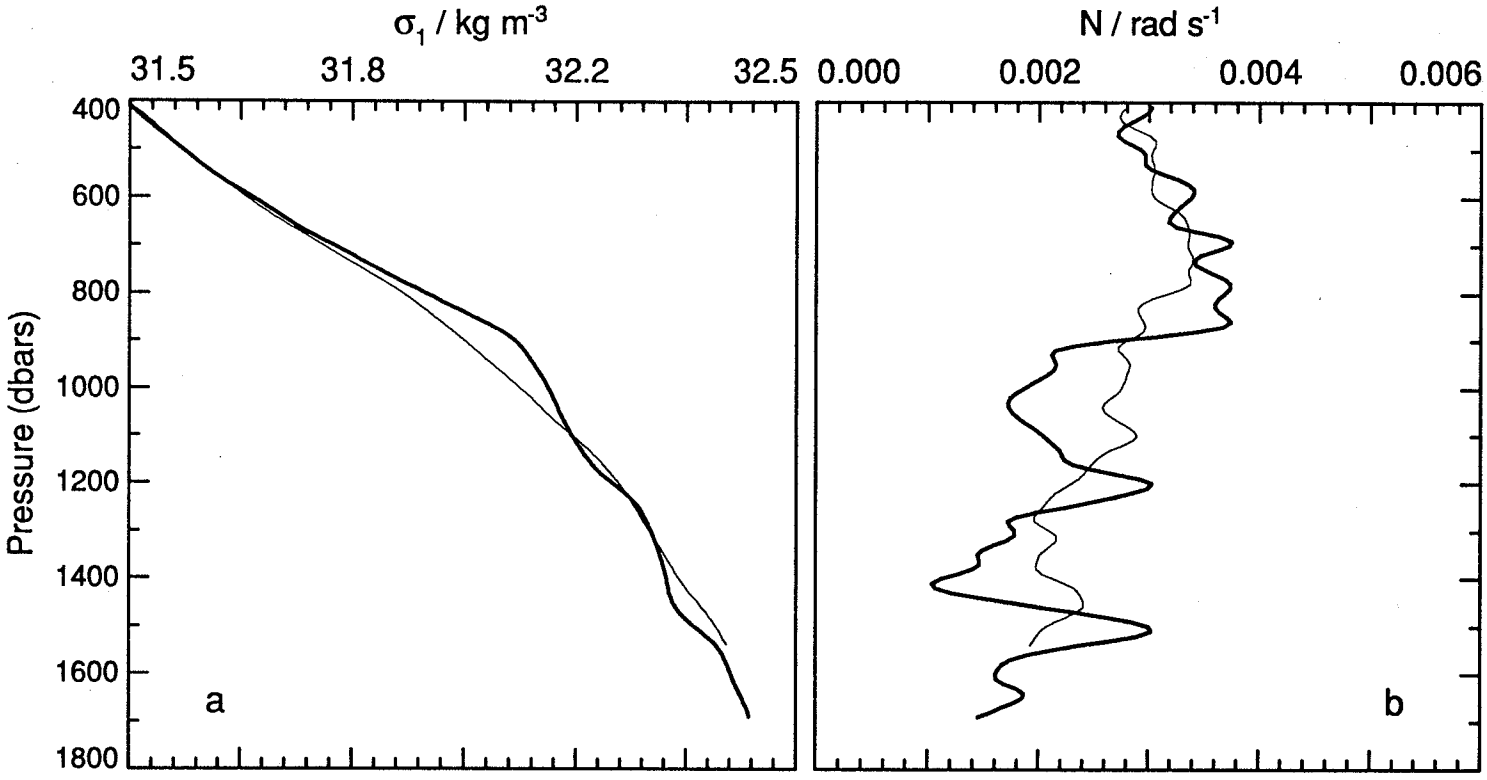

Figure 3.10. ***a***) Potential density σ_1 for the Meddy center (dark line) and the far-field (light line). ***b***) Buoyancy frequency N for the Meddy center (dark line) and the far-field (light line).

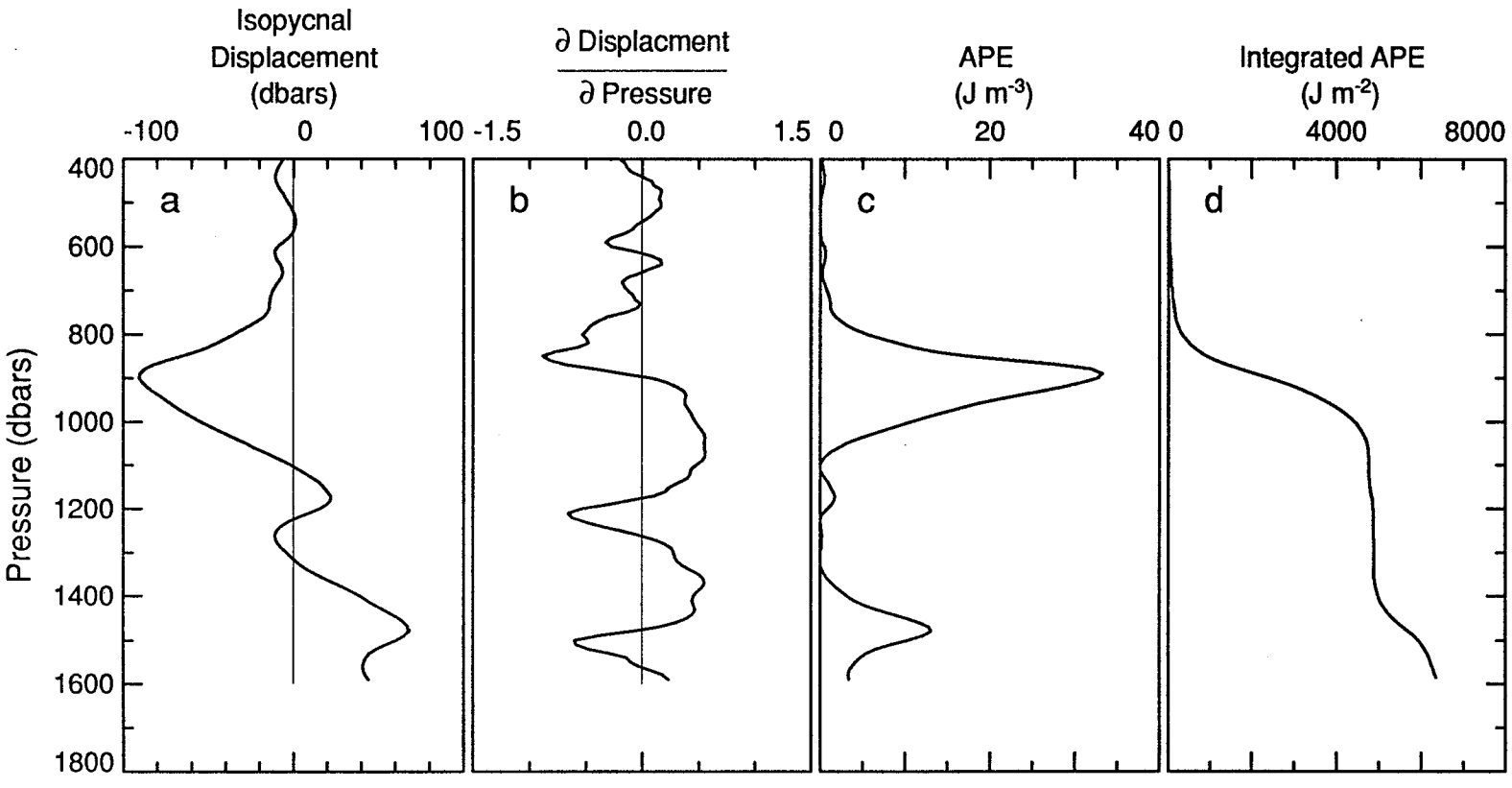

Figure 3.11. All the panels display results from an average of CTD data in the center of the Meddy referenced to the far-field. ***a***) Isopycnal displacement. ***b***) Rate of isopycnal displacement. ***c***) Vertical distribution of available potential energy density. ***d***) Vertical integration of available potential energy density.

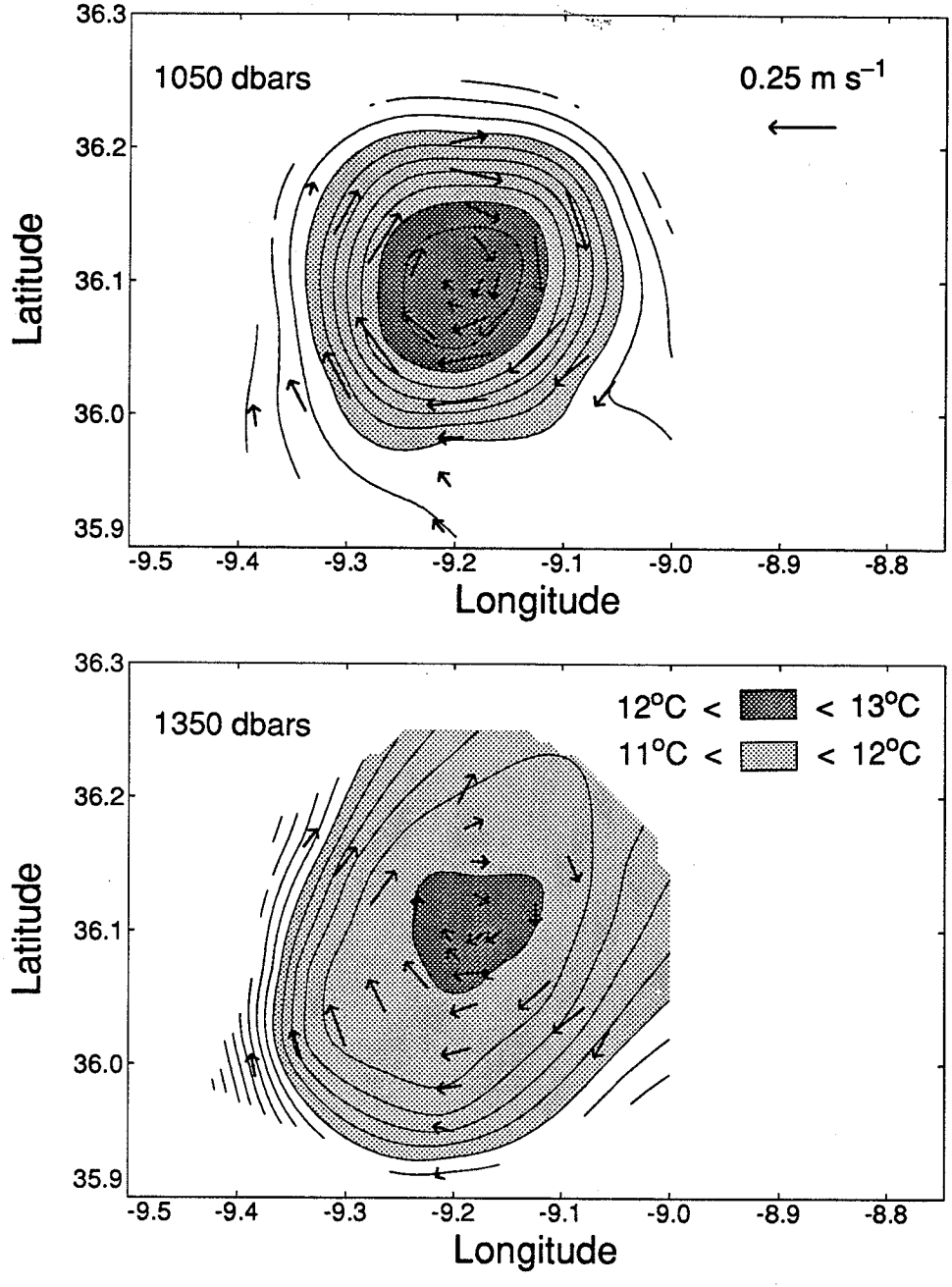

Figure 3.12. Referenced XCP velocity vectors overlaid on temperature contours on horizontal surfaces through the Meddy.

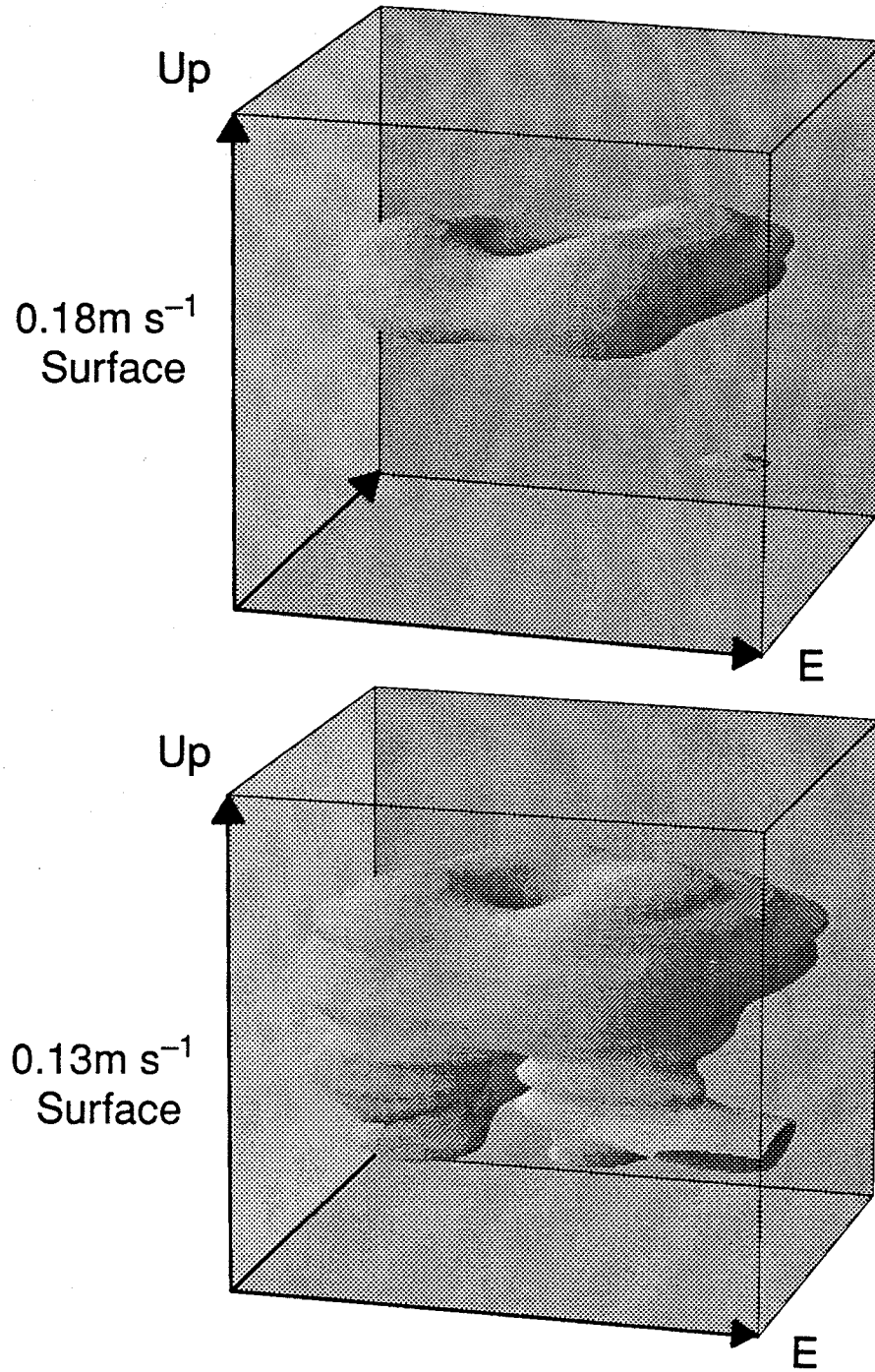

Figure 3.13. Three-dimensional perspective of Meddy velocity structure, showing surfaces of constant velocity magnitude. The box is approximately 35 km by 35 km by 900 m.

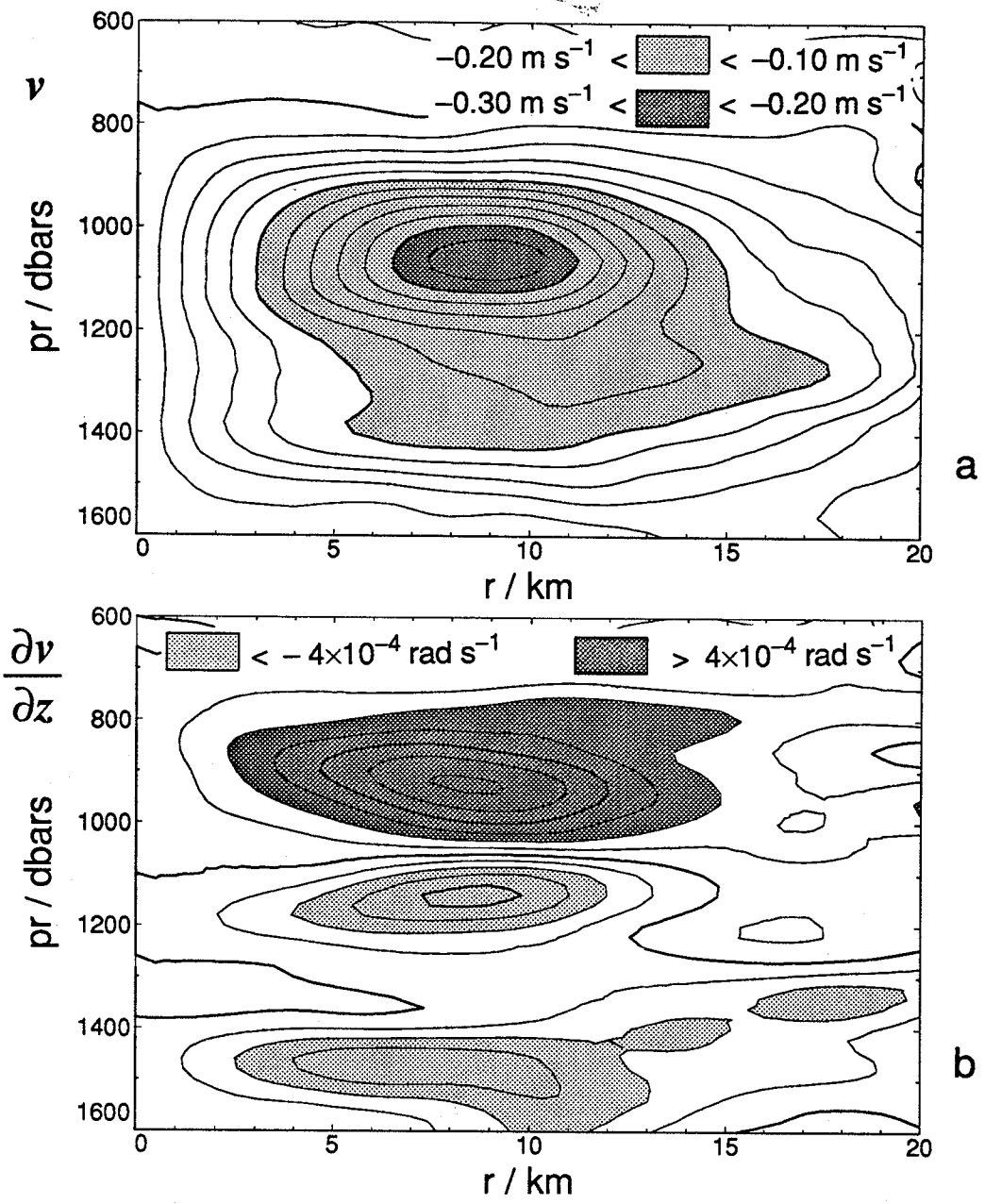

Figure 3.14. *a*) Contours of azimuthal velocity v in the r-z plane. The contour interval is 0.02 m s^{-1}. *b*) Contours of $\partial v/\partial z$ in the r-z plane. The contour interval is 2×10^{-4} rad s^{-1}.

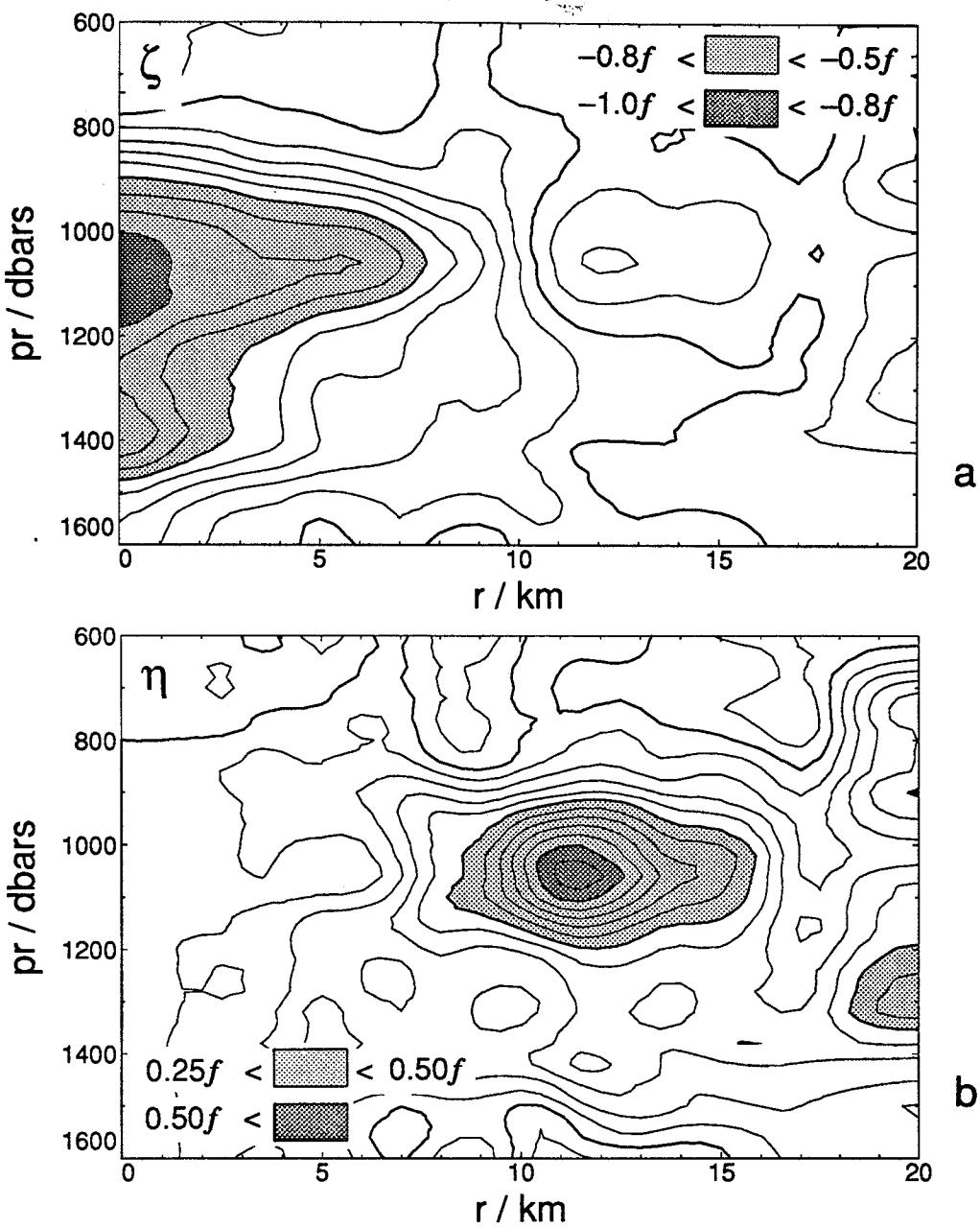

Figure 3.15.*a*) Contours of relative vertical vorticity ζ in the r-z plane. The contour interval is $0.1f$. *b*) Contours of rate-of-strain η in the r-z plane. The contour interval is $0.05f$.

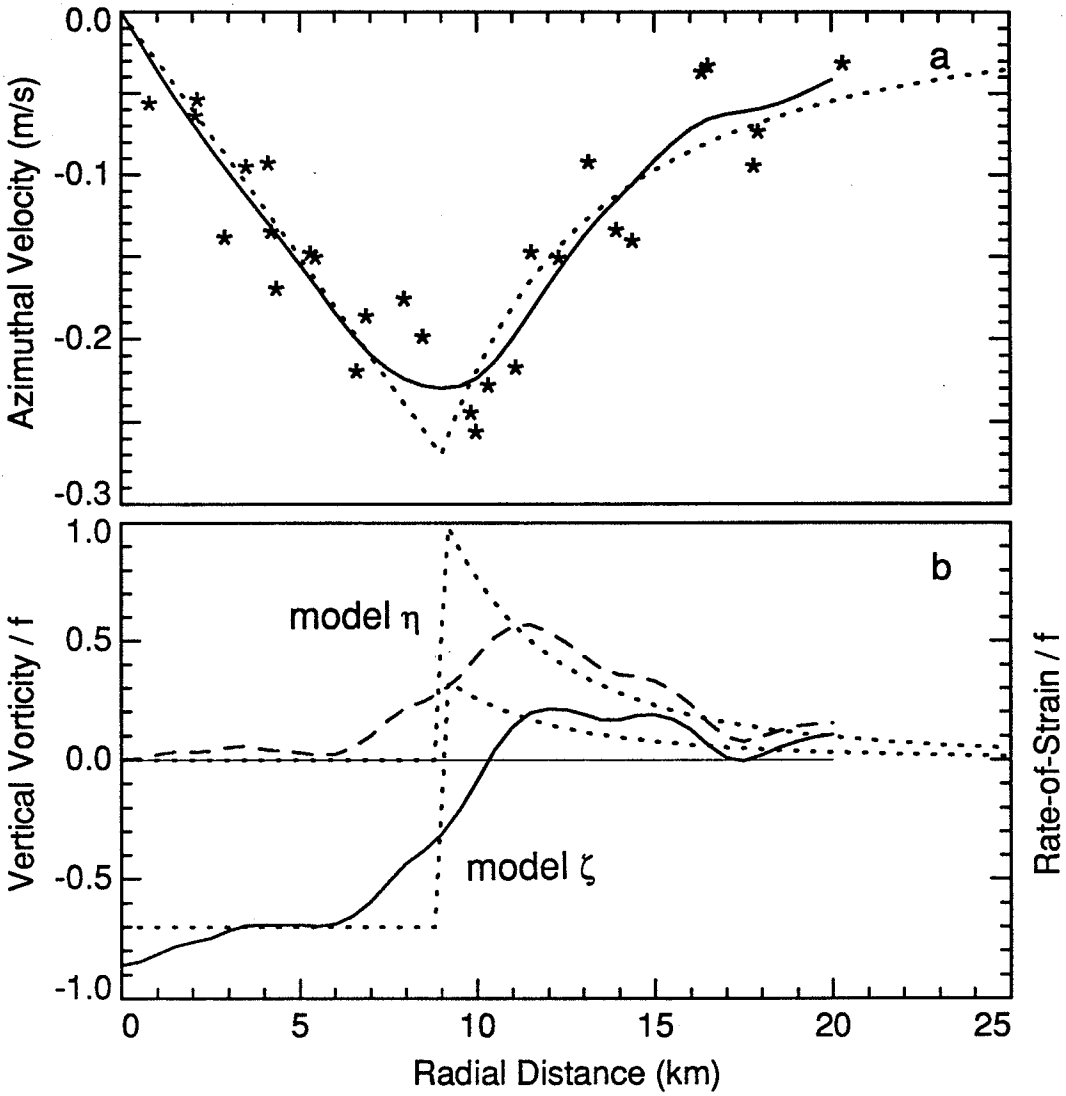

Figure 3.16. *a*) Radial distribution of azimuthal velocity in Meddy. Stars are 100-m average of elliptically referenced XCP velocities centered at 1050 dbars. The dotted line is from a model Meddy, having solid-body rotation to R_{max} and an r^{-2} decay beyond R_{max}. The solid line is the azimuthal velocity at 1050 dbars from Figure 3.14. *b*) Radial distribution of vertical vorticity ζ (solid line) and rate-of-strain η (dashed line), both normaled by f, and taken from Figure 3.15 at 1050 dbars. Model values of ζ and η are given by the dotted line.

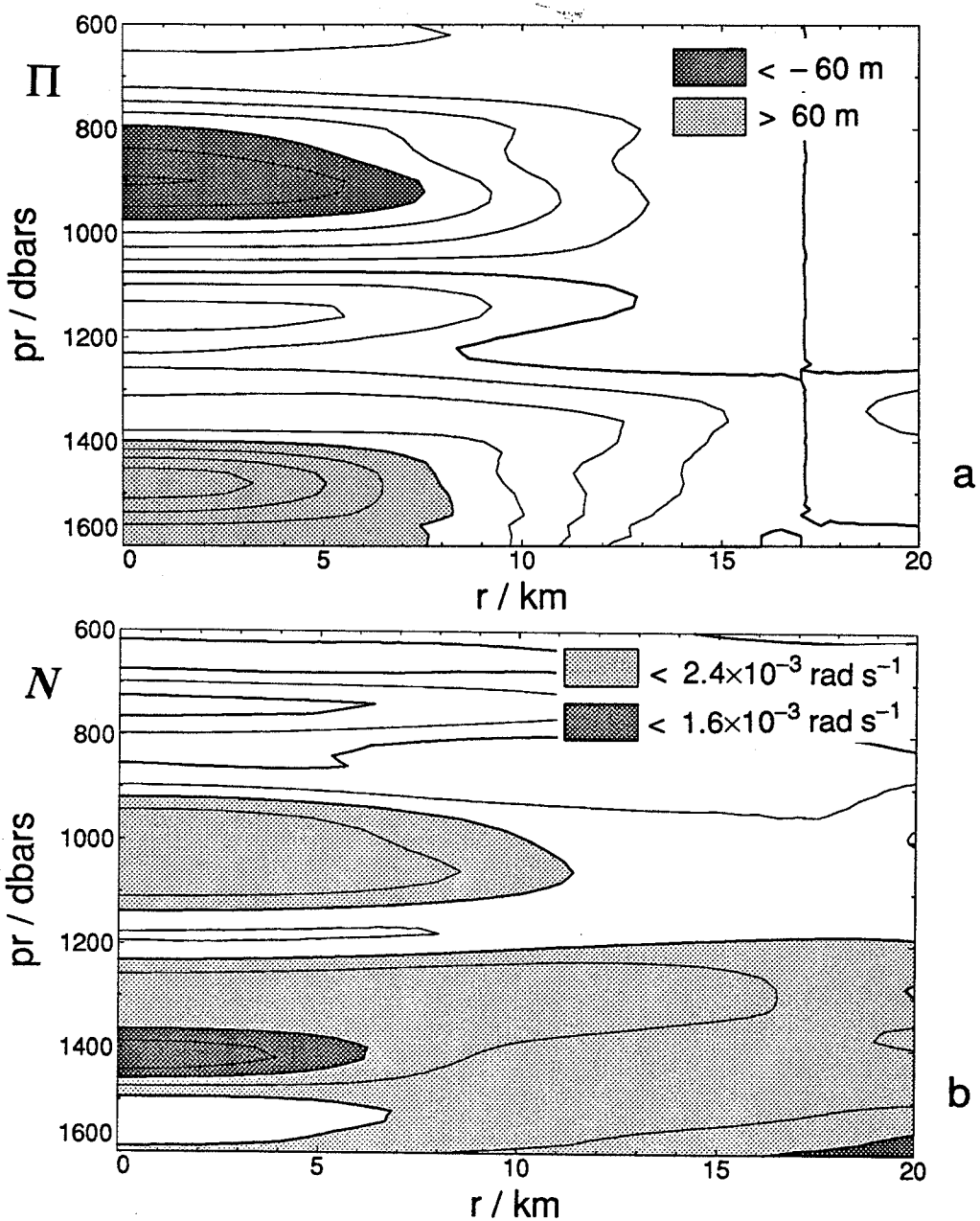

Figure 3.17. *a*) Contours of isopycnal displacement from a reference at 17 km radius. The contour interval is 15 m. *b*) Contours of buoyancy frequency N in the r-z plane. The contour interval is 4×10^{-4} rad s^{-1}.

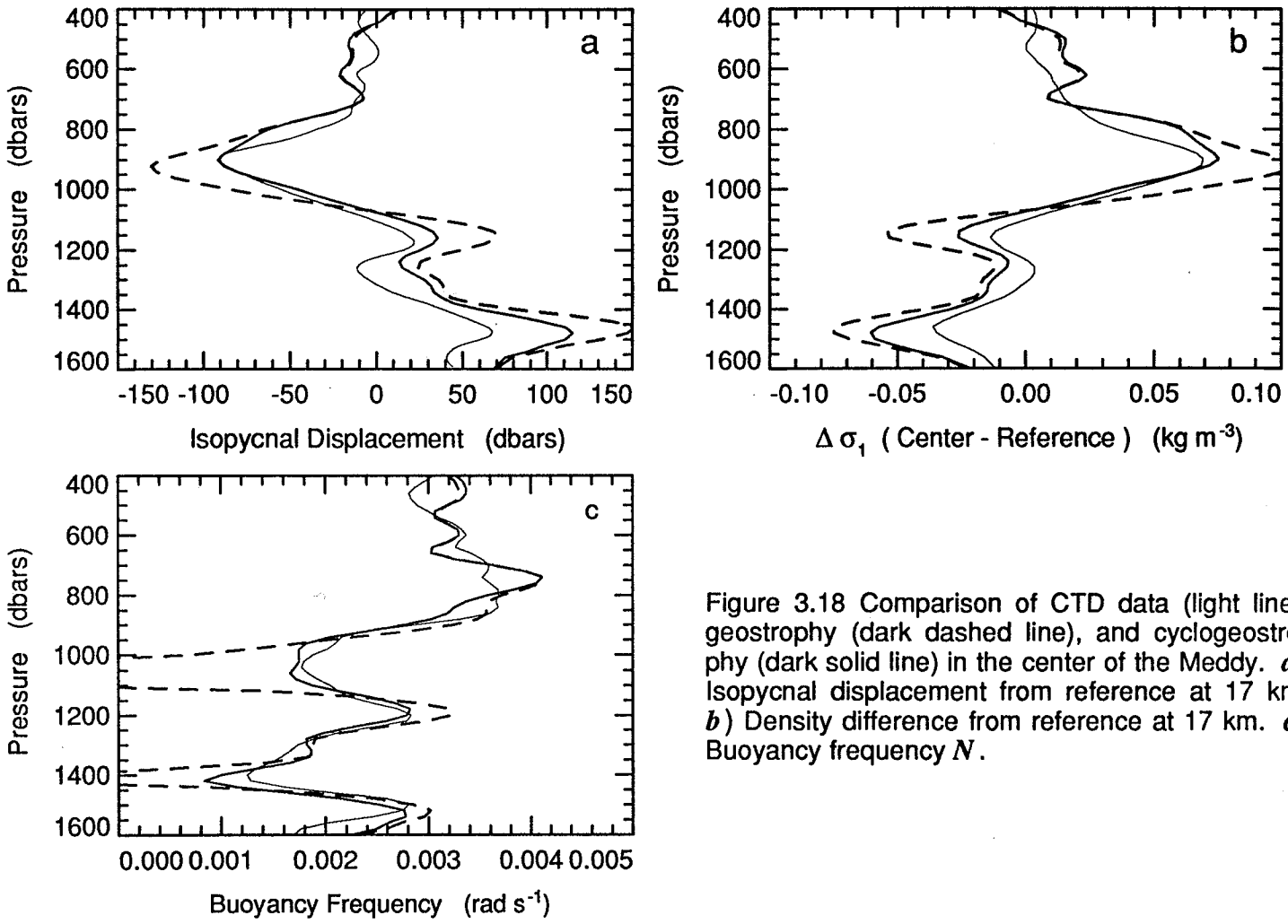

Figure 3.18 Comparison of CTD data (light line), geostrophy (dark dashed line), and cyclogeostrophy (dark solid line) in the center of the Meddy. ***a***) Isopycnal displacement from reference at 17 km. ***b***) Density difference from reference at 17 km. ***c***) Buoyancy frequency N.

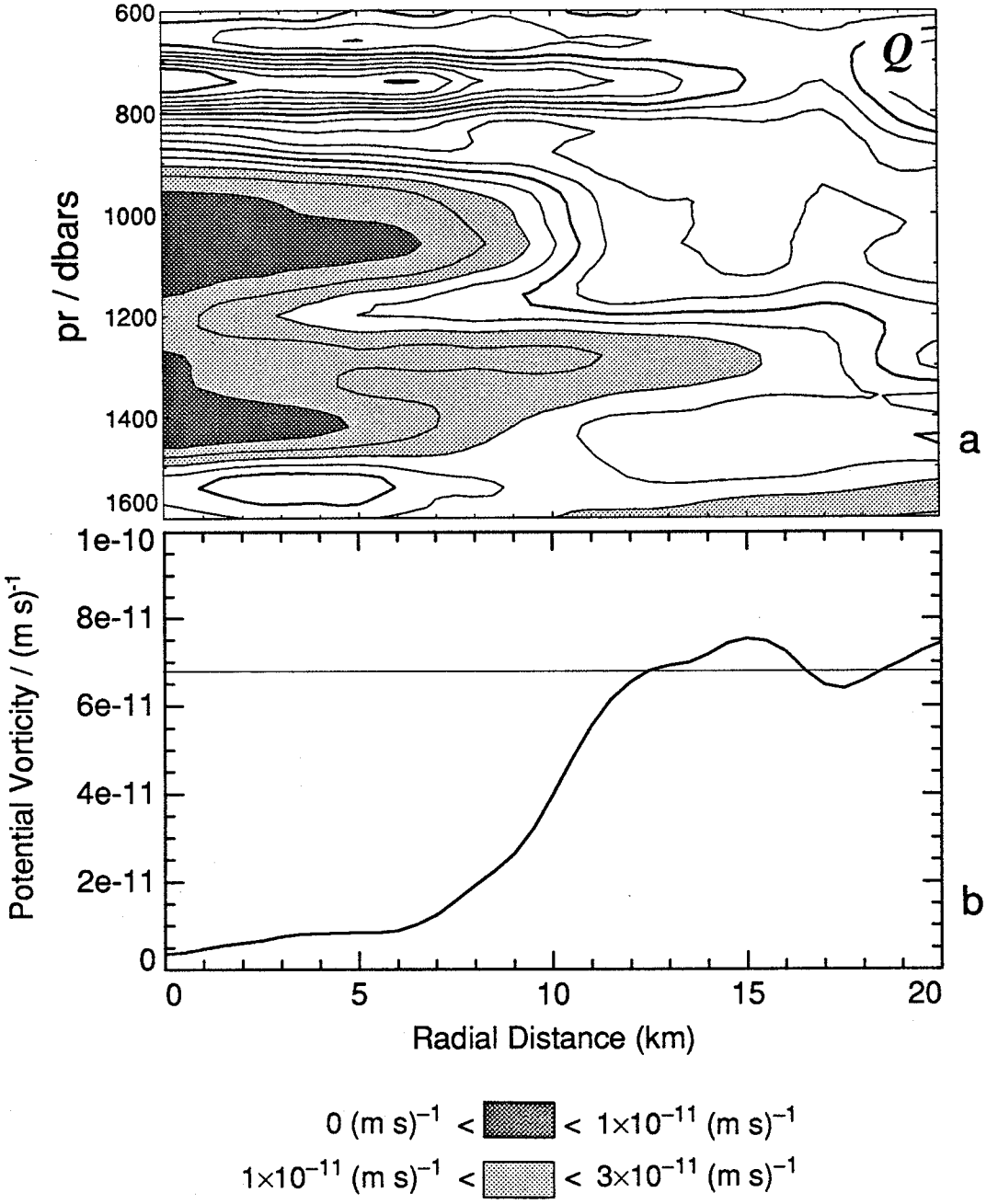

Figure 3.19. ***a***) Contours of potential vorticity Q in the r-z plane. The contour interval is 1×10^{-11} (m s)$^{-1}$. ***b***) Potential vorticity at 1050 dbars extracted from ***a***). The light line is the background level of 6.8×10^{-11} (m s)$^{-1}$.

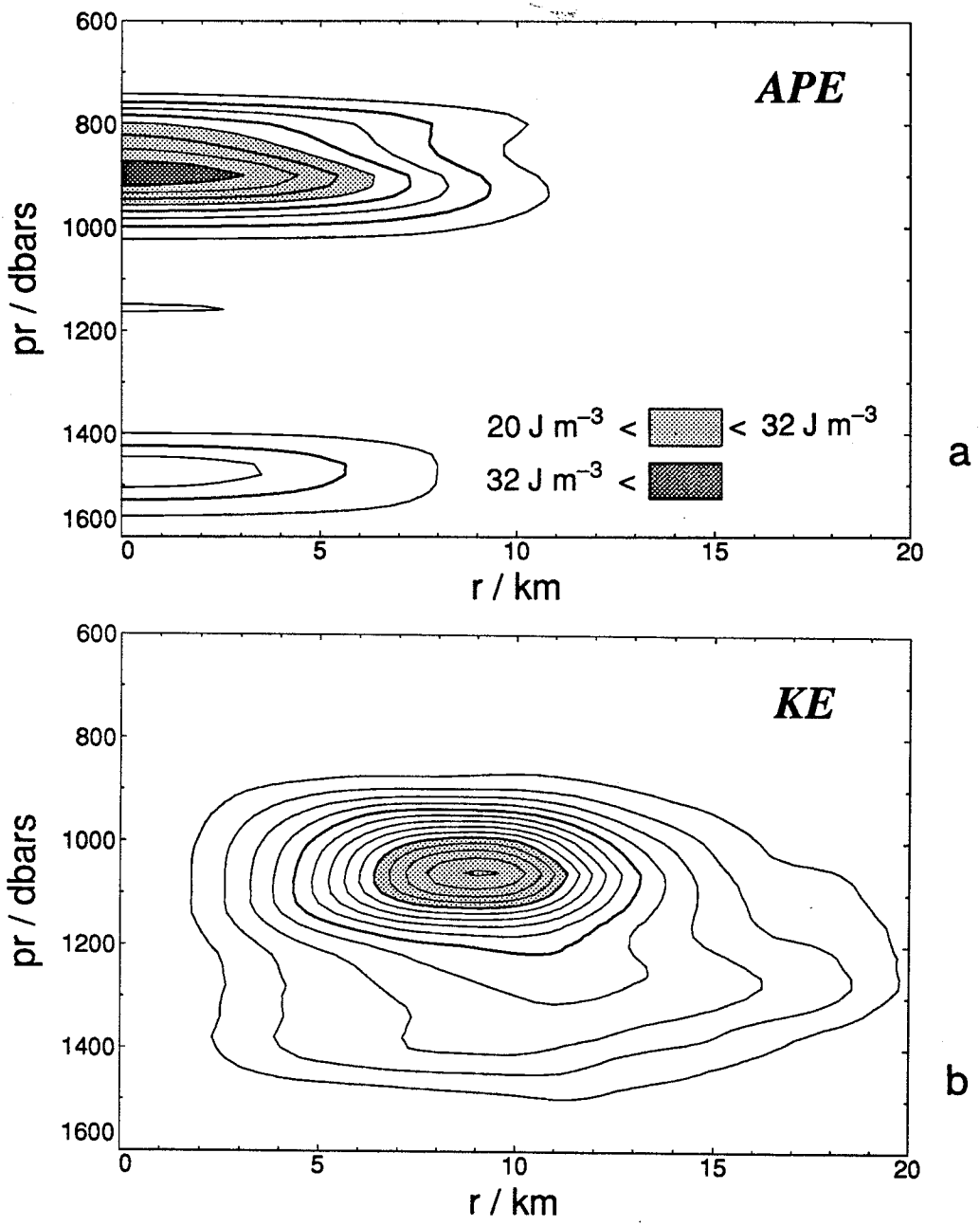

Figure 3.20. Contours of potential energy density (panel *a*) and kinetic energy density (panel *b*) in the *r*-*z* plane. The contour interval in *a*) is 4 J m^{-3}, while in *b*) the interval is 2 J m^{-3}.

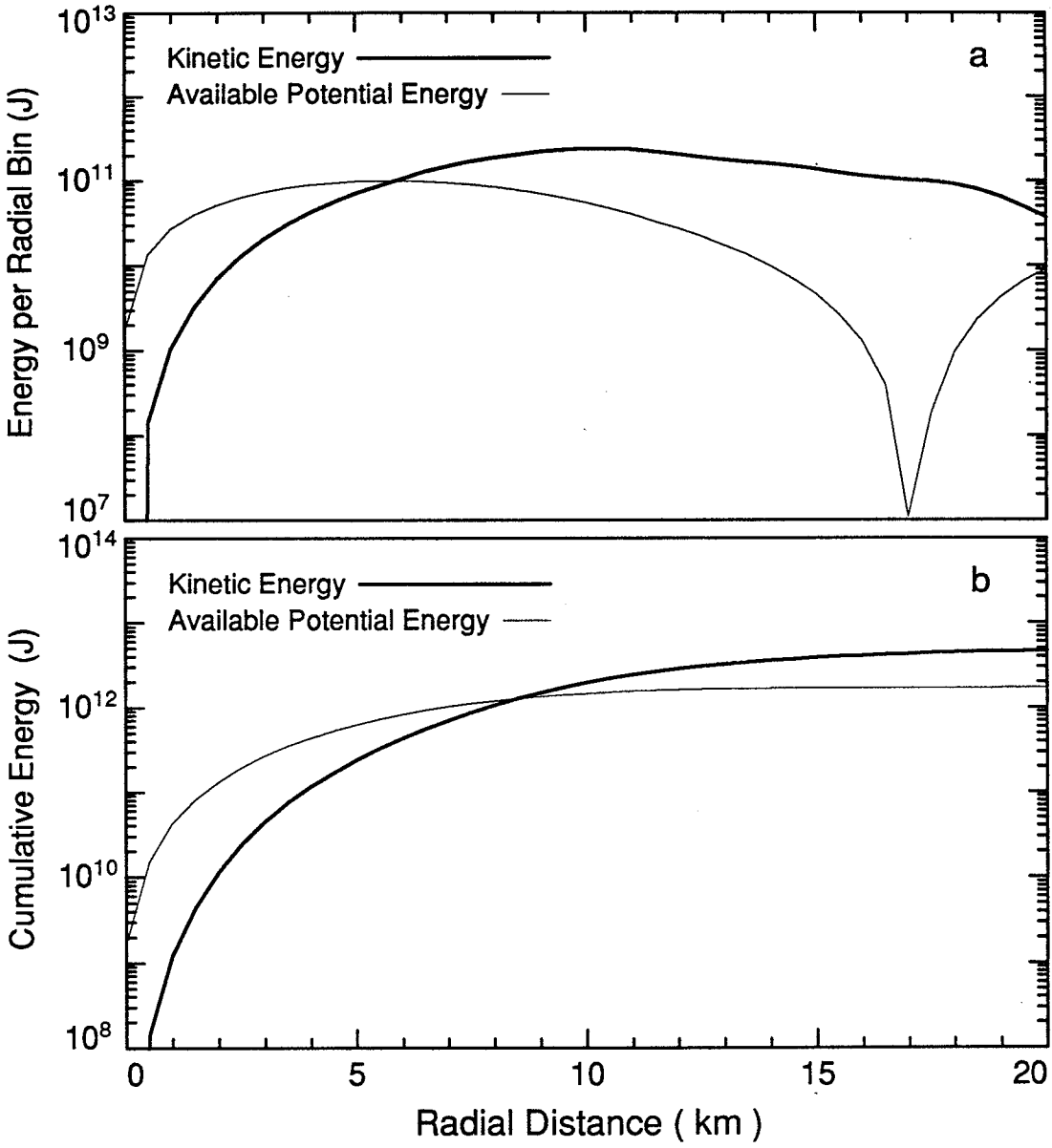

Figure 3.21. Radial distributions of energy in the Meddy. ***a***) Energy contained in radial bins of 0.5 km width. Measuring the isopycnal displacements referenced to those at 17 km creates the "notch" in ***APE*** at 17 km. ***b***) Cumulative energy.

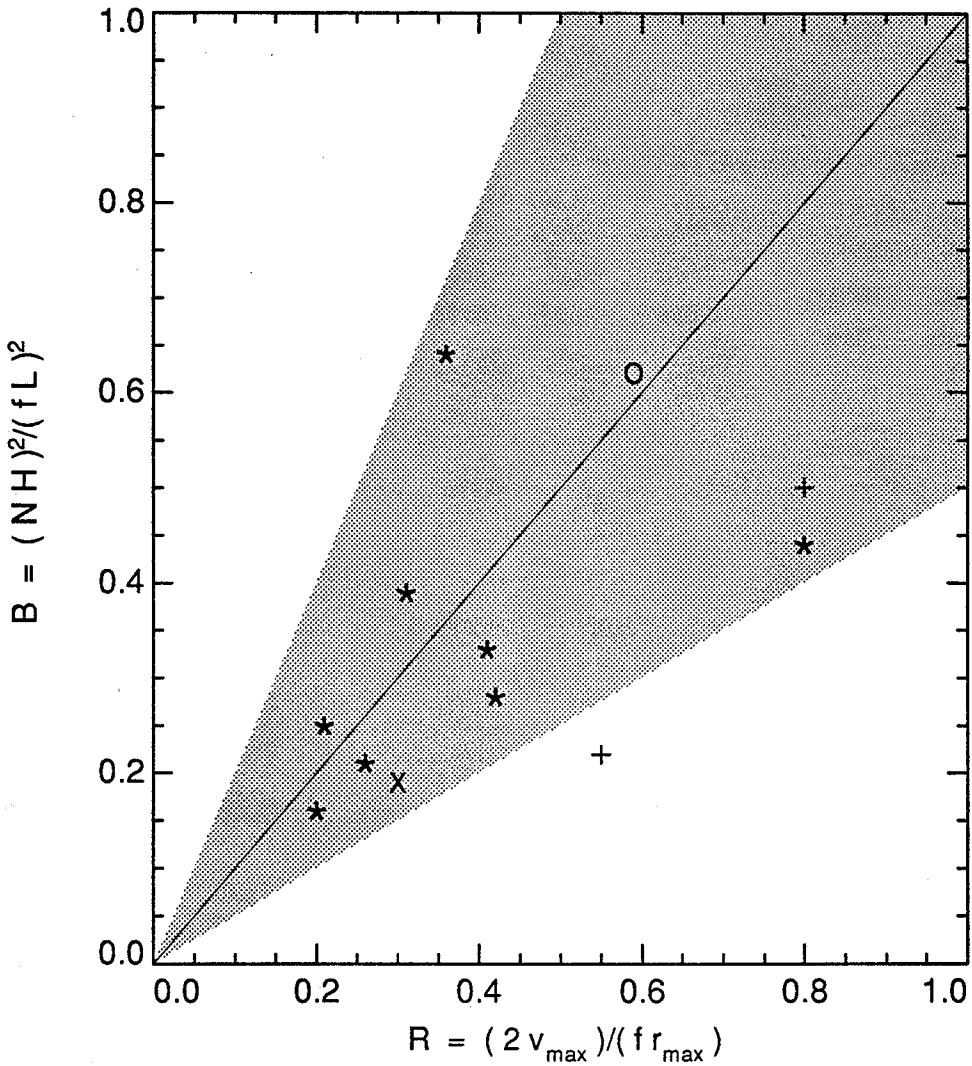

Figure 3.22. Scatter-plot of Burger number B and Rossby number R for the Cadiz Meddy (o), the Meddy "Sharon" (x), Meddies from Table 1.1 (*), and two other eddies (D'Asaro, 1988a; Elliott & Sanford, 1986b) (+). The straight line from the origin and the shaded region show the spread of values.

Chapter 4. Origin and Generation of the Cadiz Meddy

4.0 Introduction

The unique aspect of the Gulf of Cadiz Meddy was that it was recently formed and presumably still in the vicinity of its formation site. This raises the issue of where and how Meddies form. It is likely that there are several generation sites and mechanisms, creating Meddies with a variety of characteristics. In this chapter, I will focus on the origin and generation of the Cadiz Meddy.

4.1 The Mediterranean Outflow in the Gulf of Cadiz

As a precursor to discussion of the origin and generation mechanisms, a brief summary of the Mediterranean outflow in the Gulf of Cadiz is presented.

The Mediterranean outflow arises from dense water forming by evaporation and cooling in the Mediterranean Sea. The evaporation and the spilling of dense water over the sills at the Strait of Gibraltar into the Gulf of Cadiz are balanced by inflow of surface waters from the Atlantic. The inflow and outflow from the Mediterranean are governed in the simplest form by mass and salt conservation (Bryden & Stommel, 1984), such that

$$q_A + q_M = E \tag{4.1}$$

$$S_A\, q_A + S_M\, q_M = 0$$

where q here denotes mass flow, S salinity, E net evaporation over the Mediterranean, and the subscripts A and M the Atlantic and Mediterranean waters, respectively. With the observed E at 57,000 $m^3\, s^{-1}$ in the western basin of the Mediterranean and the salinity difference $S_M - S_A$ of 1.7 psu, an outflow of 1.2 Sv is produced (1 Sverdrup = $10^6\, m^3\, s^{-1}$). Fluctuations, of both tidal (Lacome & Richez, 1982) and large-scale meteorological (Candela et al., 1989) origin, can change the outflow strength by more than 50%. The outflow is characterized by warm ($\approx$ 13.0 °C) and saline ($\approx$ 38.4 psu) waters.

As the outflow leaves the Strait, it is denser than the ambient Gulf of Cadiz water and thus hugs the bottom and flows down slope. Due to the constraints of geostrophy, it also turns northward following the topography of the continental shelf. Within the first 50 km, the outflow entrains Gulf of Cadiz waters and its temperature and salinity decrease. The outflow is split by initial source conditions, topographic steering, and by differential entrainment into two different water types, the "upper" and "lower" cores of the Mediterranean outflow. A series of papers by Madelain (1970), Zenk (1970, 1975a,b, 1980), Zenk & Armi (1990), Ambar et al. (1976), Ambar & Howe (1979a,b), Ambar (1983), Howe et al. (1974), Howe (1982, 1984), and Gründlingh (1981) describes in greater detail the path and structure of the outflow to the region south of Portugal.

The outflow of the Mediterranean is not steady, but is marked by episodic pulses of increased transport and meanders (Thorpe, 1976; Gründlingh, 1981; and Stanton, 1983). Far from the Strait, the variability is caused mainly by tidal fluctuations within the Gulf of Cadiz and large-scale meteorological pressure events modifying the outflow regimes at the Strait.

4.2 Formation Site of Meddy

A prominent feature of the Cadiz Meddy is its two vertically distinct cores, each with its own specific water property. The upper core is identified by 12.2 °C and 36.5 psu water, while the lower core is slightly cooler and more saline, at 12.0 °C and 36.65 psu. I hypothesize that the two cores of the Meddy were entrained simultaneously during the formation of the Cadiz Meddy and that little subsequent mixing or entraining of ambient water into the cores occurred. Possible formation sites can thus be found by tracking the above water properties on isopycnals on which the upper and lower Meddy cores are centered (32.14 σ_1 and 32.30 σ_1, respectively) to the locations where those properties are vertically aligned. The two "cores" of the Meddy have densities consistent with only the "lower" core of the Mediterranean outflow. The upper core of the outflow tends to have densities near 31.9 σ_1, while the lower core is near 32.25 σ_1. The term "core" will be used primarily for either of the two distinct lenses that comprise the Meddy. If a core of the Mediterranean outflow is referred to, it will be done so explicitly.

There are two possible violations of the above assumption which must be addressed. First, entrainment could have occurred during formation, and second, the two cores could have formed separately and then coalesced later, but prior to our observation.

As to the first possible violation, we assume that there is minimal entrainment of ambient Gulf of Cadiz water into the core of the Meddy during formation, hence the core waters have the same properties as the source waters at the time of formation. This is consistent with warm-core rings in the Gulf Stream system (Smith & Baker, 1985) and laboratory experiments of boundary current instability (Griffiths & Linden, 1981). On the other hand, the numerical and experimental work of Stern & Whitehead (1990) suggests that entrainment of ambient waters does occur. They observe the anticyclonic vorticity water in the interior of the boundary current entraining the cyclonic vorticity water on the outer edge of the current (Figure 4.1). However, in buoyancy driven boundary currents like the Mediterranean outflow, the cyclonic and anticyclonic vorticity waters have similar T and S properties (e.g., Howe, 1984); thus, although differing vorticities might be entrained, differing water properties are not.

As to the second possible violation, vertical alignment of initially horizontally separated eddies has been observed in the ocean (Cresswell, 1982) and in numerical models (McWilliams, 1989; Polvani, 1991). However, Polvani (1991) found, using a two-layer quasi-geostrophic "contour surgery" model, that only vortices whose radii are comparable to or larger than the Rossby deformation radius (R_d) can align. Additionally, the centers of the vortices must be initially closer than 3.3 R_d, or else the two vortices merely rotate about one another. The value of R_d for the Meddy can be estimated as

$$R_d = \frac{N H}{2 f} \tag{4.2}$$

Assuming a layer depth H of 650 m and a background stratification of 2.4 $\times 10^{-3}$ rad s^{-1}, one obtains a value of 9 km, which is the same as the radius of maximum velocity R_{max}. The Cadiz Meddy therefore exists at a limit of possible alignment. The second criterion states that the vortices must have originated within 30 km of each other before alignment could occur. Thus the Meddy could have obtained its two cores by alignment, but the source waters of the upper and lower Meddy cores, as a conservative estimate, must have originated within 30 km of one another. For this discussion, we

will assume that the two cores formed simultaneously.

The data from CTD casts during our experiment throughout the Gulf of Cadiz were searched for the temperature of the upper and lower Meddy core isopycnals. The results are plotted in Figure 4.2. The figure shows the 12 to 12.5 °C waters for the upper core isopycnal (light shade) and the 11.9 to 12.4 °C waters for the lower core isopycnal (dark shade). The two regions meet at the mouth of a canyon south of Portugal, and this location is thus selected as the most likely formation region.

The canyon region also agrees with crudely back-extrapolating the Meddy position using the translation speed found in Section 3.1. If the Meddy had maintained the same course and speed, its position would have also been in that canyon region (Figure 4.2), 30 days prior to our survey. These two separate determinations of the formation region support the selection of a Meddy formation site at the mouth of a canyon region south of Portugal. This location is interesting not only because of the abrupt topography of the canyon, but because the isobaths converge there, forcing the topography-following currents to likewise converge.

In the next section, characteristics of the Meddy and the Mediterranean outflow in the formation region will be used to determine which generation mechanisms may be responsible.

4.3 Meddy Generation Mechanisms

In the past several years, six different mechanisms for the generation of Meddies have been proposed. They include

(i) interaction of meanders in the surface Azores current and the mean Mediterranean salt tongue at mid-depth (Käse & Zenk, 1987; Beckmann & Käse, 1989),

(ii) instability of the northward flowing Mediterranean outflow along the western coast of Portugal (Käse et al., 1989),

(iii) geostrophic adjustment of a mixed patch (McWilliams, 1985 & 1988),

(iv) transport intermittency in the otherwise stable outflow current (Nof, 1991),

(v) separation from the coast of a boundary current whose potential vorticity was

modified by boundary-layer friction (D'Asaro, 1988b), and

(vi) instability of buoyancy-driven coastal currents (e.g., Griffiths & Linden, 1981).

Each of the above mechanisms will be examined and evaluated. The Meddy description in Chapter 3, providing radius, thickness, energy, and vorticity scales, aids in the evaluation. Additional CTD and XCP data provide similar information in the outflow.

4.3.1 Meanders in the Azores Current

Käse & Zenk (1987) and Beckmann & Käse (1989) propose that Meddies can be formed from the interaction of meanders in the surface Azores current and the mean Mediterranean salt tongue at mid-depth. Eddies shed from the Azores current will have a surface vorticity signature which will supposedly decay after formation due to intense stirring near the surface. The mid-depth Meddies will survive and enter the westward circulation of the Canary Current and North Equatorial Current systems. This hypothesis is supported by observations of satellite-tracked surface drifters following anticyclonic paths corresponding to Meddy features at 1100 m. The features were visualized by a coarse CTD survey and two mooring stations, and seemed to be advecting around a larger cyclonic cell. The Meddies generated in this fashion should have the T-S characteristics of the mean salt tongue at the generation site, near 36° N and 22° W. However, the mean salinity at 1000 meters in that region is only 35.8 psu, which is 0.7 psu lower than the Cadiz Meddy.

Beckmann & Käse (1989) model the movement and dynamics of a Meddy formed from the instability of a meandering zonal front, representing the Azores Current. A 9-layer quasigeostrophic model produces a Meddy moving to the south-southwest.

Meddies produced by this mechanism would originate far to the southwest of the Gulf of Cadiz, and would propagate even further away. Also, the maximum salinity found in the Meddy core through this mechanism would not exceed 36.0 psu. Therefore, the mechanism of Käse & Zenk (1987) is not consistent with the Cadiz Meddy.

4.3.2 Instability of northward current off western Portugal

Käse et al. (1989) advanced the hypothesis that Meddies are generated by the instability of the Mediterranean outflow after it has turned northward at Cape St. Vincent. Käse supports this idea with a CTD survey which shows four isolated high salinity features off the western Portuguese coast. These features have maxima in dynamic topography at 1000 dbar relative to 3000 dbar associated with them, indicating anticyclonic rotation. Peak azimuthal velocities ranged from 0.05 to 0.12 m s^{-1}, obtained from geostrophy. Numerical modeling of a meridional jet, representing the northward-traveling outflow, produces both cyclonic and anticyclonic eddies. However, the cyclonic eddies produced are bounded by the jet and coastline and do not survive, leaving only the anticyclonic eddies. The modeled eddies have a barotropic component and a surprisingly strong surface signature (7 cm s^{-1}). Analysis of GEOSAT altimetry (Stammer et al., 1991) supports this modeling result, and shows strong correlations between surface topography and Meddy positions.

Although this mechanism has been shown to produce Meddies, it is doubtful that it could have produced the Cadiz Meddy. Once formed, the generated Meddies would tend to propagate to the southwest, to the region between the Azores and Madeira (Figure 1.1). To return to the Gulf of Cadiz, the Meddy would have to travel around or through the Horseshoe Seamounts and the Gettysburg Bank. Neither is probable, and from Section 4.1 we already have a likely formation site within the Gulf of Cadiz.

4.3.3 Geostrophic adjustment

The classic generation mechanism for a subsurface anticyclonic eddy is gravitational collapse and geostrophic adjustment (McWilliams, 1985 & 1988). Local diapycnal mixing in a stratified fluid leads to a neutrally buoyant region of weaker stratification. Under the effect of gravity coupled with ambient stratification, the patch of mixed water collapses. Due to conservation of volume, the water is forced radially outward. The Coriolis force turns the outward flow to the right (in the northern hemisphere), creating an anticyclonic circulation. During adjustment, a portion of the initial energy content of the patch is radiated away in the form of inertial-gravity waves. After a time on the order of f^{-1}, the adjustment process is complete, and the initial patch is now a rotating lens in hydrostatic and gradient-wind balance.

The typical assumption is that the initial patch of water contains available potential energy but no kinetic energy. Thus, the initial relative vorticity in the mixed region is zero. Under these conditions, McWilliams (1988) developed a model that describes the final, equilibrium state of a patch of mixed water within a uniformly stratified background. The model depends on three parameters: the amplitude of the density anomaly γ, the initial radial scale of the mixed patch r_{0m}, and a vertical structure parameter β. The existence of the Cadiz Meddy places constraints on several other parameters: the Rossby number defined here as $R = \zeta/f$, the thickness ratio h/H (where h and H are the thicknesses of the resulting eddy and source waters, respectively), and the energy Burger number B_E which is the ratio of the horizontal kinetic energy (KE) and the available potential energy (APE).

McWilliams (1988) examines possible outcomes of the adjustment process by sampling his model parameter space. The only combination of parameters that produces an eddy similar in some respects to the Cadiz Meddy is given in Table 4.1. The original mixed region has a moderate density perturbation amplitude, a Gaussian density perturbation profile, and a large aspect ratio (tall and thin). A value of B_E greater than 1 and a large Rossby number are obtained for the adjusted eddy. Due to McWilliams's (1985, 1988) scaling, an R of 0.5 denotes the onset of inertial instability, while in this paper a scaling giving a value of -1 is used. However, the eddy was reduced to only 39% of the mixed region's original thickness, where z_{0s} is the final eddy thickness and the initial thickness is 1. For the Cadiz Meddy thickness of 600 m, this requires a mixed region 1500-m thick. Using salinity greater than 36.1 psu or temperature greater than 12 °C as criteria, the thickness of the outflow did not exceed 700 m in the hypothesized formation region during the Gulf of Cadiz expedition, nor in previous Mediterranean outflow surveys (Madelain, 1970; Ambar & Howe, 1979a; Zenk & Armi, 1990; Ochoa & Bray, 1991).

Table 4.1 McWilliams's (1988) Results for Cadiz-like Eddy

r_{0m}	γ	β	R	z_{0s}	B_E
0.25	0.4	1.0	0.445	0.394	1.343

Although the entire parameter space describing the characteristics of the mixed region was not sampled, the tendencies of the resulting adjusted eddies show that to achieve large Rossby and energy Burger numbers the mixed region must undergo a large amount of compression, allowing the original APE to be converted into KE. Therefore, even though geostrophic adjustment may play a part in the generation of the Cadiz Meddy, a more important constraint is that the source waters have either a significant amount of negative relative vorticity ζ or kinetic energy KE.

4.3.4 Transport intermittency

The variable transport of the Mediterranean outflow from tides (Lacome & Richez, 1982) and atmospheric pressure disturbances (Gründlingh, 1981; Candela et al., 1989) is well documented. Nof (1991) presents a generation method that incorporates this intermittency of the outflow. The mean boundary current is assumed to be dynamically stable, but pulses in the net transport can be unstable. Nof separates the volume of the pulse from that of the mean current, and assumes that, in any adjustment process, conservation of volume (or equivalently mass), potential vorticity, and angular momentum are obeyed. He then shows a consistent outcome of the adjusted pulse is a linear series of touching eddies. However, he does not state why or where the eddies form, only that the end condition (the eddies) is consistent with conservation laws. The size and intensity of the eddies are a function of the size of the transport pulse and the Rossby radius of deformation R_d, while the number of eddies (n) is assumed *a priori*. The eddies are governed by cyclogeostrophy, and the water in the pulse is assumed to have no angular momentum and vorticity other than planetary.

The only scales specified are the half-length and depth of the pulse (b and H respectively), and the Rossby radius of deformation R_d defined by Nof as $(g'H)^{1/2}/f$. Assuming the parameter $\varepsilon = (b/R_d)^2 \ll 1$, an analytical solution is developed for the half-width of the pulse (w) and the radius (r), thickness (h), and velocity (v) of the resulting eddies. The resulting eddies are assumed to be circular with the thickness following a parabola, with a maximum in the center and zero at the eddy boundary. This geometry constrains the eddy velocity field to be in solid body rotation. With the choice of small ε, the eddies are shown by Nof to have a core vorticity of $-f$. Subsequent numerical solutions by Nof show that the analytical solutions are valid even as ε approaches 1. The solutions in dimensional form are

$$
\begin{aligned}
v(r) &= -\frac{f}{2}r \\
h(r) &= \frac{H}{8R_d^2}(R^2 - r^2) \\
R(n) &= \frac{b}{(n^2-1)^{1/2}} \\
w(n) &= \frac{n\pi b^3}{64\,R_d^2(n^2-1)^2}
\end{aligned}
\qquad (4.3\text{-}4.6)
$$

where n is the number of eddies formed from the pulse.

Laboratory experiments were carried out by Nof in a rotating cylindrical tank filled with saline water. Dyed, fresher water was introduced at the surface, and formed a surface boundary current flowing anticyclonically around the tank. Two experiments were performed. First, the injection of dyed water was terminated, and the current quickly broke up into a linear series of eddies along the boundary. Second, the injection of dyed water was allowed to continue. Even though waves along the boundary current interface appeared in the second experiment (as they did initially in the first before termination of the injected fluid), no eddies formed. All other aspects of the two experiments were identical. Thus, Nof claims, the termination of the inflow creating a pulse of fluid was responsible for the creation of the eddies. Nof's discussion of the laboratory experiments was entirely qualitative however, with no indication of the eddy's vorticity, its thickness with respect to the thickness of the boundary current, or the radius of the eddy with respect to the deformation radius. Equation 4.4 predicts that, for an eddy with a radius on the order of the deformation radius, the final thickness would only be 1/8 that of the boundary current, which is in contradiction to that observed.

Applying Nof's generation model to the Mediterranean outflow, I could not reproduce an eddy with the characteristics of the Cadiz Meddy. I first assume a Meddy with a final radius R of 9 km, a source water thickness H of 700 m, and an R_d as defined in (4.2) of 9 km. Solving for the maximum depth of the Meddy using (4.4) gives $h = 87$ m. Trying another approach, I estimate the length $2b$ of a pulse to be on the order of 60 km, again with $H = 700$ m and R and $R_d = 9$ km. The above combinations result in three eddies being formed, with an initial width $2w$ of 1.4 km. The thickness of the eddies remains 87 m. The half-width of the outflow during the Cadiz experiment was on the order of 5 to 10 km. Thus, the mechanism of Nof (1991) produces a Meddy with

an order of magnitude error in both the final Meddy thickness and in the original outflow width. Some of this difference may be accounted for in the definition of R_d. However, to obtain a Meddy with a thickness on the order of the initial source waters, the final radius R of the Meddy must be almost 3 times R_d. The Meddy could no longer be considered a submesoscale feature. As in the McWilliams (1988) mechanism discussed in Section 4.6, compression of the initial mixed volume is much greater than is observed. This compression can be reduced by allowing the formation waters to contain negative relative vorticity.

In conclusion, I determine that the generation mechanism of Nof (1991) was not the cause of the Cadiz Meddy. First, and most importantly, I find no combination of parameters that produces an eddy consistent with observations. Also, with the source of the outflow intermittency presumably near the Strait of Gibraltar, the origin of the Cadiz Meddy over 100 km downstream indicates that the mechanism of Nof was inhibited until the canyon region. The cause of this inhibition is not known, but might be related to the separation of the outflow from the bottom once the outflow reaches its equilibrium depth. At that point, any constraints that bottom boundary layer dynamics have on the outflow are removed. Finally, Ambar & Howe (1979a) have suggested that some of the observed variability in the outflow is not transport intermittency, but instead a result of a meandering outflow.

4.3.5 Boundary torques

In the previous two sections, I've shown that geostrophic adjustment of a mixed patch cannot produce an eddy with characteristics consistent with those of the Cadiz Meddy unless an unreasonable amount of isopycnal compression occurs. Assuming that the potential vorticity is conserved during the formation process (refer to Section 4.4), then negative relative vorticity and/or vertical shear is required in the outflow. D'Asaro (1988b) argues, specifically for eddies found in the Arctic Ocean but applicable for Meddies as well, that the potential vorticity of the source waters can be reduced by boundary torques. The proposed mechanism allows the vorticity in the Meddy to be created by boundary layer friction as the Mediterranean outflow follows topography. Meddies would spin off as the outflow separates from the coast near Cape St. Vincent, or as portions of the outflow separate from the canyons and are no longer confined by bottom or side topography (Figure 4.3). Due to the flow being geostrophically driven,

the topographic boundary is to the right of the flow and the frictional torques impart anticyclonic vorticity. This vorticity, governed by boundary-layer effects and not by geostrophy, can be below $-f$, thus creating a vortex with negative potential vorticity Q. The eddy, after separating from topography, then undergoes inertial instability and entrains surrounding waters having positive Q until the eddy has $Q \geq 0$. This would account for the many eddies, particularly in the Arctic, with $\zeta \approx -f$.

D'Asaro (1988b) uses a one-dimensional barotropic expression for the u-momentum equation to motivate a discussion of frictional torques generating vorticity. The governing equation is

$$\frac{\partial u}{\partial t} = -\frac{C}{H(y)} \bar{u}\, u(y) \tag{4.7}$$

where C is a drag coefficient, $H(y)$ is the flow depth, and $\bar{u}$ is the magnitude of the laterally averaged flow speed. Solving (4.7) for $u(t)$, we obtain

$$u(t) = u_o \exp\left[-\frac{C\,\bar{u}}{H}\, t\right] \tag{4.8}$$

where u_o is the initial downstream velocity. Thus, with any value of the parameters, the mean velocity will decay exponentially in time.

To study the creation of relative vorticity, the curl of (4.7) is taken, letting $\zeta = -\partial u / \partial y$, such that

$$\frac{\partial \zeta}{\partial t} = -\frac{C\,\bar{u}}{H}\left[\zeta + \frac{u\,S}{H}\right] \tag{4.9}$$

where $S = \partial H / \partial y$ is the bottom slope. Solving for ζ while imposing zero relative vorticity as an initial condition yields

$$\zeta(t) = -\frac{\bar{u}\,S}{H}\left[1 - \exp\left[-\frac{C\,\bar{u}}{H}\, t\right]\right] \tag{4.10}$$

The vorticity arises in (4.10) solely from shallower waters being frictionally slowed at a higher rate than deeper waters. With no slope and no boundary friction, there would be no vorticity generation. Using optimistic values of the parameters ($u_o = 1$ m s^{-1}, $S = 0.1$, $C = 0.01$, and $H = 500$ m), a simulation of the Mediterranean outflow through the Gulf of Cadiz was made. A value of 500 m is used for H, using the thickness of the

outflow rather than the total water depth. Figure 4.4 shows the time evolution of u and ζ, as well as the distance traveled downstream. The above equations crudely model the effect of a barotropic outflow along a sloping bottom. Vorticity is created as the shallow waters slow. Then, as the mean flow decreases, the vorticity also begins to diminish. Using the above parameters, after 1 day, the mean velocity has decreased to 0.45 m s^{-1}, the outflow has traveled 60 km, and a relative vorticity of $-0.6f$ has been generated. This value of vorticity falls short of that found in the Cadiz Meddy ($-0.85f$), and a more gradual slope, a slower mean current, and a thicker outflow all contribute to a reduction in vorticity magnitude.

D'Asaro (1988b) references the current-meter data presented by Howe (1984), showing that in the Mediterranean outflow lateral shears on the order of $-f$ exist. Howe (1984) describes 12-day current records from three moorings off Cape St. Vincent. The data suggest a mean current of 0.5 m s^{-1} at 1000 m depth, with peak velocities extending 8 to 14 km offshore. The mooring array did not have the lateral resolution necessary to describe the frictional boundary layer, but, by assuming zero outflow velocity along the shelf, an average vorticity would be -0.5 m s^{-1} / 8 km $\approx -0.73f$. One standard deviation above the mean velocity was 0.65 m s^{-1}, which yields a vorticity of $-0.95f$. Undoubtedly, the lateral boundary layer profile is such that actual vorticities are more negative than $-f$, but the laterally averaged vorticity determines the core vorticity in the D'Asaro (1988b) mechanism.

Data gathered in the Gulf of Cadiz cruise from three XCP probes, dropped (by coincidence) exactly where Howe (1984) had his current moorings, show little evidence of such a strong flow. Using the salinity minimum as a layer-of-no-motion, which is consistent with Howe's (1984) data, we obtained peak velocities of 0.20 m s^{-1}, or two standard deviations below Howe's mean. This is not to say that 30 days earlier, when the Cadiz Meddy was hypothesized to have formed, the outflow was not much stronger.

An additional unknown is the characteristic of a baroclinic eddy with a core vorticity below $-f$. D'Asaro's mechanism requires that inertially unstable eddies restabilize by entraining waters of lower angular momentum, and that this process occurs gently enough that the eddy does not split apart. There is no strong evidence for this. But, with the Cadiz Meddy's core vorticity near $-0.85f$, perhaps a restabilization was not required. Also, there is evidence (MacCready & Rhines, 1992) that, for stratified flows along sloping bottoms, an arrested Ekman layer might exist. This Ekman layer would

maintain a no-slip bottom condition by means of a thermal wind balance. Thus, the boundary current would obey instability limits imposed by the geostrophic shear and might not be able to support relative vorticities below $-f$.

In summary, the maximum velocity in the outflow during the Cadiz expedition was not large enough to produce the relative vorticity of the Meddy, although the outflow velocity at the time of formation is unknown. Also, solutions to the barotropic vorticity equation (4.10) do not produce the relative vorticity of the Meddy, even when very favorable parameters are used. However, the formation area is the region where the outflow separates from topography, and any lateral shear in the outflow will contribute to the Meddy vorticity. In conclusion, there is no evidence that the Cadiz Meddy was generated primarily by means of the D'Asaro (1988b) mechanism.

4.3.6 Instability of a coastal current

Griffiths & Linden (1981) (hereafter GL81) observed instability of buoyancy-driven coastal currents in a laboratory setting. Their motivation was not the study of Meddy formation, but a general understanding of boundary current stability.

The experiments of GL81 were in a rotating cylindrical tank containing dense saline waters. A cylinder of smaller radius was aligned with the axis of rotation, and acted as the coastal boundary. Dyed, less dense water was introduced at the coastal boundary. The lighter water tended to flow outward, and to the right under the influence of Coriolis, to form a steady boundary current. However, regardless of the flow conditions, wave-like disturbances appeared on the interface of the two fluids and grew to increasingly large amplitude (Figure 4.5).

The laboratory experiments of GL81 share several characteristics with observations in the Gulf of Cadiz. In the laboratory experiment, the boundary current instability manifested itself as a wave-like form. The crests of the wave consisted of anti-cyclonic vorticity and contained the dyed water of the boundary current. The troughs consisted of cyclonic vorticity and contained mostly undyed, ambient water, but had entrained filaments of the dyed waters. For low azimuthal mode disturbances, the cyclone-anticyclone pairs would move radially away from the boundary into the interior. A similar feature is seen in the Gulf of Cadiz when we examine the structure of isopycnals. The isopycnal with the maximum upward displacement above the

Meddy was 32.10 σ_1, while the isopycnal of maximum depression below the Meddy was 32.30 σ_1. The depths of these two isopycnal surfaces throughout the Gulf are displayed in Figure 4.6. In both views, the lightest of the four gray scales is the shallowest depth, the darkest is the most depressed. The contour interval is 25 dbars in 4.6a, and 50 dbars in 4.6b. The Meddy is indicated by a shallow upper isopycnal over a deeper lower isopycnal. However, to the east of the Meddy there is a feature that has deep upper isopycnals over shallow lower isopycnals, which suggests an isolated cyclonic feature. This cyclonic feature does not have the strong temperature or salinity characteristics of the Mediterranean outflow. The Meddy and the cyclonic feature are aligned so that they pair to self-advect away from the boundary. Since only one coarse survey of the cyclone was made, the relative motion of the two eddies could not be determined.

The results of GL81 also quantify the wavelength of the unstable wave on the boundary current, showing the wavelength to be on the order of twice the boundary current width. This result seemed to be independent of the thickness of the current, the water depth, or the density perturbation of the current. The width of the Mediterranean outflow in the formation region is between 10 and 20 km. Since one cyclonic eddy and one anticyclonic eddy comprise one wavelength, the expected resulting Meddy radius is half the current width, or about 5 to 10 km. The above agreements suggest that baroclinic instability might play an important role in Meddy formation.

4.3.7 Discussion

By insisting that the Cadiz Meddy formed both of its cores simultaneously without entraining ambient waters from the Gulf of Cadiz, the formation site was chosen to be near the canyon regions on the continental slope south of Portugal.

Of the six generation mechanisms found in the literature, two were eliminated for geographic reasons: the interaction of the surface Azores current and the mean Mediterranean salt tongue at mid-depth (Käse & Zenk, 1987; Beckmann & Käse, 1989), and the instability of the Mediterranean outflow after turning northward at Cape St. Vincent (Käse et al., 1989). Two others were eliminated because of the unreasonable amount of water column compression needed to generate the observed relative vorticity: geostrophic adjustment of a mixed patch (McWilliams, 1985 & 1988), and transport

intermittency in the otherwise stable outflow current (Nof, 1991).

The remaining two mechanisms, baroclinic instability of buoyancy-driven coastal currents (Griffiths & Linden, 1981) and boundary layer friction modifying potential vorticity of the outflow (D'Asaro, 1988b), cannot be eliminated or verified so easily. The first requires that the boundary current contain vertical shear, while the second requires lateral shear. Unfortunately, the data spacing in the boundary current from the Cadiz Cruise is such that we are unable to adequately resolve the lateral shear. A gross estimate is the maximum velocity divided by the distance from land, with the alongshore velocity assumed to be zero. More lateral resolution in the outflow is required to show a necessary condition exists for barotropic instability, which is that the gradient of absolute vorticity must vanish within the boundary current, or

$$\frac{\partial}{\partial y}\left[f - \frac{\partial u}{\partial y}\right] = 0 \tag{4.11}$$

somewhere (Holton, 1979). For an f–plane approximation, where the gradients of f are negligible, the necessary condition reduces to the Rayleigh inflection-point theorem (e.g., Drazin and Reid, 1981) which states that a necessary condition for instability is that the velocity should have an inflection point, or

$$\frac{\partial^2 u}{\partial y^2} = 0 \tag{4.12}$$

If one assumes a reasonable lateral velocity profile (e.g., Figure 4.3), an inflection point will occur somewhere to the seaward side of the velocity maximum. However, even in controlled laboratory experiments, it is difficult to measure the velocity and density (and thus the potential vorticity) structure with sufficient accuracy to allow direct application of the necessary conditions for baroclinic or barotropic instability (Griffiths & Linden, 1981).

In summary, I am left with two alternatives. (i) Baroclinic instability of the Mediterranean outflow, although not verified, is likely to occur. The scales of the instability and the scales of the resulting Meddy are in close agreement. A companion cyclonic feature containing lesser amounts of the source waters is predicted and observed. Yet, the relationship between the strength of the current and the resulting vorticity of the Meddy is not understood. (ii) Generation of relative vorticity through boundary friction can provide a mechanism to explain the vorticity of the Meddy. The lateral shear

required to form a Meddy having the observed vorticity has occurred in the past, but was not present during the Cadiz Cruise. However, in the region where the Meddy is thought to have been formed, the convergence of bathymetry and the appearance of a canyon act as a break from topography, which is suggested for eddy formation.

In conclusion, the velocity structure of the boundary current cannot be ignored when considering Meddy formation, and the most likely mechanism is baroclinic instability, augmented by lateral boundary shear. Regardless of the generation mechanism, the potential vorticity Q of the source waters and of the Meddy must be the same. The only changes possible to Q occur through diffusive or frictional processes. Neither is a fundamental aspect of baroclinic instability. The very low potential vorticity found in the Meddy must therefore also exist in the Mediterranean outflow. How the outflow obtains its anomalous Q and the creation of a Meddy from that anomaly will be the focus of the remainder of this chapter.

4.4 Potential Vorticity in the Mediterranean Outflow

As stated above, only mixing and frictional processes modify the Q of a water parcel, while hydrodynamic instabilities do not. The analysis of the Cadiz Experiment data in the Mediterranean outflow by Baringer (1991) suggests that the highest total stress, nearly 5 Pa, occurs on the first 25 km of the outflow. This is also the region of highest dissipation (Lueck, 1991). The stress decreases to 1 Pa for the next 75 km, and perhaps to 0.5 Pa thereafter (Baringer, personal communication, 1992). I hypothesize that most of the Q modification of the outflow by bottom friction also occurs at that same high stress location. The values of Q continue to change downstream by entrainment, but the flux of Q along the Mediterranean outflow remains constant. Thus, the Q anomaly of the Cadiz Meddy may be determined far upstream.

The above process is somewhat analogous to two-dimensional flow over a flat plate, shown in Figure 4.7. Here, all the vorticity in the boundary layer is generated at the leading edge (e.g., Morton, 1984), which is presumably a high dissipation region. Thereafter, the vorticity is advected downstream and experiences vertical diffusion, forming a boundary layer of increasing thickness. The vorticity (or Q anomaly in this analogy) of any parcel thus decreases downstream, but the area integral of vorticity (the circulation) in the boundary layer remains constant. To support this claim, the change in Q along the outflow will be examined.

4.4.1 An expression for potential vorticity in the outflow

The potential vorticity Q of the Meddy was discussed in Section 3.9. Here, the Q of the outflow will be examined. The derivation will follow that of Section 3.9, but with slight modifications. Again, starting with Ertel's vorticity,

$$Q = -(f\hat{\mathbf{k}} + \vec{\zeta}) \cdot \frac{\nabla \rho}{\rho} \tag{4.13}$$

The conservation of Q assumes that ρ is a conserved quantity, that is, $d\rho/dt = 0$, and that any frictional or viscous forces are negligible. Since the potential vorticity Q is not modified by either baroclinic, barotropic, or ageostrophic instabilities of the Mediterranean outflow, the Q anomaly that exists in the Meddy must also exist in the outflow.

Expanding (4.13) while noting that i) the horizontal gradients of vertical velocity are much smaller than vertical gradients of horizontal velocity, ($\left|\frac{\partial w}{\partial x}\right|, \left|\frac{\partial w}{\partial y}\right| \ll \left|\frac{\partial u}{\partial z}\right|, \left|\frac{\partial v}{\partial z}\right|$), ii) the downstream gradient of lateral velocity is much smaller than the lateral gradient of downstream velocity ($\left|\frac{\partial v}{\partial x}\right| \ll \left|\frac{\partial u}{\partial y}\right|$), and iii) the downstream gradient of density is much smaller than the lateral gradient of density ($\left|\frac{\partial \rho}{\partial x}\right| \ll \left|\frac{\partial \rho}{\partial x}\right|$), then

$$Q = -\frac{1}{\rho}(f + \zeta)\frac{\partial \rho}{\partial z} - \frac{1}{\rho}\frac{\partial \rho}{\partial y}\frac{\partial u}{\partial z} \tag{4.14}$$

where the vertical component of vorticity $\zeta = -\partial u/\partial y$. Now, let

$$\rho = \bar{\rho}(z) + \rho'(x, y, z) \tag{4.15}$$

where $\bar{\rho}$ is the mean vertical structure of density and ρ' is the density anomaly from the Mediterranean outflow. Next, assume the outflow is in thermal wind balance, so that

$$\frac{1}{\rho}\frac{\partial \rho'}{\partial y} = \frac{f}{g}\frac{\partial u}{\partial z} \tag{4.16}$$

Using (4.16), the expression (4.14) for Q becomes

$$Q = \frac{1}{g}\left[- f S_z^2 \right. \tag{4.17}$$

where $\bar{N}$ is the mean stratification, N' is the stratification anomaly, and S_z^2 is defined as

$$S_z^2 = \left[\frac{\partial u}{\partial z} \right]^2 \tag{4.18}$$

Equation (4.17) can be simplified in terms of nondimensional parameters, so

$$Q = \frac{f\overline{N}^2}{g} \left[(1 + \frac{\zeta}{f})(1 + \frac{N'^2}{\overline{N}^2}) - \frac{S_z^2}{\overline{N}^2} \right] \tag{4.19}$$

Defining the Rossby number R_o as ζ / f , the gradient Richardson number R_i as $\overline{N}^2 / S_z^2$, and the normalized buoyancy gradient anomaly G as $N'^2 / \overline{N}^2$, then

$$Q = \frac{f\overline{N}^2}{g} \left[(1 + R_o)(1 + G) - R_i^{-1} \right] \tag{4.20}$$

or

$$Q = \frac{f\overline{N}^2}{g} \left[1 + (R_o + G + R_o G - R_i^{-1}) \right]$$

(Kunze, personal communication, 1991; Kunze and Sanford, 1992). As was shown in Chapter 3, a potential vorticity modifying term X and a potential vorticity anomaly Q' can be defined, such as

$$Q = \overline{Q} \left[1 + X \right] = \overline{Q} + Q' \tag{4.21}$$

where the ambient potential vorticity is again

$$\overline{Q} = \frac{f\overline{N}^2}{g} \tag{4.22}$$

the modifying term is

$$X = R_o + G + R_o G - R_i^{-1} \tag{4.23}$$

and the potential vorticity anomaly is

$$Q' = \overline{Q} X \tag{4.24}$$

As in the Meddy, the ambient potential vorticity $\overline{Q}$ in the outflow is modified by X, a sum of nondimensional terms. The rotational inhibiter of the twisting term R_i^{-1} that appeared in the derivation of Q for the Meddy does not appear here. Remember that the Q anomaly in the center of the Meddy was dominated by the R_o term (Figures 3.15a, 3.19) and the G term (Figures 3.10, 3.18b). The components of X are computed for two data sections of the Cadiz Cruise. Line 04 is in the formation region of the

Meddy, while Line F is halfway between the Meddy formation region and the Strait of Gibraltar (refer to Figures 2.2 and 2.10).

4.4.2 Determination of G

The vertical profile of the ambient stratification $\overline{N}^2$ was computed by averaging over estimates of N^2 obtained from nine CTD casts in the Gulf of Cadiz. Only those casts that showed no visible signature of the Mediterranean outflow or of the Meddy were used. From these casts, the vertical gradient of σ_1 was computed by derivatives of smoothing spline fits. The smoothing spline acts as a Butterworth low-pass filter, and the 3-dB point of the filter was chosen as 100 m. The 100-m vertical scale was subjectively chosen as representative of the scale of vertical density gradients in the Meddy and of the outflow within the formation region. Smaller vertical scales emphasize perturbations in the flow, while larger scales obscure the signal of the feature we wish to examine.

The individual vertical profiles of N^2 were interpolated onto a grid of monotonically increasing σ_1, with an increment of 0.001 σ^1. The N^2 profiles were then averaged on potential density surfaces to form an estimate of $\overline{N}^2$. The average profile from -600 to -1700 m generally resembles the Garrett-Munk (GM81) model of vertical stratification $N(z) = 5.2 \times 10^{-3} \exp(z/1300)$ (Munk, 1981). The root-mean square variation of the individual N^2 estimates is about 1×10^{-6} (rad s^{-1})^2 down to -1200, decreasing to 2×10^{-7} (rad s^{-1})^2 at -1700 m depth, while the variation in depth of the isopycnals is about 10 m down to -1200 m, increasing to 30 m at -1700 m depth. The variation in isopycnal displacement above -1200 m is similar to that predicted by the GM81 internal wave model. The variation below that depth is presumed to be caused by increased levels of internal wave energy, or by Mediterranean outflow finestructure which has been advected into the Gulf of Cadiz.

At each CTD location along lines F and 04, profiles of normalized buoyancy gradient anomaly G were computed by $(N^2 - \overline{N}^2)/\overline{N}^2$. The vertical scale used for the spline fits for N^2 was 100 m along Line 04. However, along Line F the outflow is still a bottom boundary current, and the vertical scale was reduced to 30 m. Figure 4.8 shows the distribution of G along Lines F and 04 superimposed upon contours of salinity. Note that in this figure, and those to follow, the scales used for Line F and Line 04

differ. Above the boundary current in Line F, very large values of G occur because the isopycnals are compressed. In the well mixed outflow, the minimum values possible for G are found (−1). Along Line 04, the outflow again has low values of G. In the region below the salinity maximum in the Gulf of Cadiz (≈ −1200 m), large variations of G, both positive and negative, occur. The source of these variations is the same as that of the large isopycnal depth variations discussed above.

4.4.3 Determination of R_i^{-1}

Vertical profiles of R_i^{-1} were constructed by combining data from concurrent (within 1 hour and 1 km) XCP profiles and CTD casts, as well as the $\overline{N}^2$ estimate determined in the previous section. The data from XCPs provide direct estimates of S_z^2 as a function of depth. Again, the vertical gradients were computed by smoothing spline fits of velocity (for S_z^2), with vertical smoothing scales of 100 and 30 m for Lines 04 and F, respectively. The CTD cast provided an estimate of σ_1 with depth, which was then associated with the S_z^2 at the same depth. The value of $\overline{N}^2$ at that density surface was then used in determining R_i^{-1}.

Figure 4.9 shows the distribution of R_i^{-1} along Lines F and 04 superimposed upon contours of salinity. At Line F, R_i^{-1} far exceeding 1 exists above and within the high salinity core of the outflow. When R_i^{-1} exceeds 4, Kelvin-Helmholtz instability and turbulence production can occur, resulting in localized mixing and further reduction in G. Again, high values of R_i^{-1} occur in the outflow at Line 04, as well as elsewhere in the Gulf of Cadiz below the salinity maximum.

4.4.4 Determination of R_o

The independent determination of lateral shear needed to determine R_o suffers from the XCP being a relative velocity profiler and the need to have two estimates of velocity at each depth increment. The calculation of lateral shear can be subdivided into two separate components. The first, determining the lateral shear between two adjacent XCP velocity profiles along a section, requires that the two velocity profiles (hereby denoted as a "profile pair") be known to within the same constant. Thus the velocities do not need to be absolute, just referenced consistently. Referencing the XCPs to the salinity minimum (Ambar & Howe, 1979b) discussed in Appendix A is

used here, since absolute velocities are not required. An application of this method to idealized velocity profiles typical of the Mediterranean outflow is presented in Figure 4.10. Several interesting results are obtained through this example. First, there is a region where the vorticity could not be computed, because only one of the two profiles extends to that depth. Secondly, the relative vorticity is not everywhere negative, but exists in a positive sense as well. The structure of the vertical profile of vorticity depends on the vertical structure of the velocity profile pair, the bottom slope, and the lateral separation of the pair.

The second component in the determination of lateral shear, that of finding the shear between the first velocity profile and land, or, if the bottom is sloping, between the lower portion of any profile and topography, requires an absolute velocity. The assumption here is that, with a no-slip boundary, the water velocity at the boundary is zero, thus known in an absolute sense. The determination of an absolute velocity from XCP data was not entirely successful, as discussed in Appendix A. An alternative estimate of the lateral shear can be made, however, if the bottom depth is smoothly sloping and there is a well-defined bottom boundary layer in the outflow. The lateral shear can then be estimated by the product of the bottom slope and the vertical shear of the downstream component of velocity (Figure 4.10). Thus a velocity shear in the Gulf of Cadiz of -0.30 m s^{-1} over the bottom 70 m along a slope of 1:50 gives a lateral shear of -8.6 $\times 10^{-5}$ rad s^{-1}, or nearly $-f$. In fact, the typical vertical scale of the bottom boundary layer, where negative R_o would be found, is on the order of 20 m. Using the above bottom shear method, an R_o of nearly -3.5f might arise.

Figure 4.11 shows values of R_o along section F and 04, derived from the procedures discussed above, superimposed upon contours of salinity. A smoothing spline, as was used in the previous section for R_i^{-1}, was used in processing the velocity profiles. Only the component of velocity normal to the line connecting the profile pair was used. Above the outflow in Line F, R_o near and exceeding 1 is found. Within the bottom boundary layer, negative values of R_o occur, but over a very small ($\approx$ 20 m) vertical extent. Thus, regions of positive R_o dominate the Line F section plot. No large lateral shears of any sign are found along Line 04, except within the shoreward side of the outflow, where $R_o \approx -0.25$.

4.4.5 Determination of Q

The nondimensional potential vorticity factor X for Lines F and 04 is shown in Figure 4.12. The structure of X along Line F is dominated by high vertical wavenumber features, alternatingly dominated by positive X from high values of G and negative X from high R_i^{-1}. Some of this variability is due to the small vertical scale of the outflow, coupled with the problems inherent in combining data from different instrument systems (the XCP and the CTD) and from slightly different times and locations. A contour plot of Q for Line 04 is given in Figure 4.13, where the values of Q were smoothed in the vertical. (The Q field along Line F, even when smoothed, did not lend itself to contouring.) Two important results from Figure 4.13 are i) the potential vorticity in the outflow near the formation region is similar to that found in the Meddy, and ii) the potential vorticity anomaly in the outflow is dominated by vortex stretching (the G component) and vertical shear (R_i^{-1}). Remember, vortex stretching and the lateral shear (the R_o component) were dominant in the Meddy. It must also be remembered that only three XCP profiles were used in determining the Q near the coast in line 04, while 28 profiles were used in the Meddy. Also, the Meddy was surveyed about a month after formation, and Line 04 was surveyed 12 days before Line F. With the known intermittency of the Mediterranean outflow, I am primarily looking for qualitative agreement between the Meddy and the outflow.

4.4.6 Determination of the flux of Q

If no production or dissipation of Q occurs between Lines F and 04, then the flux of Q through Line F should be equal to the flux through Line 04. Here, I will examine the flux of the potential vorticity factor X. This term is chosen since it is of order one and the background levels are near zero, whereas Q itself can be an order of magnitude *below* the background levels. Thus, errors in defining the cross-sectional area of the outflow that might cause an inclusion of ambient waters containing no anomalous potential vorticity will not degrade the estimate of the flux. The flux is here defined as

$$Flux = \int_A \vec{\mathbf{u}} \cdot \hat{\mathbf{n}} \; X \; dA \tag{4.25}$$

where $\vec{\mathbf{u}}$ is the horizontal velocity vector, $\hat{\mathbf{n}}$ is the unit normal to the data line (either F or 04), and A is the cross-sectional area of the outflow. The flux is a signed quantity,

where a positive flux here results from a negative anomaly multiplied by a negative (westward) velocity.

Possible errors in the flux estimate arise from i) the errors in the potential vorticity factor X, ii) errors in the velocity reference, iii) errors in the definition of the cross-sectional area, and iv) lack of lateral resolution. The velocity required here is the absolute velocity, and I will approximate the absolute velocity by using the salinity minimum as a layer-of-no-motion. The cross-sectional area A was defined subjectively as having "outward" (westward) flow and having salinity properties consistent with the outflow. The mass transport through Lines F and 04 was also computed, as a crude indication of the validity of the XCP referencing method. The Line F transport was 1.4 Sv, while the Line 04 transport was 3.1 Sv. These estimates are consistent with historical estimates that use hydrographic sections as well as mooring data (Gründlingh, 1981; Ambar & Howe, 1979b; Zenk, 1975b), and suggest that the velocity referencing may not be a major source of error.

The estimate of X flux through Line F was 4.4 Sv (X is dimensionless) while the flux through Line 04 was 1.0 Sv. Thus, although there was a factor of two increase in mass transport from Line F to 04, there was a factor of 4.4 *decrease* in the flux of X. This large downstream change in X flux is surprising, given my initial hypothesis that the potential vorticity is modified far upstream and thereafter the flux remains constant. The flux change might be due in part to the temporal variability of the outflow and the time lag in the measurements. One reason for the flux difference is certainly the error in computing X at Line F. An error bound on X flux was obtained by "reasonably" varying parameters such as the vertical scale of the smoothing and the velocity referencing method. The X flux at Line 4 changed by ± 0.2 Sv, while at Line F the variation was ± 2.5 Sv. Finally, modification in the X flux might have occurred along the path of the outflow. This modification will be examined in the next section.

4.4.7 Viscous modification of X in the outflow

Following Pedlosky (1979), the time rate-of-change of potential vorticity is given by

$$\frac{dQ}{dt} = -\frac{1}{\rho}\nabla\rho \cdot \left[\kappa \nabla^2 \vec{\zeta}\right] \tag{4.26}$$

where κ is the eddy diffusion of momentum, and will be used here instead of kinematic viscosity. Assuming here, as in Section 4.1, that the velocity is only in the downstream (u) direction, and that u and ρ vary only in y and z, we then have

$$\frac{dQ}{dt} = -\frac{1}{\rho}\frac{\partial \rho}{\partial y}\left[\kappa_H \nabla^2 \frac{\partial u}{\partial z}\right] + \frac{1}{\rho}\frac{\partial \rho}{\partial z}\left[\kappa_V \nabla^2 \frac{\partial u}{\partial y}\right] \tag{4.27}$$

where κ_H and κ_V are the horizontal and vertical eddy diffusivities of momentum, respectively. Letting $\partial u / \partial z = S_z$ and $-\partial u / \partial y = \zeta$, and with the curvature in z much greater than that in y, the above simplifies to

$$\frac{dQ}{dt} = -\frac{\kappa_H}{\rho}\frac{\partial \rho}{\partial y}\frac{\partial^2}{\partial z^2} S_z - \frac{\kappa_V}{\rho}\frac{\partial \rho}{\partial z}\frac{\partial^2}{\partial z^2}\zeta \tag{4.28}$$

Defining N^2 as before, using the thermal wind relation, and rearranging,

$$\frac{dQ}{dt} = \frac{f\,\bar{N}^2}{g}\left\{\kappa_V \frac{N^2}{\bar{N}^2}\frac{\partial^2}{\partial z^2}\frac{\zeta}{f} - \kappa_H \frac{S_z}{\bar{N}^2}\frac{\partial^2}{\partial z^2} S_z\right\} \tag{4.29}$$

Letting the outflow remain in steady state, and realizing that the ambient potential vorticity is a constant, we then have

$$u\frac{\partial X}{\partial x} = \kappa_V \frac{N^2}{\bar{N}^2}\frac{\partial^2}{\partial z^2} R_o - \kappa_H \frac{S_z}{\bar{N}^2}\frac{\partial^2}{\partial z^2} S_z \tag{4.30}$$

From the sections above, we found that the vertical variation in R_i^{-1} was greater than that of R_o, and, assuming that κ_H is much greater than κ_V, only the last term of the right-hand-side of (4.30) remains. The vertical curvature of S_z is usually maximum where S_z is maximum, and the two terms will be of opposite sign. Thus, their product will be negative. For simplicity, the vertical curvature term will be approximated by a height scale H_z^2; thus

$$\frac{S_z}{\bar{N}^2}\frac{\partial^2}{\partial z^2} S_z \approx -\frac{R_i^{-1}}{H_z^2} \tag{4.31}$$

so

$$u\frac{\partial X}{\partial x} \approx \frac{\kappa_H R_i^{-1}}{H_z^2} \tag{4.32}$$

It is interesting to note that the *vertical* shear is coupled with the *lateral* diffusion in the downstream modification of X. From (4.32), the large R_i^{-1} at Line F would have

increased the value of X as the outflow moved downstream, changing large negative X to less negative, thus decreasing the X flux.

4.4.8 Conversion from R_i^{-1} in outflow to R_o in Meddy

Earlier, we found that the Q in the Meddy is dominated by the R_o component, while in the formation region (Line 04) the R_i^{-1} term was dominant. The reason for this conversion from R_i^{-1} to R_o during the formation process has not been given. However, the conversion is consistent with meanders within a geostrophic current in which anticyclonic curvature is introduced. The conservation of potential vorticity (to first order $(f + \zeta) / H$) then requires that the isopycnals flatten. This decreases the vertical shear through thermal wind constraints. However, the full conservation of potential vorticity requires that the reduction of the R_i^{-1} component be compensated, and this occurs by an additional increase in negative relative vorticity. A specific mechanism for the instability is not required. Meanders might easily occur from barotropic instability, or from curvature induced by variations in topography, such as canyons or changes in slope. However, the large vertical shears present support the previous conclusion that baroclinic processes may be important.

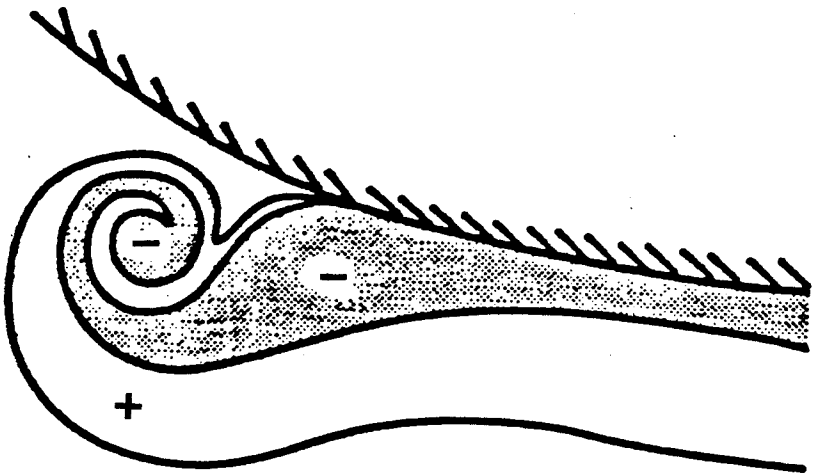

Figure 4.1. Schematic of lateral boundary layer entraining opposite signed vorticity (adapted from Stern & Whitehead (1990)).

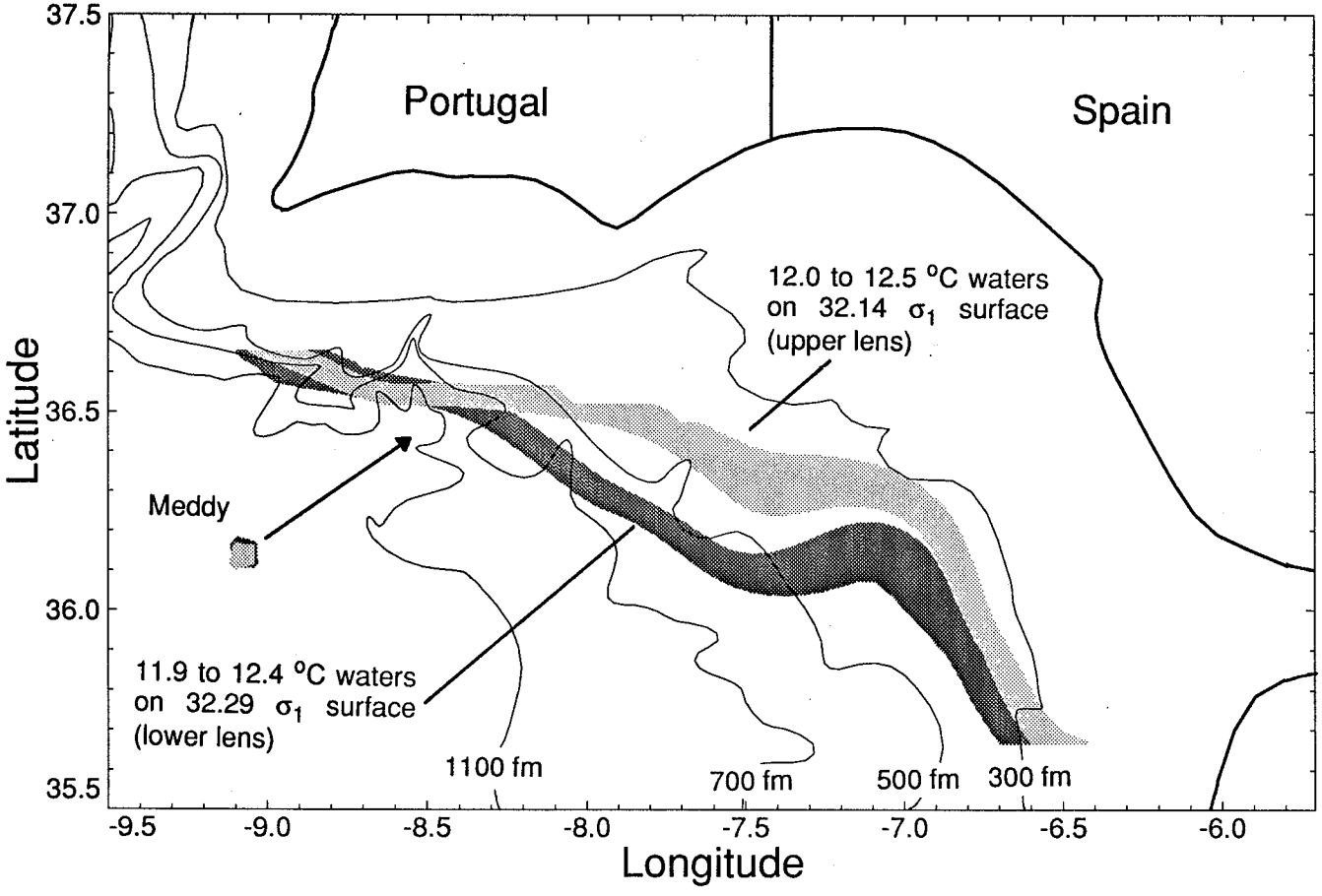

Figure 4.2.Contours of temperature on isopycnal surfaces, showing suggested formation region of the Cadiz Meddy. Also shown is the backward extrapolated path of the Meddy for one month.

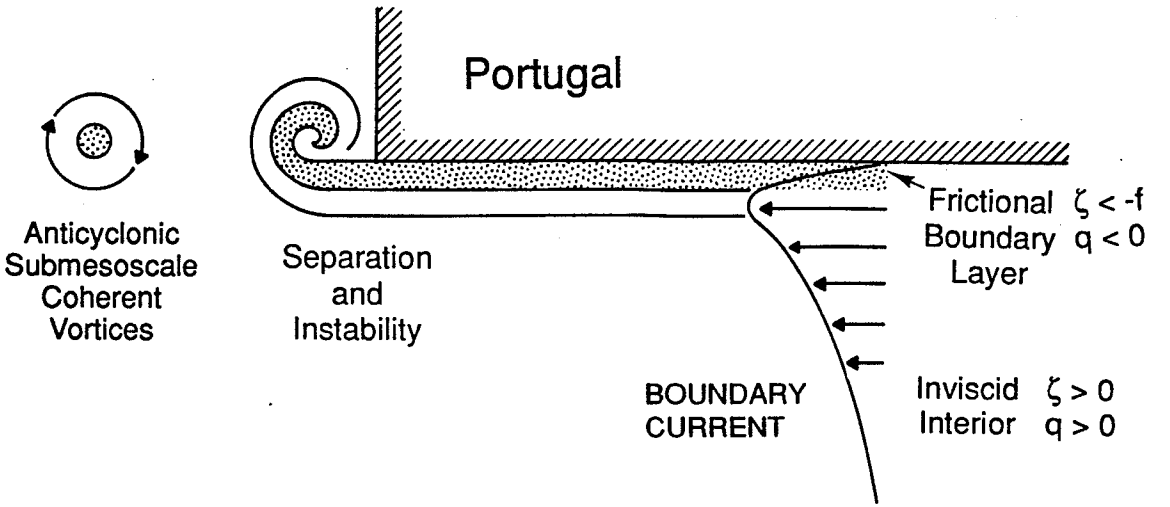

Figure 4.3. Schematic of frictional boundary layer separating from topography, creating a Meddy (adapted from D'Asaro, 1988b).

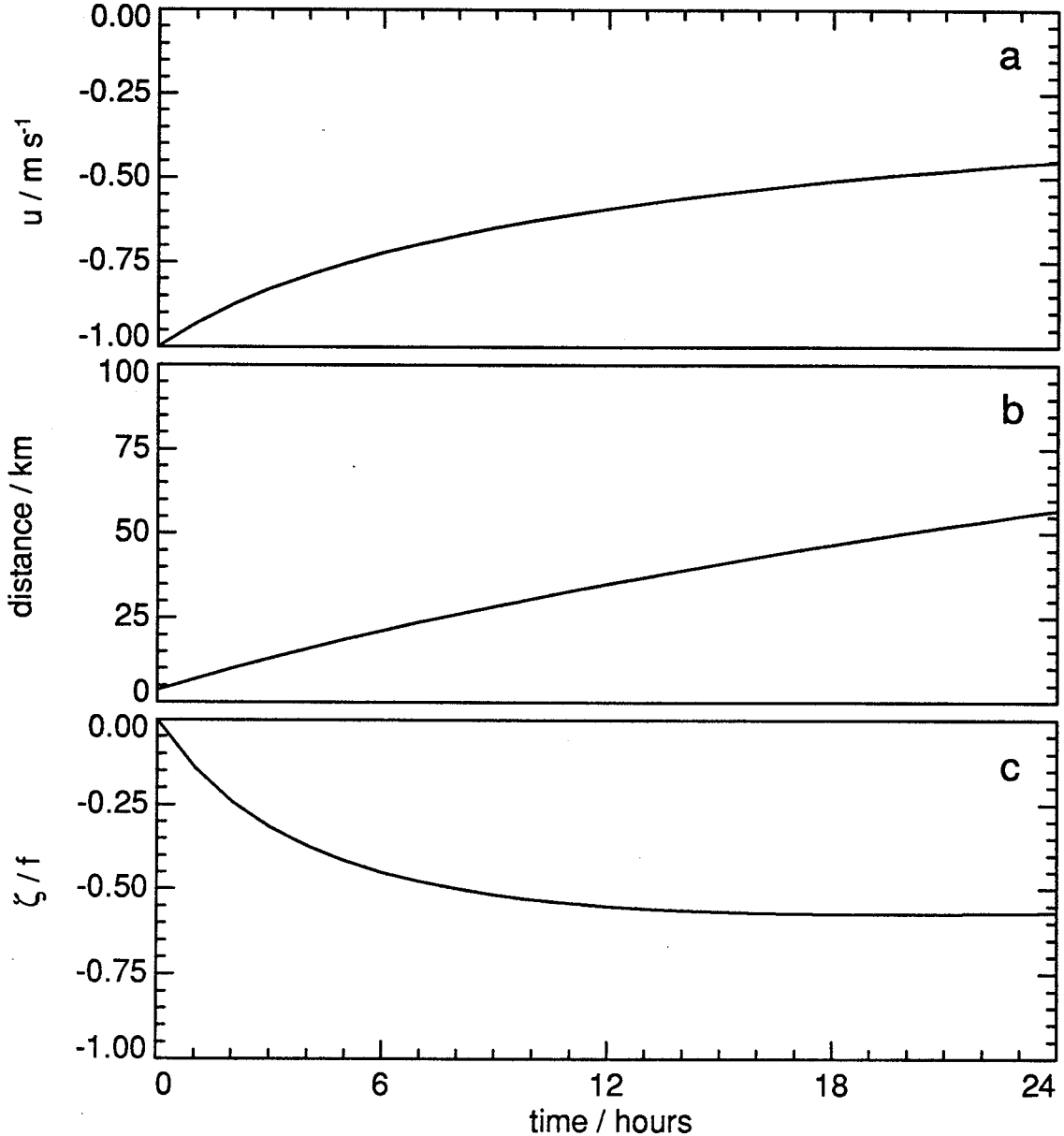

Figure 4.4. Results of along-shore momentum equation with frictional drag, showing the generation of relative vorticity from depth-dependent drag on a flow over a sloping bottom. *a*) Along-shore velocity (positive to the east). *b*) Distance traveled downstream. *c*) Relative vorticity.

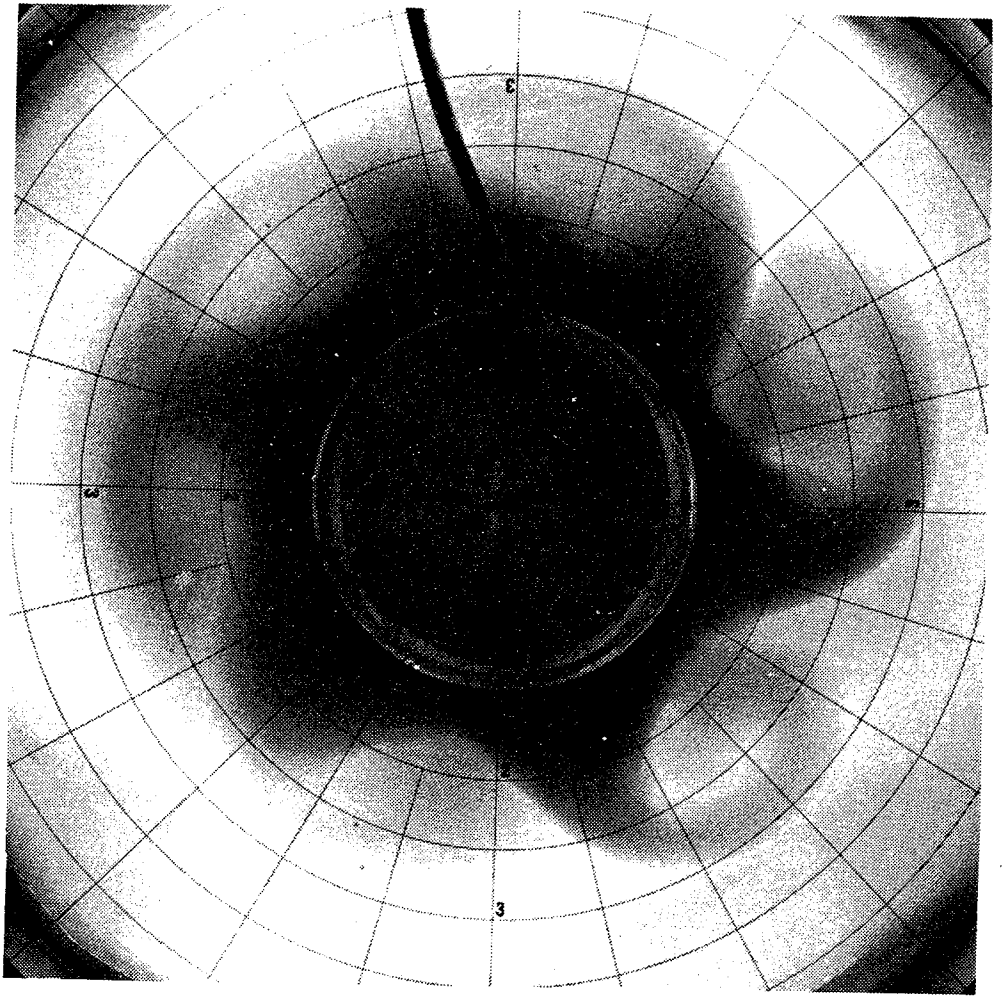

Figure 4.5. Laboratory experiment of boundary current instability (from Griffiths & Linden, 1981). Cyclonic eddies are entraining dyed boundary current waters on the counterclockwise side of each wave crest. The anti-cyclonic eddies are within the crest, and have the same dyed coloration as the boundary current.

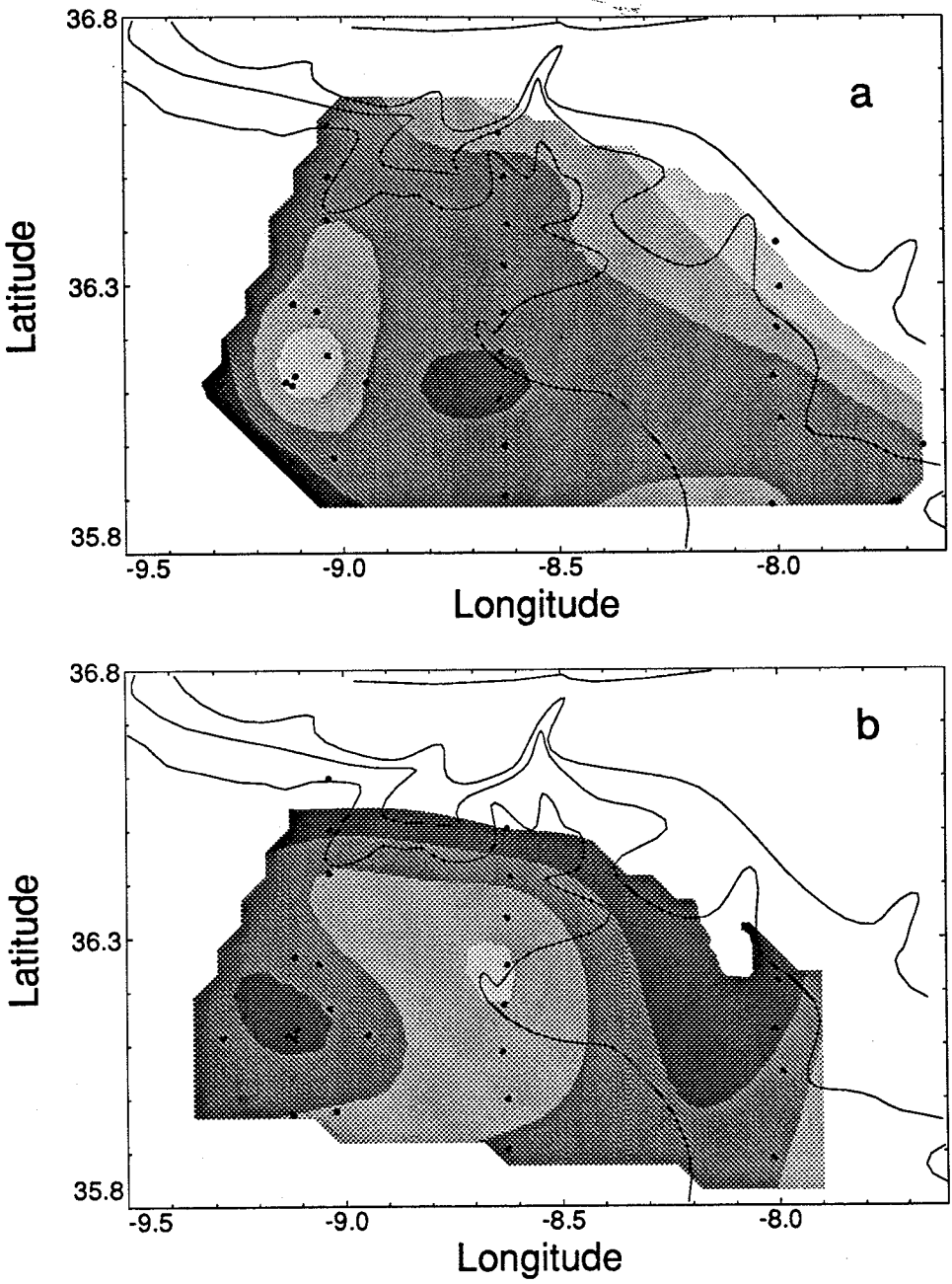

Figure 4.6. Contours of the depths of isopycnals in the Gulf of Cadiz. In both panels, the lightest gray shade is the shallowest, the darkest gray is the deepest. *a*) Depth of the isopycnal (32.1 σ_1) that had the maximum upward displacement above the Meddy. The range of contours is from 930 to 1030 dbars, with shading increments of 25 dbars. *b*) Depth of the isopycnal (32.3 σ_1) that had the maximum downward displacement below the Meddy. The range of contours is from 1290 to 1490 dbars, with shading increments of 50 dbars.

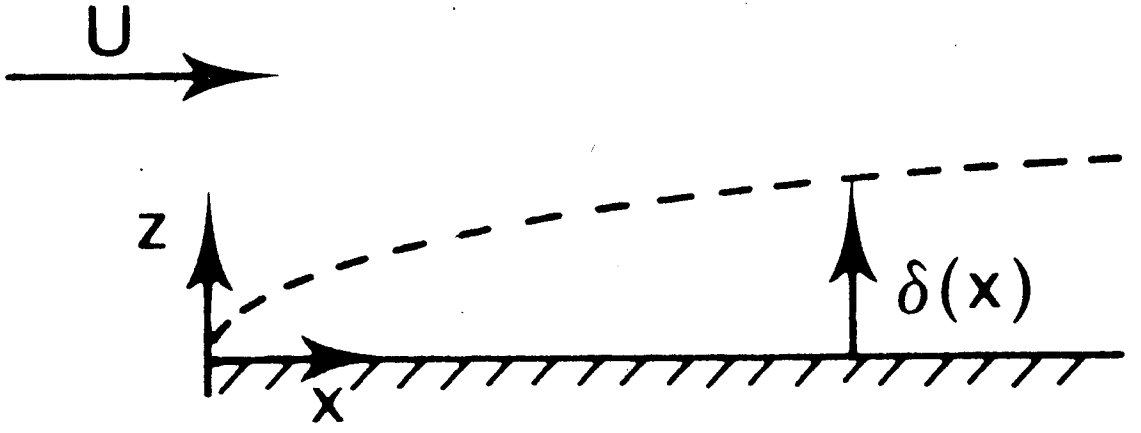

Figure 4.7. Boundary layer formed by flow over a flat plate (adapted from Morton, 1984). All the vorticity in the boundary layer is generated at the leading edge. Afterwards, the vorticity is advected downstream and is diffused vertically into a thickening boundary layer $\delta(x)$. An analogous mechanism may occur in the Mediterranean outflow, with the potential vorticity being injected far upstream and then diffusing (and entraining) along with downstream advection.

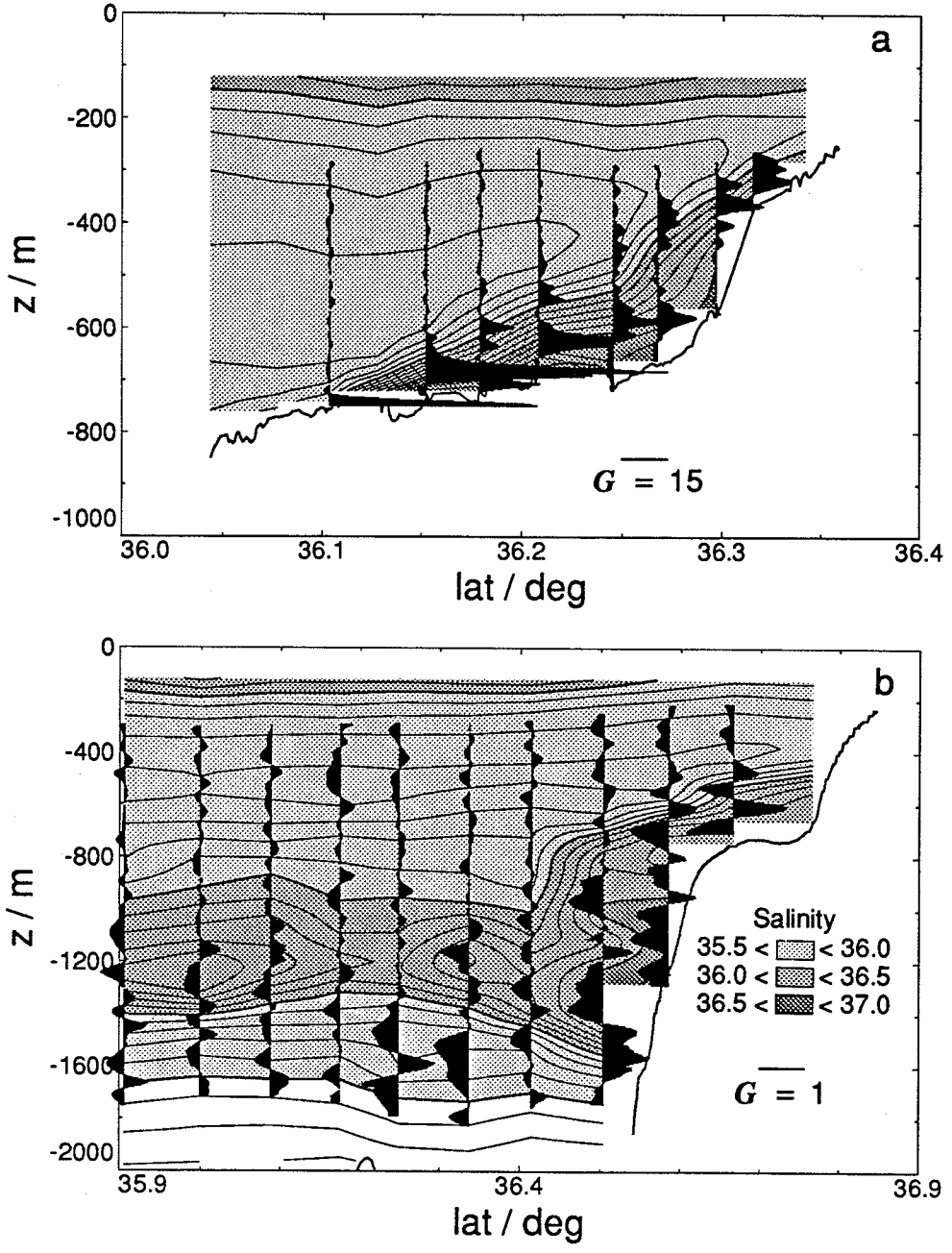

Figure 4.8. Profiles of G superimposed upon contours of salinity. The contour interval for salinity is 0.1 psu. *a*) Line F. *b*) Line 04. The two panels have different vertical and horizontal scales, as well as different scales for the G profiles.

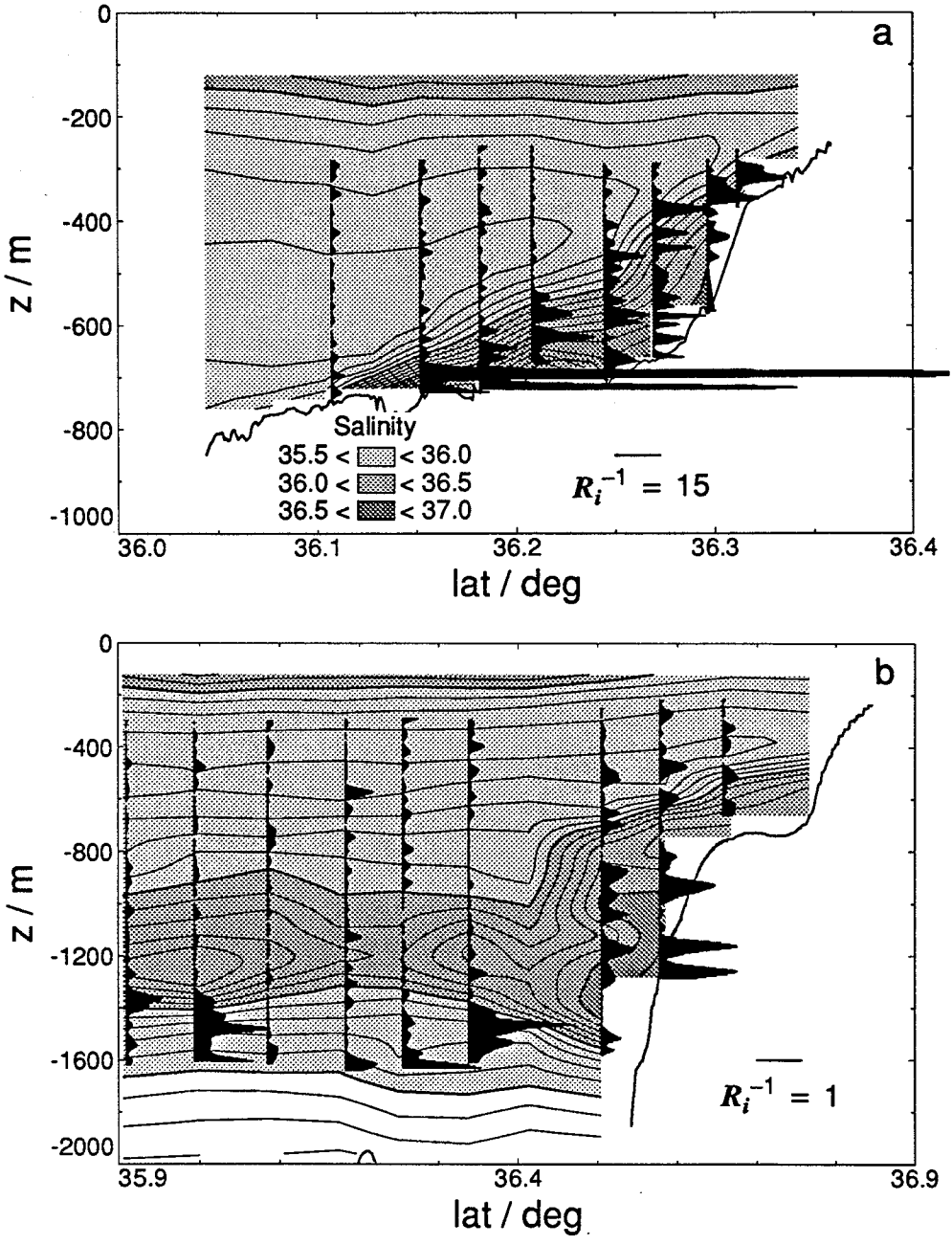

Figure 4.9. Profiles of R_i^{-1} superimposed upon contours of salinity. The contour interval for salinity is 0.1 psu. ***a***) Line F. ***b***) Line 04. The two panels have different vertical and horizontal scales, as well as different scales for the R_i^{-1} profiles.

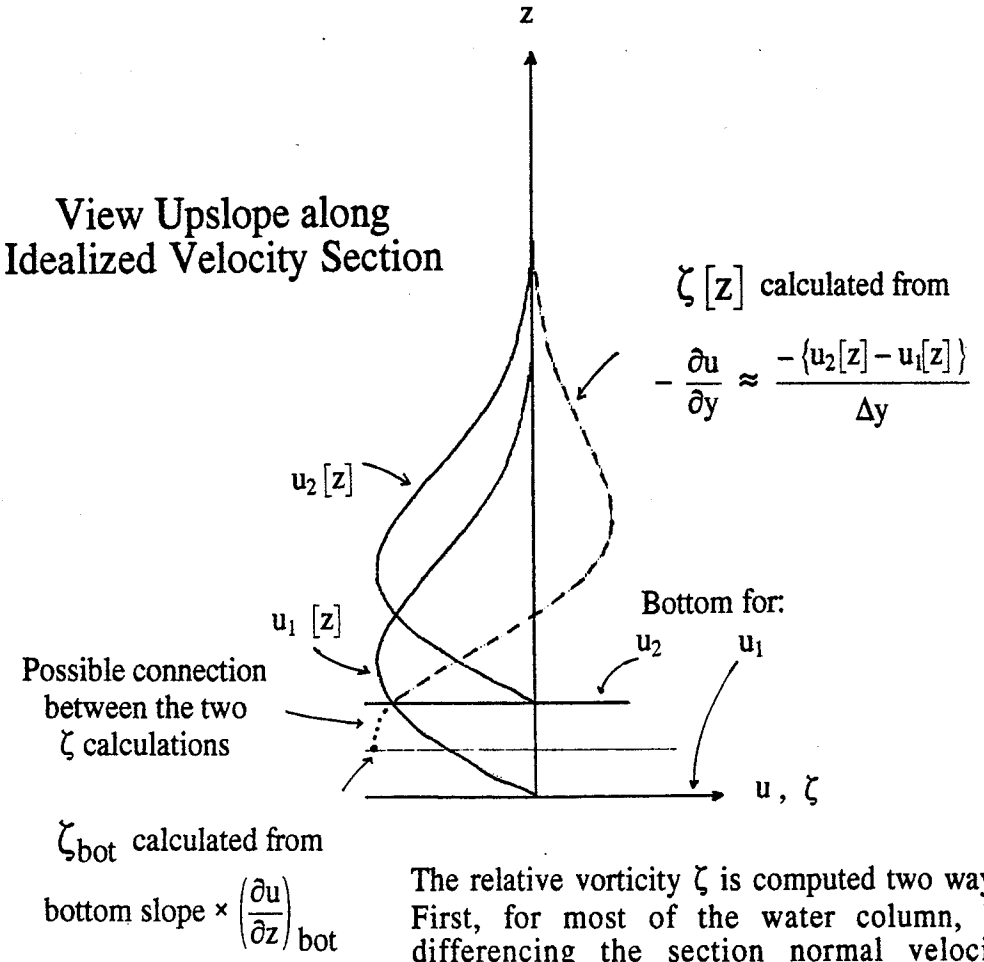

The relative vorticity ζ is computed two ways. First, for most of the water column, by differencing the section normal velocity component from two XCP profiles, and dividing by the profile separation. Secondly, just for the bottom, by multiplying the bottom slope with the section normal vertical shear at the bottom. The two estimates of ζ are then smoothly connected.

Figure 4.10. Example of the calculation of relative vorticity, using i) the velocity difference between two adjacent profiles, and ii) the bottom slope multiplied by the bottom shear.

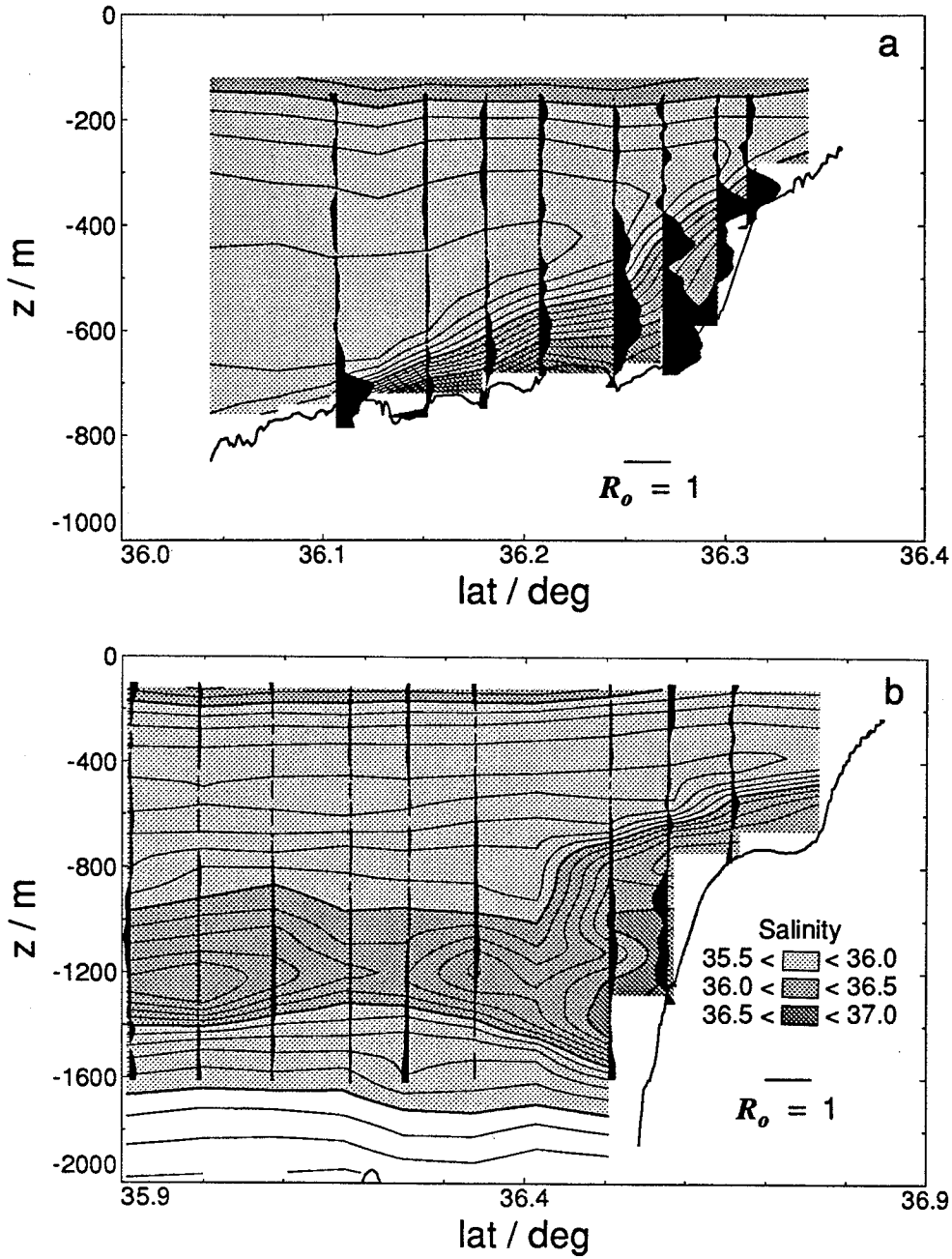

Figure 4.11. Profiles of R_o superimposed upon contours of salinity. The contour interval for salinity is 0.1 psu. *a*) Line F. *b*) Line 04. The two panels have different vertical and horizontal scales, but the same scale for the R_o profiles.

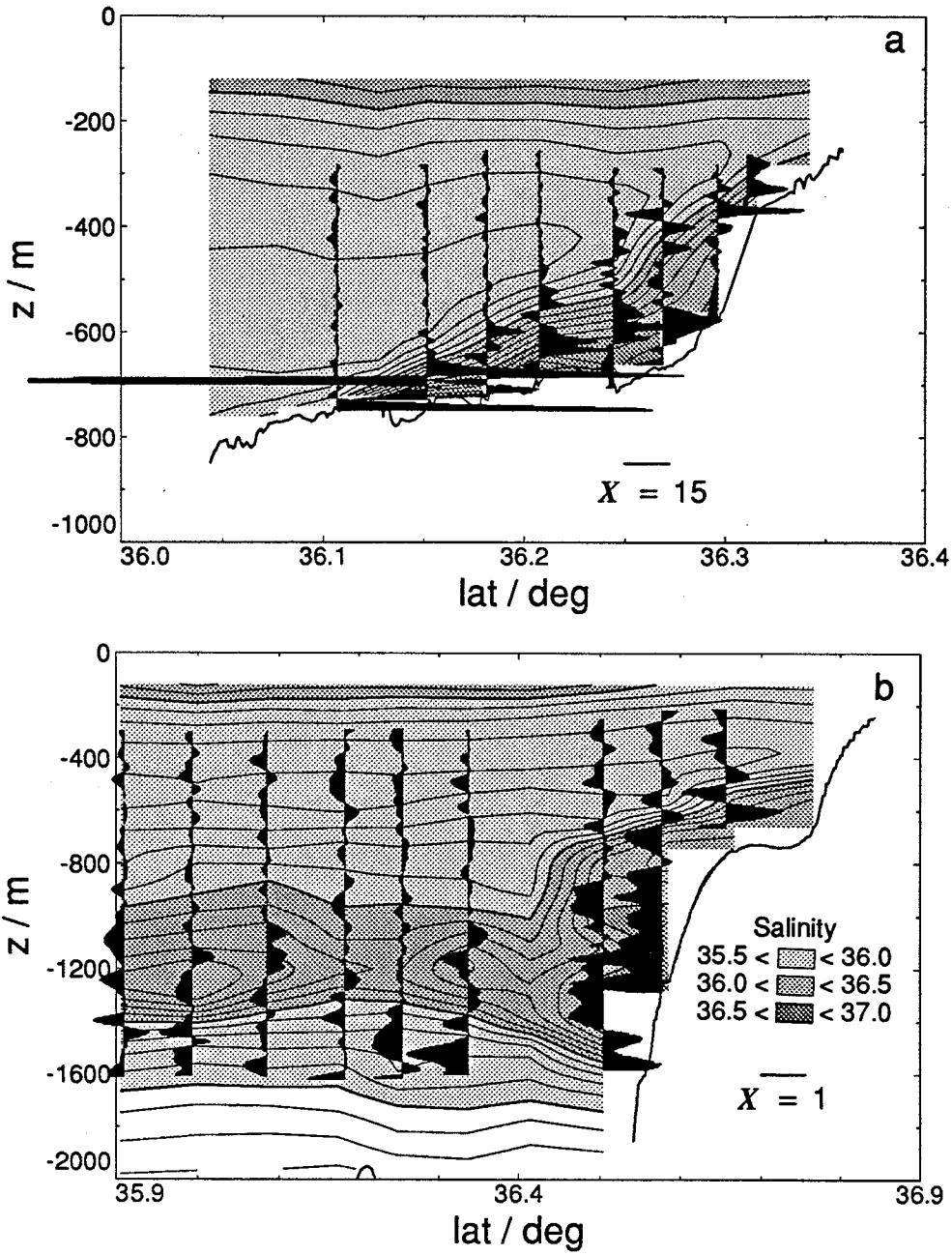

Figure 4.12. Profiles of $X = R_o + G + R_o G - R_i^{-1}$ superimposed upon contours of salinity. The contour interval for salinity is 0.1 psu. *a*) Line F. *b*) Line 04. The two panels have different vertical and horizontal scales, as well as different scales for the X profiles.

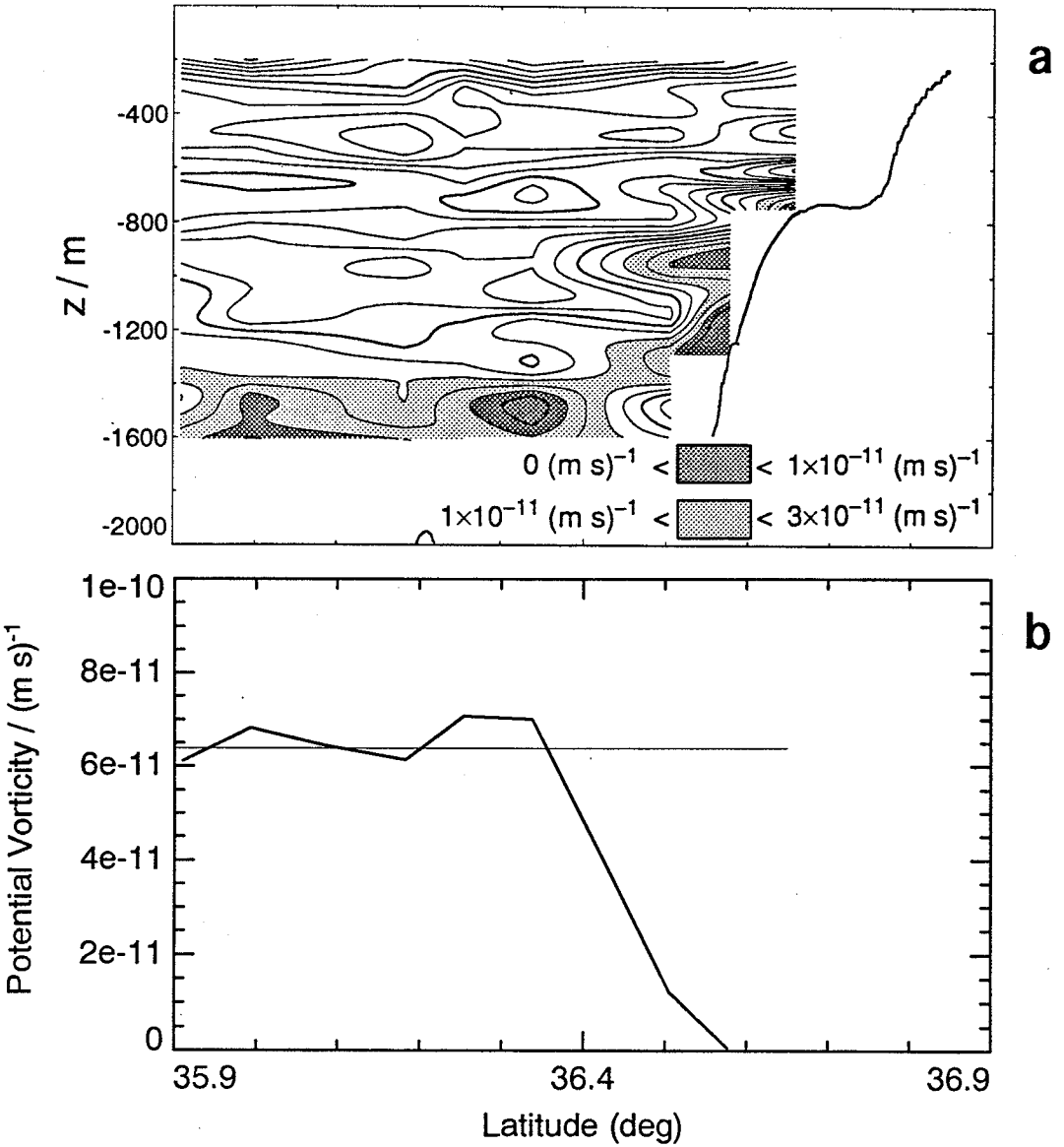

Figure 4.13. *a*) Contours of potential vorticity Q for Line 04. The contour interval is 1×10^{-11} (m s)$^{-1}$. *b*) The potential vorticity anomaly at 925 m extracted from *a*). The light line is the background level of 6.4×10^{-11} (m s)$^{-1}$.

Chapter 5. Summary and Conclusions

5.1 Summary of the Meddy formation process

The following scenario summarizes the processes that led to the Cadiz Meddy. The warm, saline, and very dense waters of the Mediterranean spill over the sills at the Strait of Gibraltar. The outflow then descends, retarded by bottom friction and propelled by gravity, and vigorously entrains the surrounding waters. The nose of the outflow is bounded above by a high entrainment region, with large vertical shears and density gradients. A bottom boundary layer exists below the nose of the outflow, again with high vertical shears and nearly zero density gradient. As the outflow descends, the effect of Coriolis forces the flow to follow along the sloping bathymetry. One effect of having the outflow moving along a sloping bottom is that strong *lateral* density and velocity gradients form. At this point, the bottom portion of the outflow contains very low values of potential vorticity Q, with negative G and positive R_i^{-1}. Within the upper portion of the outflow, G and R_i^{-1} are both positive, and the relative magnitudes of each determine the size of Q. The importance of R_o in the outflow is small compared with that of G and R_i^{-1}.

Continuing on downstream, the outflow slows as it increases its transport through entrainment. The water properties of the outflow are modified and lose some of the strong characteristics of the Mediterranean source waters. Differential entrainment and topographic steering of the outflow cause it to form two water masses, the "upper" and "lower" cores of the outflow. Finally, the combination of entrainment and descent results in an outflow that is neutrally buoyant. The outflow still hugs the coast due to the effect of Coriolis, but the steepening topography causes the bottom to drop away, removing any direct boundary layer effects.

At this point, the outflow begins to meander, perhaps by the combined effect of topography and instability processes. The "lower" core of the outflow might be more susceptible to topographic influences, and thus form meanders more easily. As the meander undergoes anticyclonic curvature, negative relative vorticity is introduced into the outflow. The conservation of potential vorticity (to first order $(f+\zeta)/H$) requires that the isopycnals flatten, reducing the thermal wind-driven vertical shear.

Thus the meander forces an increase in G and a decrease in R_i^{-1}, with a compensating decrease in R_o. Of course, any negative vorticity that existed in the outflow before the meander began also contributes to the final R_o.

If the meander continues until it pinches off, an isolated eddy of Mediterranean outflow water is formed. During the meander and pinching, little ambient Gulf of Cadiz water is entrained. Thus, the Meddy can be traced through its water properties back to its formation site. The Meddy, with its core of large negative vorticity water, is in cyclogeostrophic balance. Compared with the surrounding water, the Meddy is a stratification minimum, as is the Mediterranean outflow.

A cyclonic partner might form along with the Meddy, initiated by cyclonic curvature of the outflow. However, instead of incorporating outflow water as the anticyclonic meander does, the cyclonic meander incorporates ambient Cadiz water.

5.2 Speculations

A final thought on the Cadiz Meddy after our observations: What happened to it? A look at the regional bathymetry (Figure 1.1) might give a clue. The boundary between the Gulf of Cadiz and the eastern Atlantic is made up of a chain of islands and seamounts, with Madeira to the southwest, and the Seine, Ampere, and Horseshoe seamounts and the Gettysburg Banks to the west. The only passage for the Meddy to the Atlantic is through the Seine Abyssal Plain. It seems more likely that the Meddy would encounter topography before reaching the open ocean, and release its salt and heat relatively close to Cape St. Vincent. Evidence of a Meddy encountering seamounts is given by Richardson et al. (1989). They present SOFAR drifter tracks and CTD survey results of a Meddy attempting to pass between the Great Meteor and Hyeres seamounts south of the Azores. The rotational integrity of the Meddy was destroyed by the stirring effect of the seamounts, thus reducing the Q gradients between the Meddy core and the ambient waters and allowing increased radial exchange. Thus the source of the Mediterranean salt tongue might be the seamount barrier between the Gulf of Cadiz and the eastern North Atlantic. The salinity anomaly then advances into the Atlantic thorough mechanisms similar to the advection-diffusion model proposed by Richardson and Mooney (1975). What then accounts for the Meddy observations in the Canary Basin? The mechanism of Käse et al. (1989), in which Meddies are generated

due to instabilities of the Mediterranean outflow as the flow moves northward alone the western coast of Portugal, is the likely answer. From that formation site, the Meddies would have a fairly unobstructed path along the Iberian and Madeira abyssal plains. This might account for the characteristics of Meddies found in that region.

5.3 Conclusions

A unique aspect of the Gulf of Cadiz expedition data set was the discovery of a newly formed Meddy in the vicinity of its place of origin. The observations of the Meddy and of the Mediterranean outflow in the Gulf of Cadiz provided an opportunity to address the properties and dynamics of a young Meddy, and relate those directly to the characteristics of the Mediterranean outflow.

The primary results of this study were as follows:

- The Cadiz Meddy consisted of two vertically aligned lenses, whose water properties arose from the "lower" core of the Mediterranean outflow. The Meddy had a large negative relative vorticity ($-0.85f$) and was in cyclogeostrophic balance.

- The Cadiz Meddy had a larger negative vorticity, a larger aspect ratio, and was less massive than other historical Meddies. These characteristics are probably due to the formation region, since entrainment processes cannot account for the differences.

- The formation site of the Cadiz Meddy was near the canyon region along the continental shelf south of Portugal. This is also where the bathymetry under the outflow steepens and the outflow separates from topography.

- Pure geostrophic adjustment could not have generated the Cadiz Meddy. This mechanism, advocated in various forms by McWilliams (1985, 1988) and Nof (1991), requires an unreasonably large compression of isopycnals to create the Meddy's observed negative relative vorticity. Observations, taken during the Cadiz expedition as well as from historical sources, show that the outflow is never much thicker than the Cadiz Meddy.

- The potential vorticity Q in the Meddy was similar to that in the outflow in the formation region.

- The low Q in the Meddy was dominated by negative relative vorticity ($\propto R_o$) and negative buoyancy anomaly ($\propto G$), while the effect of the tilting term ($\propto R_i^{-1}$) was minor.

- The low Q in the Mediterranean outflow was dominated by large R_i^{-1} and negative G, while the effect of R_o was minor.

- The conversion of R_i^{-1} in the outflow to R_o in the Meddy while preserving Q is consistent with meandering in the outflow. Where anticyclonic curvature is induced, conservation of Q requires a flattening of isopycnals and the subsequent reduction in vertical shear. The cause of the meanders is not necessarily limited to a specific process.

- The flux of the potential vorticity anomaly is not conserved in the outflow immediately upstream from the formation region. Instead, the flux of negative anomaly was greater through an upstream section. The sign of the flux change following the flow downstream was consistent with viscous effects.

- The presence of seamounts and islands separating the Gulf of Cadiz from the eastern North Atlantic might impede the introduction of Cadiz Meddies into the Azores or Canary Basins. Instead, Meddies found there might have formed along the western Portuguese coast, as suggested by Käse et al. (1989).

List of References

Ambar, I., 1983: A shallow core of Mediterranean water off western Portugal. *Deep Sea Res.,* **30A,** 677-680.

Ambar, I., and M. R. Howe, 1979a: Observations of the Mediterranean outflow. I. Mixing in the Mediterranean outflow. *Deep Sea Res.,* **26A,** 535-554.

Ambar, I., and M. R. Howe, 1979b: Observations of the Mediterranean outflow. II. The deep circulation in the vicinity of the Gulf of Cadiz. *Deep Sea Res.,* **26A,** 555-568.

Ambar, I., M. R. Howe, and M. I. Abdullah, 1976. Physical and chemical description of the Mediterranean outflow in the Gulf of Cadiz. *Deutsche Hydrogr. Zeit.,* **29,** 58-68.

Armi, L., and H. Stommel, 1983: Four views of a portion of the North Atlantic subtropical gyre. *J. Phys. Oceanogr.,* **13,** 828-857.

Armi, L., and W. Zenk, 1984: Large lenses of highly saline Mediterranean water. *J. Phys. Oceanogr.,* **14,** 1560-1576.

Armi, L., D. Hebert, N. Oakey, J. Price, P. L. Richardson, T. Rossby, and B. Ruddick, 1989: Two years in the life of a Mediterranean salt lens. *J. Phys. Oceanogr.,* **19,** 354-370.

Baringer, M. O., 1991: Large-scale structure of the Mediterranean Outflow. *Report on the Second Gulf of Cadiz Experiment Workshop,* APL-UW TM 6-91, Applied Physics Laboratory, University of Washington, Seattle, WA, 63 pp.

Beckmann, A., and R. Käse, 1989: Numerical simulation of the movement of a Mediterranean water lens. *Geophys. Res. Lett.,* **16,** 65-68.

Berestov, A. L., et al., 1986: Thermohaline, hydrochemical and dynamical characteristics of an intrusive lens of Mediterranean water as based on the data collected during Mesopolygon-85 expedition. *Intrathermocline eddies in the ocean,* Academy of Sciences of the USSR, Moscow, 35-49.

Bryden, H. L., and H. M. Stommel, 1984: Limiting process that determine basic features of the circulation of the Mediterranean Sea. *Oceanol. Acta,* **7,** 289-296.

Candela, J., C. D. Winant, and H. L. Bryden, 1989: Meteorologically forced subinertial flows through the Strait of Gibraltar. *J. Geophys. Res.,* **94,** 12,667-12,679.

Chen, C.-T., and F. J. Millero, 1977: Speed of sound in seawater at high pressures. *J. Acoust. Soc. Am.,* **62,** 1129-1135.

Cresswell, G. R., 1982: The coalescence of two East Australian Current warm-core eddies. *Science,* **215,** 161-164.

D'Asaro, E., 1988a: Observations of small eddies in the Beaufort Sea. *J. Geophys. Res.,* **93,** 6669-6684.

D'Asaro, E., 1988b: Generation of submesoscale vortices: a new mechanism. *J. Geophys. Res.,* **93,** 6685-6693.

Drazin, P. G., and W. H. Reid, 1981: *Hydrodynamic stability.* Cambridge University Press, 527 pp.

Dunlap, J. H., 1989: Accurate determination of ship's velocity using Loran-C. *Proc. Oceans '89,* **3,** 860-862.

Elliot, B., and T. Sanford, 1986a: The subthermocline lens D1. Part I: description of water properties and velocity profiles. *J. Phys. Oceanogr.,* **16,** 532-548.

Elliot, B., and T. Sanford, 1986b: The subthermocline lens D1. Part II: kinematics and dynamics. *J. Phys. Oceanogr.,* **16,** 549-561.

Flierl, G., and R. Mied, 1985: Frictionally-induced circulation and spin-down of a warm-core ring, *J. Geophys. Res.,* **90,** 8917-8927.

Gill, A. E., 1982: *Atmosphere-ocean dynamics.* Academic Press, 662 pp.

Griffiths, R. W., and P. F. Linden, 1981: The stability of buoyancy-driven coastal currents. *Dyn. Atmos. Oceans,* **5,** 281-306.

Gründlingh, M. L., 1981: On the observation of a solitary event in the Mediterranean outflow west of Gibraltar. *"Meteor" Forsch.-Ergebn., ser. A,* **23** 15-46.

Haynes, P., and M. McIntyre, 1987: On the evolution of vorticity and potential vorticity in the presence of diabatic heating and frictional or other forces. *J. Atmos. Sci.,* **44** 828-841.

Hebert, D., 1988a: *Mediterranean salt lens*. Ph.D. thesis, Dalhousie University, 187 pp.

Hebert, D., 1988b: The available potential energy of an isolated feature. *J. Geophys. Res.*, **93**, 556-564.

Hebert, D., N. Oakey, and B. Ruddick, 1990: Evolution of a Mediterranean salt lens: scalar properties. *J. Phys. Oceanogr.*, **20**, 1468-1483.

Holton, J. R., 1979: *An introduction to dynamic meteorology*. Academic Press, 391 pp.

Howe, M. R., 1982: The Mediterranean water outflow in the Gulf of Cadiz. *Oceanogr. Mar. Biol. Ann. Rev.*, **20**, 37-64.

Howe, M. R., 1984: Current and hydrographical measurements in the Mediterranean undercurrent near Cape St. Vincent. *Oceanol. Acta*, **7(2)**, 163-168.

Howe, M. R., M. I. Abdullah, and S. Dietal, 1974: An interpretation of the double T-S maxima in the Mediterranean outflow using chemical tracers. *J. Mar. Res.*, **32**, 377-386.

Joyce, T. M., 1989: On in situ "calibration" of shipboard ADCPs. *J. Atmos. Oceanic Technol.*, **6**, 169-172.

Käse, R. H., and W. Zenk, 1987: Reconstructed Mediterranean salt lens trajectories. *J. Phys. Oceanogr.*, **17**, 158-163.

Käse, R. H., A. Beckmann, and H. H. Hinrichsen, 1989: Observational evidence of salt lens formation in the Iberian Basin. *J. Geophys. Res.*, **94**, 4905-4912.

Kennelly, M. A., J. H. Dunlap, T. B. Sanford, E. L., Kunze, M. D. Prater, and R. G. Drever, 1989a. The Gulf of Cadiz Expedition: R/V *Oceanus* Cruise 202. APL-UW TR 8914, Applied Physics Laboratory, University of Washington, Seattle, WA, 115 pp.

Kennelly, M. A., T. B. Sanford, and T. W. Lehman, 1989b. CTD Data from the Gulf of Cadiz Expedition: R/V *Oceanus* Cruise 202. APL-UW TR 8917, Applied Physics Laboratory, University of Washington, Seattle, WA, 129 pp.

Kennelly, M. A., M. D. Prater, and T. B. Sanford, 1989c. XBT and XSV Data from the Gulf of Cadiz Expedition: R/V *Oceanus* Cruise 202. APL-UW TR 8920, Applied Physics Laboratory, University of Washington, Seattle, WA, 209 pp.

Kennelly, M. A., M. D. Prater, J. H. Dunlap, E. L Kunze, and T. B. Sanford, 1989d. XCP Data from the Gulf of Cadiz Expedition: R/V *Oceanus* Cruise 202. APL-UW TR 8925, Applied Physics Laboratory, University of Washington, Seattle, WA, 203 pp.

Killworth, P. D., 1983: On the motion of isolated lenses on a beta-plane. *J. Phys. Oceanogr.,* **13,** 368-376.

Kunze, E., 1986: The mean and near-inertial velocity field in a warm-core ring. *J. Phys. Oceanogr.,* **16,** 1444-1461.

Kunze, E., and T. B. Sanford, 1992: Measurement of submesoscale Ertel vorticity near a seamount. *J. Phys. Oceanogr.* (submitted).

Lacombe, H., and C. Richez, 1982: The regime of the Strait of Gibraltar. *Hydrodynamics of semi-enclosed seas,* Proc. 13th Inter. Liege Colloquium on Ocean Hydrodynamics, Elsevier Oceano. Series, 34, J. C. J. Nihoul, Ed., 13-73.

Lueck, R., 1991: Bottom stress. *Report on the Second Gulf of Cadiz Experiment Workshop,* APL-UW TM 6-91, Applied Physics Laboratory, University of Washington, Seattle, WA, 63 pp.

MacCready, P., and P. B. Rhines, 1992: Slippery bottom boundary layers on a slope. *J. Phys. Oceanogr.* (submitted).

Madelain, F., 1970: Influence de la topographie du fond sur L'ecoulement Mediterraneen entre le Detroit de Gibraltar et le Cap Saint-Vincent. *Cahiers Oceanogr.,* **22,** 43-61.

McDowell, S. E., and H. T. Rossby, 1978: Mediterranean water: an intense mesoscale eddy off the Bahamas. *Science,* **202,** 1085-1087.

McWilliams, J. C., 1985: Submesoscale, coherent vortices in the ocean. *Reviews of Geophysics,* **23,** 165-182.

McWilliams, J. C., 1988: Vortex generation through balanced adjustment. *J. Phys. Oceanogr.,* **18,** 1178-1192.

McWilliams, J. C., 1989: Statistical properties of decaying geostrophic turbulence. *J. Fluid Mech.,* **198,** 199-230.

McWilliams, J. C., and P. R. Gent, 1986: The evolution of sub-mesoscale, coherent vortices on the β-plane. *Geophys. Astrophys. Fluid Dynamics,* **35,** 235-255.

Morton, B. R., 1984: The generation and decay of vorticity. *Geophys. Astrophys. Fluid Dynamics,* **28,** 277-308.

Munk, W., 1981: Internal waves and small-scale processes. *Evolution of physical oceanography,* B. Warren and C. Wunsch, Eds., MIT Press, pp. 264-291.

Nof, D., 1982: On the β-induced movement of isolated baroclinic eddies. *J. Phys. Oceanogr.,* **11,** 1662-1672.

Nof, D., 1991: Lenses generated by intermittent currents. *Deep-Sea Res.,* **38,** 325-345.

Ochoa, J., and N. Bray, 1991: Water mass exchange in the Gulf of Cadiz. *Deep-Sea Res.,* **38,** S465-S503.

Pedlosky, J., 1979: *Geophysical fluid dynamics.* Springer-Verlag, 624 pp.

Piip, A. T., 1969: Large cells of Mediterranean water in the Madeira-Canaries region. *Trans. Amer. Geophys. Union (EOS)* **50,** 193.

Polvani, L. M., 1991: Two-layer geostrophic vortex dynamics. Part 2. Alignment and two-layer V-states. *J. Fluid Mech.,* **225,** 241-270.

Prater, M. D., 1991: A method for depth and temperature correction of expendable probes. *J. Atmos. Oceanic Technol.,* **8,** 888-894.

Reid, R. O., B. A. Elliot, and D. B. Olson, 1981: Available potential energy: a clarification. *J. Phys. Oceanogr.,* **11,** 15-29.

Richardson, P. L., and K. Mooney, 1975: The Mediterranean outflow—a simple advection-diffusion model. *J. Phys. Oceanogr.,* **5,** 476-482.

Richardson, P. L., D. Walsh, L. Armi, M. Schröder, and J. F. Price, 1989: Tracking three Meddies with SOFAR floats. *J. Phys. Oceanogr.,* **19,** 371-383.

Ruddick, B., and D. Hebert, 1988: The mixing of Meddy "Sharon". *Small-scale turbulence and mixing in the ocean,* Proc. 19th Inter. Liege Colloquium on Ocean Hydrodynamics, Elsevier Oceano. Series, 46, J. C. J. Nihoul, Ed., 249-261.

Sanford, T.B., 1971: Motionally induced electric and magnetic fields in the sea. *J. Geophys. Res.,* **76,** 3476-3492.

Sanford, T. B., 1982: Velocity profiling: some expectations and assurances. *Proc. IEEE Conf. on Current Meas.,* 101-112.

Saunders, P. M., 1981: Practical conversion of pressure to depth. *J. Phys. Oceanogr.,* **11,** 573-574.

Saunders, P. M., and N. P. Fofonoff, 1976: Conversion of pressure to depth in the ocean. *Deep-Sea Res.,* **23,** 109-111.

Schultz Tokos, K. L, 1989: *Kinematics and dynamics of a Mediterranean salt lens.* M.S. thesis, University of Rhode Island, 95 pp.

Schultz Tokos, K., and T. Rossby, 1991: Kinematics and dynamics of a Mediterranean salt lens. *J. Phys. Oceanogr.,* **21,** 879-892.

Sippican Ocean Systems Inc., 1983: *Operation and Maintenance Manual: MK9 Oceanographic Data System.* Sippican Ocean Systems Inc., 216 pp.

Smith, R. C., and K. S. Baker, 1985: Spatial and temporal patterns in pigment biomass in Gulf Stream warm-core ring 82B and its environs. *J. Geophys. Res.,* **90,** 8859-8870.

Stammer, D., H. H. Hinrichsen, and R. H. Käse, 1991: Can Meddies be detected by satellite altimetry? *J. Geophys. Res.,* **96,** 7005-7014.

Stanton, B. R., 1983: Low frequency variability in the Mediterranean outflow west of Gibraltar. *Deep Sea Res.,* **30A,** 743-761.

Stern, M. E., and J. A. Whitehead, 1990: Separation of a boundary jet in a rotating fluid. *J. Fluid Mech.,* **217,** 41-69.

Thorpe, S. A., 1976: Variability of the Mediterranean undercurrent in the Gulf of Cadiz. *Deep-Sea Res.,* **23,** 711-727.

Vastano, A. C., and D. E. Hagan, 1977: Observational evidence for transformation of tropospheric waters within cyclonic rings. *J. Phys. Oceanogr.,* **7,** 938-943.

Yegorikhin, V. D., et al., 1987: An intrathermocline lens of Mediterranean water in the tropical North Atlantic. *Oceanology,* **27,** 121-127.

Vorob'yev, V. N., Ye. Yu. Klyuykov, Ye. M. Ovchinnikov, and P. P. Provotorov, 1988: Thermohaline Structure of a lens of Mediterranean water in the Canary Basin. *Oceanology,* **28,** 711-715.

Zenk, W., 1970: On the temperature and salinity structure of the Mediterranean water in the northeast Atlantic. *Deep Sea Res.,* **17,** 627-631.

Zenk, W., 1975a: Some current and temperature observations in the Mediterranean outflow west of Gibraltar; a data report. *"Meteor" Forsch.-Ergebn., ser. A,* **15,** 20-48.

Zenk, W., 1975b: On the Mediterranean outflow west of Gibraltar. *"Meteor" Forsch.-Ergebn., ser. A,* **16,** 23-24.

Zenk, W., 1980: The sub-Mediterranean undercurrent. *Deep Sea Res.,* **27A,** 97-98.

Zenk, W., and L. Armi, 1990: The complex spreading pattern of Mediterranean water off the Portuguese continental slope. *Deep Sea Res.,* **37,** 1805-1823.

Zubin, A. B., and R. V. Ozmidov, 1988: A lens of Mediterranean water in the vicinity of the Ampère and Josephine seamounts. *Trans. U.S.S.R. Academy of Sciences, Earth Sci. Sec.,* **292,** 197-200.

Appendix A. Referencing the XCP Velocities

Introduction

The XCP measures relative velocity; that is, the horizontal velocity is known only to a depth invariant offset (Sanford, 1982). This is expressed as

$$v_{xcp}(z) = v_{abs}(z) - \overline{v}^* \tag{A.1}$$

The offset, $\overline{v}^*$ (Sanford, 1971), is the conductivity weighted vertical average of horizontal velocity. If the electrical conductance of the seabed is small compared with that of the water column, and if the conductivity of the seawater is nearly constant with depth, then $\overline{v}^* \approx \overline{v}$, the barotropic water velocity. If $\overline{v}^*$ is known or can be estimated, then the absolute velocity can be determined from (A.1). However, the desired end result of the XCP referencing is a velocity profile not referenced to earth (as an absolute velocity), but referenced to the translating Meddy. The translation velocity of the Meddy, as well as the XCP drop locations referenced to the moving Meddy, is obtained by the method of Section 2.3.

Three methods of referencing the XCPs to the Meddy were attempted. The first assumed a layer of constant-but-unknown-motion, while the second used a computed layer-of-known-motion. The third method references the XCP velocities directly with respect to the Meddy, and although perhaps not as general as the first two methods, proved to better represent an axially symmetric eddy. The assumption of axial symmetry does not rule out the possibility of ellipticity.

Layer-of-unknown-motion

The first approach follows Ambar and Howe (1979b), who used hydrographic data in studying the Mediterranean outflow through the Gulf of Cadiz to assume a reference layer-of-no-motion. This layer was assumed to be within the transition region between the eastward flowing North Atlantic water at the surface and the deeper westward flowing Mediterranean Outflow water. The interface between the two water types was taken to be the salinity minimum just above the Mediterranean water intrusion. Recent work (Baringer, personal communication, 1991) suggests that the layer-of-no-motion interface should be slightly deeper than this minimum, due to the inflowing Atlantic waters entraining high-salinity Mediterranean waters near the interface. Ambar and

Howe (1979a) found the salinity minimum above the outflow at -400 to -600 m. The salinity minimum near the Meddy was found from CTD data at ≈ -550 m. At best, the layer-of-no-motion might be valid as a time-mean estimate; it is probably not valid at any one time due to internal wave fluctuations. In this dissertation, the salinity minimum reference layer was assumed not to be stationary, but to be moving at a constant but unknown speed. Thus, to first order, the XCP data were referenced so that each horizontal component of velocity had a zero mean between -500 and -600 m.

As a second-order correction, we assume that the reference layer is moving, but at an unknown, constant velocity. An analytical representation of an axially symmetric Meddy was developed, having solid-body rotation out to a radius R, and r^{-1} decay thereafter. The model had six parameters: the radius $R_{\max}$; $V_{\max}$, the azimuthal water velocity at $R_{\max}$; the center of the Meddy, X and Y; and the translation speed of the reference layer, U and V. A nonlinear least-squares fit of the parameters to the data at various depths was used, with the results shown in Figure A.1. The reference layer was found to be moving approximately 3 cm s^{-1} to the north. The center of the Meddy was estimated to be at -9.19 ^{o} E and 36.11 ^{o} N. The XCP velocity vectors at -1050 m referenced by this method are given in Figure A.2.

Layer-of-known-motion

The second approach used the combined RDI acoustic Doppler current profiler (ADCP) data with the LORAN-C positioning of the ship. The ADCP measures the velocity of the water at a given layer relative to the ship ($v_{w/s}(z)$), while the LORAN-C measurements give the velocity of the ship relative to the ground, that is, to earth's fixed reference frame ($v_{s/g}$). The addition of these two measurements gives the "absolute" or "true" velocity of the water relative to ground ($v_{abs}(z)$). Using measurements from the XCP, the ADCP, and LORAN-C,

$$v_{abs}(z) = v_{w/s}(z) + v_{s/g} = v_{xcp}(z) + \overline{v}^{*} \tag{A.2}$$

With < > denoting a vertical average over a range where the XCP and the ADCP have data in common,

$$< v_{abs}(z) > \; = \; < v_{w/s}(z) > \; + \; v_{s/g} \; = \; < v_{xcp}(z) > \; + \; \overline{v}^* \tag{A.3}$$

Solving for $\overline{v}^*$,

$$\overline{v}^* \; = \; < v_{xcp}(z) > \; - \; \left[< v_{w/s}(z) > \; + \; v_{s/g} \right] \tag{A.4}$$

Using (A.2) and (A.4), a vertical profile of absolute velocity is obtained, such that

$$v_{abs}(z) \; = \; v_{xcp}(z) \; - \; < v_{xcp}(z) > \; + \; \left[< v_{w/s}(z) > \; + \; v_{s/g} \right] \tag{A.5}$$

In the implementation of the method, the ADCP and the XCP velocity data were averaged over the interval -100 to -190 m. This particular interval was chosen for three reasons:

i) the high vertical wavenumber internal wave signals in the instantaneous velocities obtained by the XCP are averaged out,

ii) both the XCP and the ADCP returned good data over that interval, and

iii) the interval was deeper than the mixed layer and other near surface effects.

A method given by Joyce (1989) was used to compute $< v_{abs}(z) >$ by combining the ADCP and the LORAN-C velocities while correcting for possible errors in the ADCP alignment and the ship's gyro. A time-series of $< v_{abs}(z) >$ was obtained, then low-pass filtered using a 3-dB point of 2 hours to reduce the velocity variance due to noise in the LORAN-C measurements. The filtered $< v_{abs}(z) >$ time-series was then sampled at the times of XCP drops, and the resulting velocity values were used to modify $v_{xcp}(z)$. Figure A.3 presents vector plots of $< v_{abs}(z) >$ in the reference layer, estimates of $\overline{v}^*$, and the referenced XCP velocities at -1050 m. Due to the noise in the LORAN-C velocity estimates (rms error in velocity near 0.1 m s^{-1} most of the time) and the difference in the ADCP and the LORAN-C responses to changes in ship speed, the results of this method were not used in this dissertation. The LORAN-C data also suffered from low signal-to-noise ratios as well as small crossing angles between stations, which contributed to the degradation of the velocity estimates. However, the method does promise to be a useful way to reference XCP velocities.

Layers-of-relative-motion

This final method is probably the most arbitrary and the least flexible of the three referencing techniques. However, this method, directly derived from the XCP data, produces the most axially symmetric Meddy. Shown in Figure A.4 are the velocity profiles from XCP drops 2501 and 2507, which from Figure 2.7b are on nearly opposite sides of the Meddy. The mean velocity from -400 to -700 m has been removed from the profiles. In the v velocity component, a strong vertical shear across the Meddy is observed. If the XCP velocities are referenced to either the layer above or below the Meddy, the Meddy would appear distorted, as if the Meddy were in a mean flow. Figure A.5a shows the mean velocity from -1500 to -1600 m relative to the reference layer, which is the same as the vertical shear over the 1000 m separating the two layers. The mean velocity difference is 6 cm s^{-1} to the north and 2 cm s^{-1} to the west. To correct the distortion of using just the upper layer as a reference, one-half of the velocity difference between the reference layer and the deeper layer was added to each velocity profile, or

$$v(z) = v_{400\text{–}700}(z) + \frac{v_{400\text{–}700} - v_{1500\text{–}1600}}{2}$$

where "400-700" denotes a reference to the -400 to -700 meter level, and "1500-1600" denotes the -1500 to -1600 meter average reference to $v_{400\text{–}700}$. Since the structure of the shear through the Meddy was not known, a more elegant interpolation between the two layers was not attempted. The resulting XCP velocity vectors at -1050 m are shown in Figure A.5b.

Discussion

The final method described was used to reference the XCPs in this dissertation. The first method, although producing in Figure A.2 the same qualitative picture of the Meddy velocity structure as in Figure A.5b, is flawed in that it is unlikely that over the 16 hours of the fine-scale Meddy survey any layer was moving with a constant velocity due to internal wave and tide activity. The second method, using the ADCP and LORAN-C, suffers from extremely high noise levels in the LORAN-C velocities. In addition, the 90 m interval used for the vertical average is probably insufficient to completely average out the vertical wavenumber structure of the XCP and ADCP velocity profiles, which is a source of additional noise.

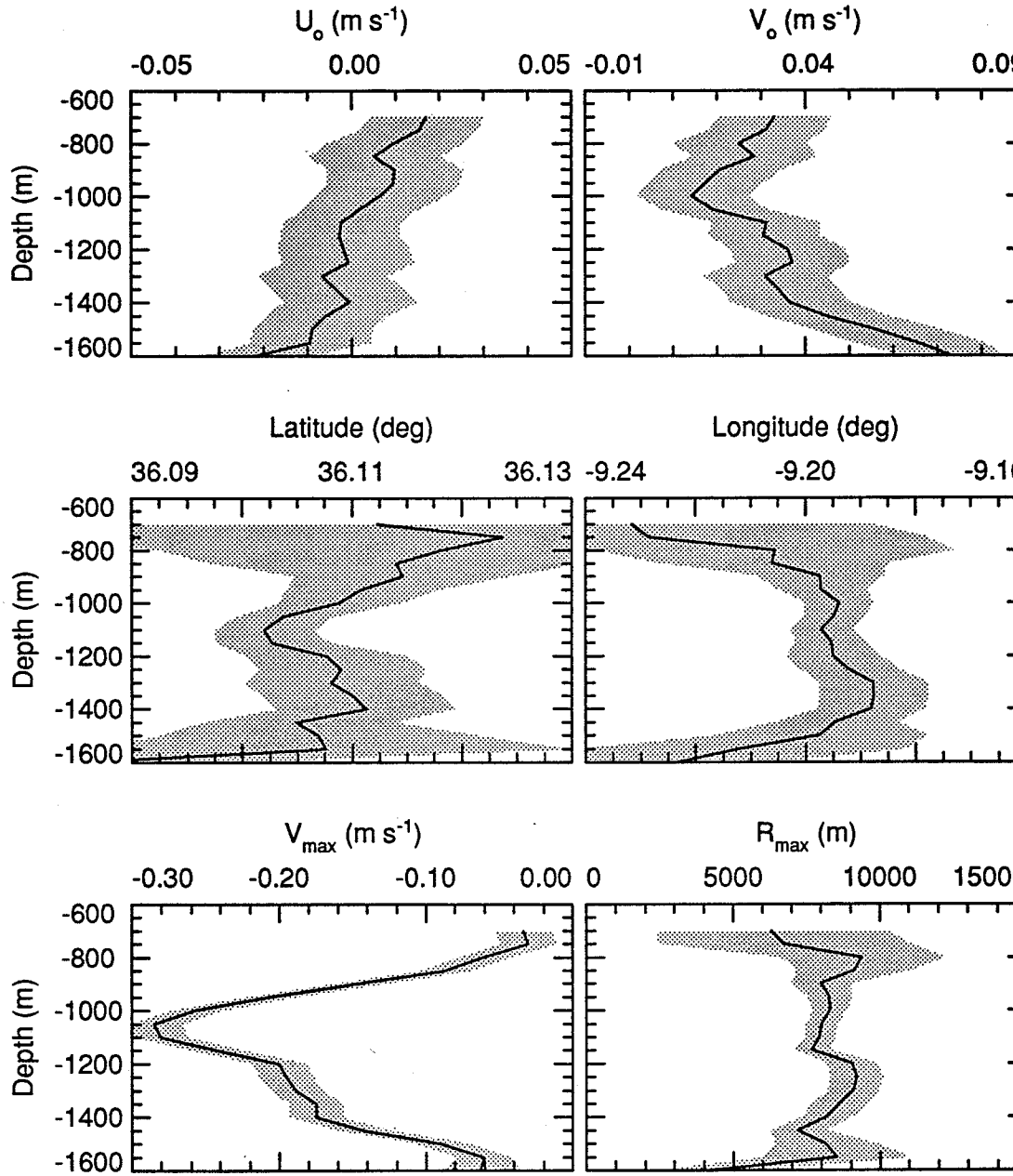

Figure A.1. Results of Meddy model fit to XCP velocity data. Fit was done on data averaged over 50 m, at 50 m intervals from -700 to -1600 m. The shaded regions denote the 3σ error range, with the combination of XCP velocity and the radial position of the XCP drop assumed to have an equivalent accuracy of 2 cm s^{-1}.

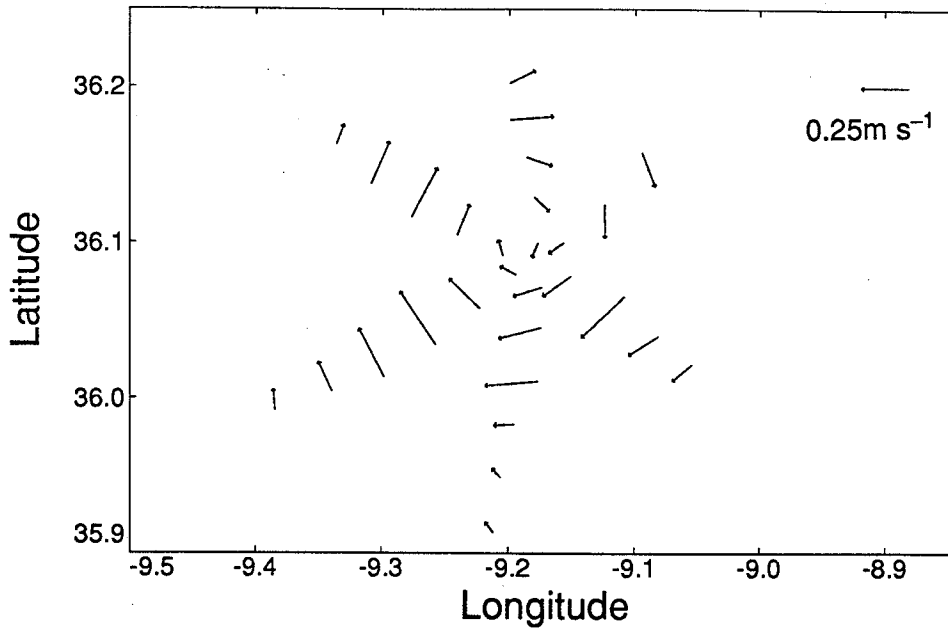

Figure A.2. XCP velocity vectors at -1050 m, referenced by combining layer of constant velocity at -500 to -600 with the results of a Meddy model fit to a uniformly moving layer.

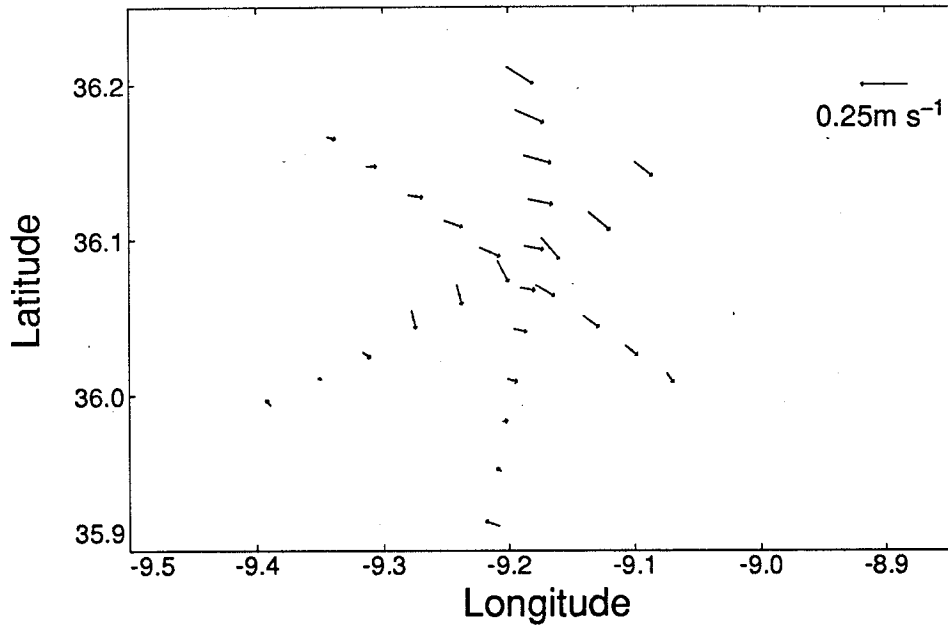

Figure A.3a. Absolute velocity vectors for the -100 to -190 m layer, obtained by combined ADCP and LORAN-C velocities.

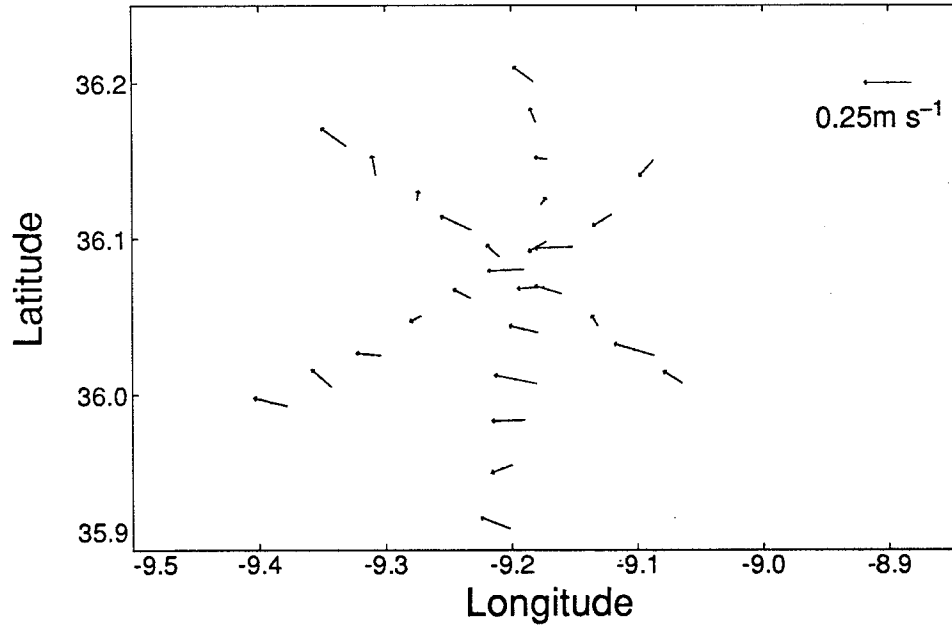

Figure A.3b. Estimates of $\overline{v}*$ vectors computed by $< v_{abs}(z) > - < v_{xcp}(z) >$.

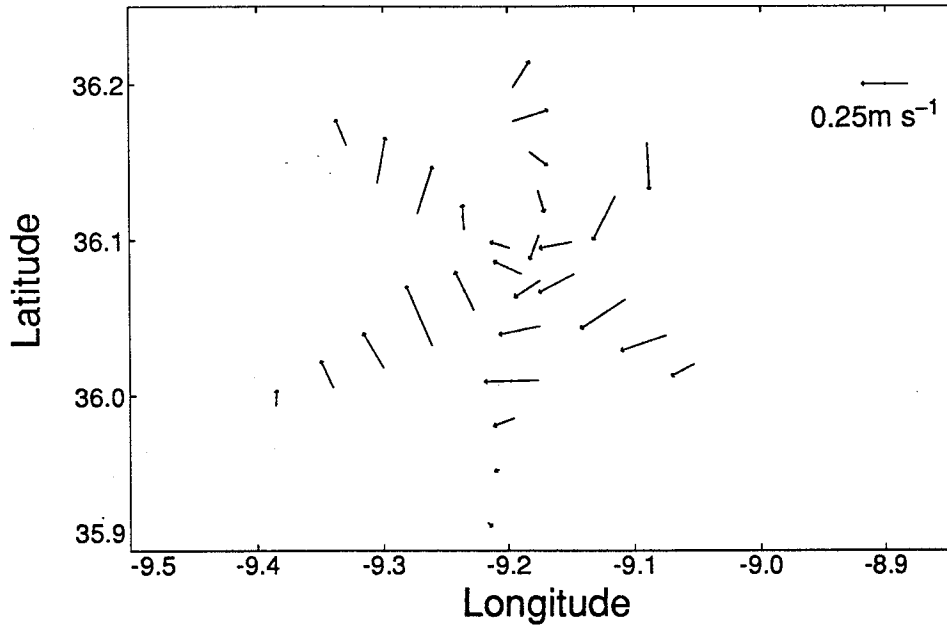

Figure A.3c. XCP velocity vectors at -1050 m, referenced by the combination of ADCP and LORAN-C velocity data.

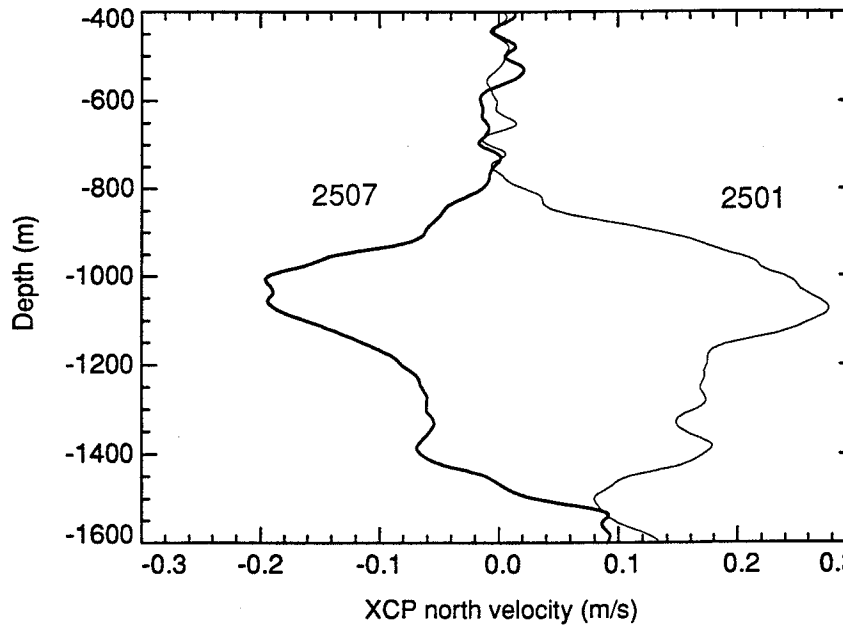

Figure A.4. The north velocity component for XCP 2501 (light) and XCP 2507 (dark), referenced to the -400 m to -700 m layer. The background vertical shear on which the Meddy is superimposed is evident.

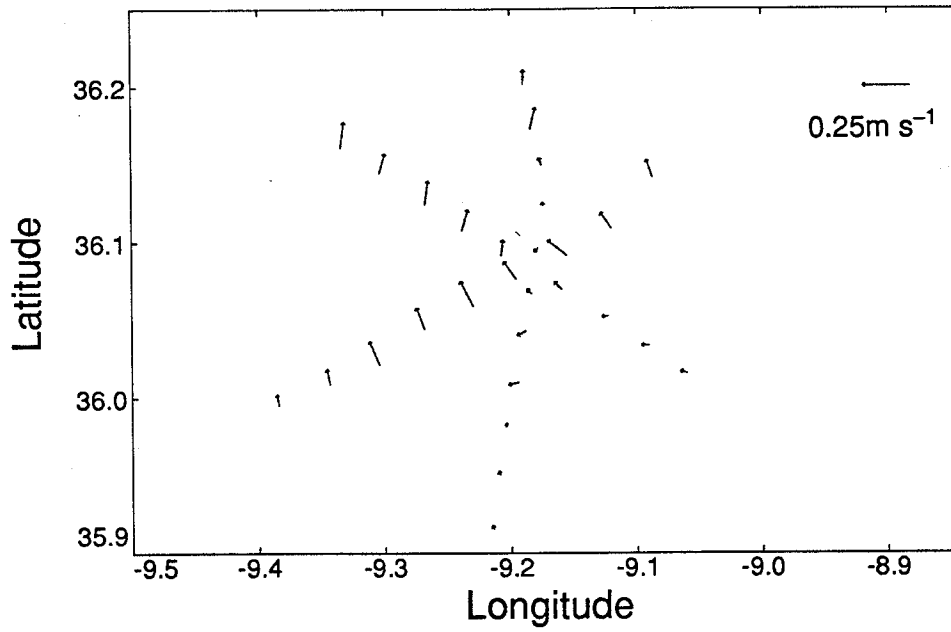

Figure A.5a. XCP velocity vectors averaged from -1500 m to -1600 m referenced to the -400 m to -700 m layer. This shows the horizontal distribution of the vertical shear in which the Meddy exists.

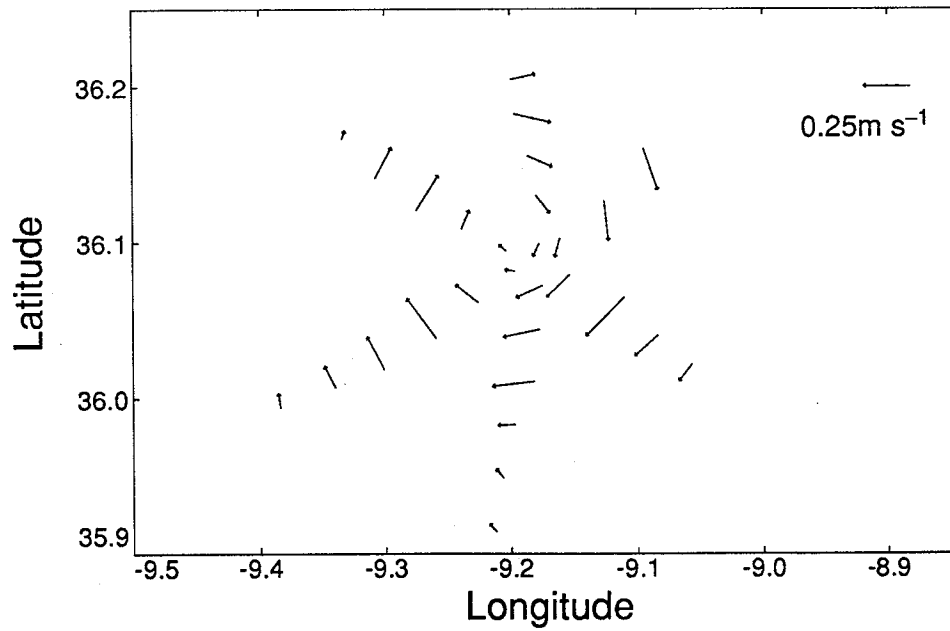

Figure A.5b. XCP velocity vectors at -1050 m, referenced by the mean velocity of the -400 m to -700 m layer and the -1500 m to -1600 m layer.

Appendix B. Estimating Salinity from Sound Velocity and Temperature

For the Gulf of Cadiz cruise, we anticipated that reasonable estimates of salinity could be obtained from the combination of sound speed from XSVs and temperature from XBTs—thus the ship could continue steaming and the typical 90 minute CTD station could be avoided.

The equations for sound speed in seawater, accepted as the current standard in the oceanographic community, were developed by Chen and Millero (1977) as a fit to laboratory data, and can be expressed as

$$U_{sw}^{P} = U_{pw}^{P} + (U_{pw}^{o} - U_{sw}^{o}) \tag{B.1}$$

where U is sound speed; the subscripts sw and pw denote seawater and pure water, respectively; the superscripts P and o denote *in situ* pressure and zero pressure, respectively; and A, B, and C are functions of temperature and pressure. The XSV measures U_{sw}^{P}, and the other values of sound speed can be obtained from expressions independent of the salinity S. Given T, the pressure P inferred from the time-of-fall of the expendable probes, and the sound speed U_{sw}^{P}, the above polynomial can be solved (or "inverted") for S. However, the sound speed is a strong function of temperature and pressure, and only weakly dependent on salinity. Thus, the inversion of (B.1) produces salinities that are highly sensitive to temperature and pressure. The sensitivity of sound speed to the variables required is presented in Table B.1, and was computed numerically.

Table B.1. Sensitivity of Chen & Millero (1977) Inversion

Variable	Sensitivity	Accuracy for 0.1 psu	Accuracy of Probes
P	-0.0138 psu / dbar	7.2 dbars	2% of depth
T	-2.8775 psu / °C	0.035 °C	0.15 °C
U	0.8340 psu / m s^{-1}	0.12 m s^{-1}	0.25 m s^{-1}

The sound velocity equation of Chen & Millero itself has an uncertainty of 0.2 m s^{-1}. From Table B.1, this uncertainty can lead to an error of 0.2 psu in salinity. For comparison purposes, the sensitivities of the standard salinity computation from temperature, pressure, and conductivity (C) are given in Table B.2.

Due to the sensitivity of the sound velocity inversion to pressure, temperature, and sound velocity, computing salinity from an expendable conductivity cell of moderate accuracy is far better than from an expendable sound velocity probe of very good accuracy.

However, due to the lack of salinity data around the Meddy, computed salinity was used to form a qualitative picture of the Meddy structure. The two expendable probes were deployed simultaneously from the two sides of the R/V *Oceanus*'s fantail, and form a "drop-pair". The high vertical wavenumber features from the temperature and the sound speed from a drop pair were correlated, and the sound speed profile was adjusted in depth (e.g., Prater, 1991) to maximize the correlation. Then, salinity was computed using (B.1). To remove systematic offsets from the resulting salinity profile, all the profiles were detrended to match the salinity measured by the CTDs near the Meddy at 300 and 1600 dbars. The final salinity profiles are presented in Figure B.1. Within 7 km of the Meddy center, the vertical profiles of salinity from the XSV-XBT combination show the same structure as the CTD casts (Figure B.2), although the actual value of salinity may be in error by up to 0.3 psu. The region of homogeneous salinity in the upper Meddy core appears from Figure B.1 to extend to 6 or 7 km. Additional details of the salinity estimate from expendable probes are given in Kennelly et al. (1989c).

Table B.2. Sensitivity of Standard Salinity Computation

Variable	Sensitivity	Accuracy Needed for 0.1 psu
P	-0.0004 psu / dbar	250 dbars
T	-0.9145 psu / °C	0.11 °C
C	9.7095 psu / S m^{-1}	0.01 S m^{-1}

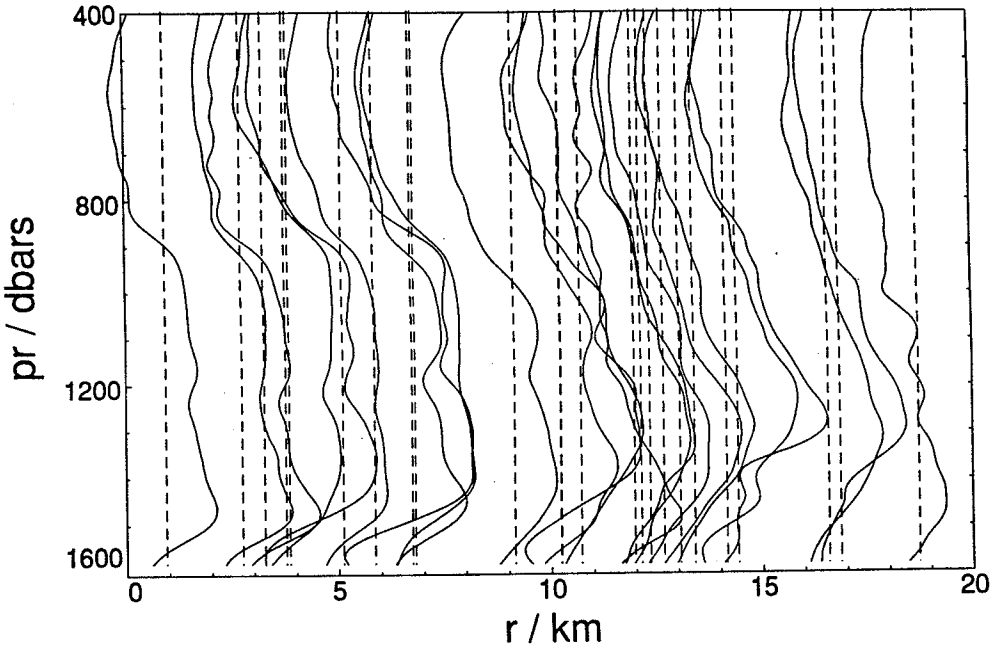

Figure B1. Salinity profiles computed from XSV and XBT data. The dashed line denotes the drop position; the salinity is scaled and offset so that the dashed line is also the 35.5 psu line for each drop; 1 psu is equivalent to 2.3 km.

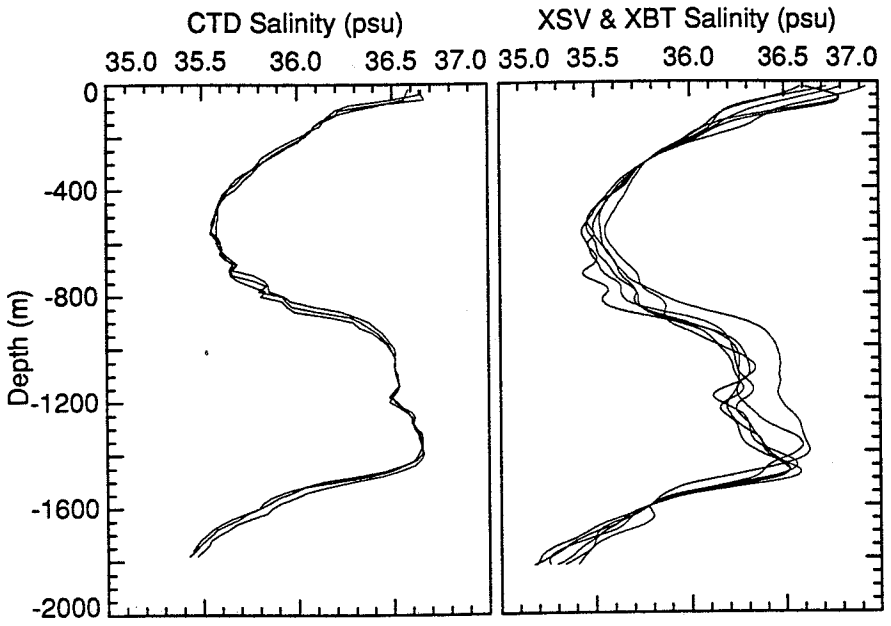

Figure B2. Comparison of salinity from CTD with that computed from XSV and XBT data in the center of the Meddy.

Appendix C. Diffusion of Heat Radially from a Cylinder

Diffusion of heat from a cylindrical column of water serves as a simplistic model for the distribution of temperature in the Meddy. The diffusion model is useful in a qualitative description of the radial temperature structure, even though the decay of Meddies is more likely due to lateral intrusions and double diffusive processes (Ruddick & Hebert, 1988), and the potential vorticity anomaly of the Meddy (Section 3.9) inhibits the motions that might contribute to lateral eddy diffusivity.

For a domain of infinite extent, and with no vertical variation in the initial temperature distribution, the governing equation for the diffusion of temperature is

$$\frac{\partial r}{\partial t} = \kappa \left[\frac{\partial^2 T}{\partial r^2} + \frac{1}{r} \frac{\partial T}{\partial r} \right] \tag{C.1}$$

where κ is thermal diffusivity. The initial temperature distribution is

$$T(r, 0) = T_{\min} + (T_{\max} - T_{\min}) H(r_o) \tag{C.2}$$

where $H(r_o)$ is 1 for $r < r_o$ and zero elsewhere.

Equation (C.1) is solved by separation of variables and using the Hankel transform of the initial condition. The details of the solution method will not be presented. The resulting temperature structure is given by

$$T(r, t) = T_{\min} + (T_{\max} - T_{\min}) \int_0^\infty r_o J_1(r_o \lambda) J_0(\lambda r) \exp(-\lambda^2 \kappa t) \, d\lambda \tag{C.3}$$

where J_0 and J_1 are Bessel functions of the first kind of order 0 and 1, respectively.

Figure C.1 shows examples of a radial temperature distribution for parameters ($T_{\min} = 10.5$ °C, $T_{\max} = 12.0$ °C, and $r_o = 10$ km) typical of the upper core of the Meddy. As the value of κt increases, the peak temperature in the model decreases, as does the temperature gradient. The radius of the "half-temperature anomaly", $(T(0,t) + T_{\min}) / 2$, increases from an initial value of r_o.

This model is used to describe the radial temperature distribution of the Meddy in Section 3.2, and the nondimensional parameter $\kappa t / r_o^2$ is a useful measure of the relaxation of that distribution.

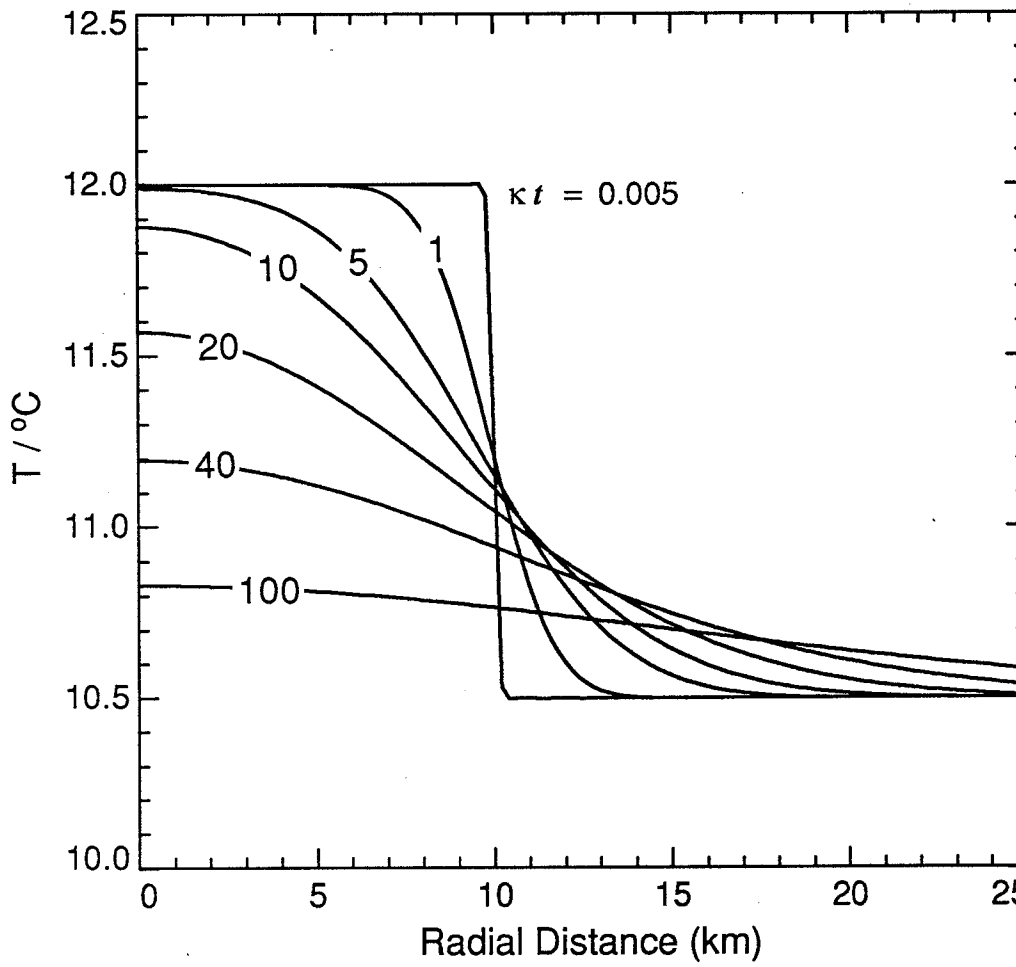

Figure C1. Diffusion of heat radially from a cylindrical body of warmer water. Temperature versus radial distance as a function of nondimensional time κt.

Appendix D. Fundamental Frequency of Solid Body Rotating Eddy

The observation that the lower core of the Meddy was more elliptic than the upper core, and had a connection through its temperature field back to the Mediterranean outflow, led to the hypothesis that the lower core is "younger" than the upper core. Younger here means that the lower Meddy has not come to the same level of equilibrium with its environment as the upper core has. An independent measure of a Meddy's age was sought, to confirm the above idea.

For an eddy in cyclogeostrophic balance (Section 3.8), the force balance on a parcel of water consists of the outward pressure gradient, the outward centrifugal force, and the inward Coriolis force. A parcel that is displaced outward will be returned toward its original position by an imbalance of these forces and will oscillate about that position with a deterministic frequency. The process is analogous to the displacement of a water parcel in a stratified fluid resulting in the buoyancy frequency.

To simplify the analysis, a barotropic eddy in solid body rotation is assumed, so $\omega = v/r$ is a constant with respect to r. Also, the parcel will conserve angular momentum as it is displaced. The cyclogeostrophic balance gives

$$\frac{v^2}{r} + fv = v(\omega + f) = \frac{1}{\rho}\frac{\partial P}{\partial r} \tag{D.1}$$

Let the subscript 1 denote variables associated with the equilibrium position and 2 those associated with the displaced position. Also, let v denote velocity in equilibrium, and u denote velocity not in equilibrium. The conservation of angular momentum gives

$$v_1 r_1 = u_1 r_2 \tag{D.2}$$

Thus a water parcel from an equilibrium position has been displaced to a nonequilibrium position. The momentum balances at r_2 are

$$v_2(\omega + f) = \frac{1}{\rho}\left(\frac{\partial P}{\partial r}\right)_2 \tag{D.3}$$

$$u_1\left(\frac{u_1}{r_2} + f\right) \neq \frac{1}{\rho}\left(\frac{\partial P}{\partial r}\right)_2$$

The displaced parcel will undergo a restoring acceleration of

$$u_1 \left(\frac{u_1}{r_2} + f \right) - v_2 (\omega + f) \tag{D.4}$$

or

$$\omega \frac{r_1^2}{r_2} \left(\omega \frac{r_1^2}{r_2^2} + f \right) - \omega r_2 (\omega + f)$$

If we do some algebraic manipulation and assume

$$r_2 - r_1 = \Delta r \tag{D.5}$$

$$r_2 + r_1 = 2r$$

$$r_2^2 + r_1^2 = 2r^2$$

then the acceleration in (D.4) reduces to

$$-\Delta r \, |\zeta| \, (\zeta + f) \tag{D.6}$$

or

$$-\Delta r \, f^2 \, |R_o| \, (R_o + 1)$$

where the vorticity $\zeta = 2\omega$ and the Rossby number $R_o = \zeta / f$. Choosing a coordinate system such that x is positive outward from the equilibrium position of a parcel, the resulting wave equation

$$\ddot{x} + f^2 |R_o| (R_o + 1) x = 0 \tag{D.7}$$

describes the oscillations of the displaced parcel, having the fundamental frequency

$$\textit{frequency} = f \, [\, |R_o| \, (R_o + 1)]^{1/2} \tag{D.8}$$

Equation (D.8) is evaluated and plotted in Figure D.1. The frequency goes to zero at R_o of 0 and -1, where the restoring force also goes to zero. There is no real frequency below R_o of -1, which is a confirmation of the inertial stability limit.

It is difficult to incorporate the above result in terms of the original hypothesis. The upper core R_o is closer to -1 than the lower core R_o, and both are below -0.5. Thus the upper core has a slower fundamental period than the lower core, about 2.5 days and 2 days, respectively. If the age of an eddy is expressed in terms of the number of fundamental periods that occur over a given time, then the upper core is aging more slowly than the lower. If the water properties throughout the core are different, the slower

period would allow more time for the displaced parcel to mix with its surroundings, and aid in the homogenization of the core. The maximum radial velocities produced by this restoring mechanism are given by

$$\dot{x} = A f [|R_o| (R_o + 1)]^{1/2} \tag{D.9}$$

where A is the displacement amplitude. For the upper core of the Meddy, with R_o = -0.85, $f = 8.6\times10^{-5}$, and a displacement of 500 m, the radial velocity reaches 0.015 m s^{-1}. A velocity this small would be difficult to observe in a Meddy where the mean velocity is 0.23 m s^{-1}.

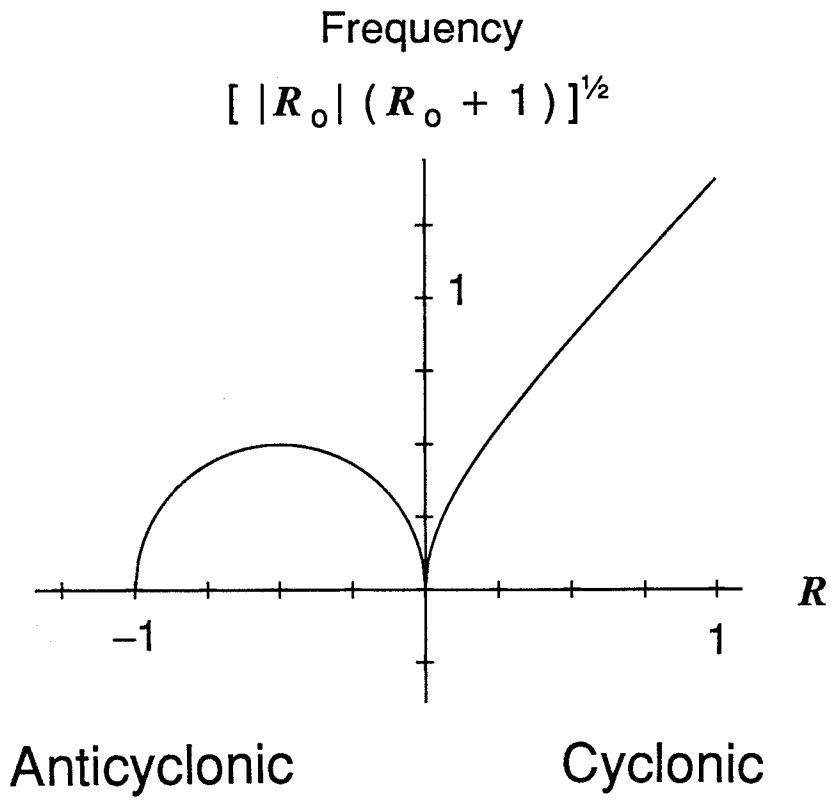

Figure D.1 Normalized frequency of a radially displaced water parcel in a barotropic, solid-body rotating eddy. No frequency exists below the inertial stability limit of R_o = -1. For dimensional frequency, multiply the ordinate values by the Coriolis frequency f.

Vita: Mark Dennis Prater

Birth: Marion, Ohio, May 27, 1956

1974: Graduate, Marion Harding High School, Marion, Ohio

1974-1978: B.S. (Civil Engineering) The Ohio State University, Columbus, Ohio

1978-1980: M.S. (Civil Engineering) The Ohio State University, Columbus, Ohio
Thesis: *The Effect of Basin Oscillations on the Formation of Sandusky Bay*
Advisor: Professor Keith W. Bedford

1981-1985: Research Hydraulic Engineer
Coastal Engineering Research Center,
U.S. Army Corps of Engineers Waterways Experiment Station,
Vicksburg, Mississippi

1985-1992: Ph.D. (Physical Oceanography) University of Washington, Seattle
Dissertation: *Observations and Hypothesized Generation of a Meddy in the Gulf of Cadiz*
Advisor: Professor Thomas B. Sanford

Selected Publications

Prater, M.D., 1991: A Method for Depth and Temperature Correction of Expendable Probes. *Journal of Atmospheric and Oceanic Technology,* **8,** 888-894.

Prater, M.D. and T.B. Sanford, 1991: "Potential Vorticity Connection between a Gulf of Cadiz Meddy and the Mediterranean Outflow" *EOS,* **72** (No. 51 supplement), 55.

Prater, M.D. and T.B. Sanford, 1990: "Generation of Meddies off Cape St. Vincent, Portugal" *EOS,* **71**, 1416.

Prater, M.D. and T.B. Sanford, 1989: "Observations of an Intense, Young Meddy" *EOS,* **70**, 1159.

Prater, M.D., J.A. Carlson and T.B. Sanford, 1987: "Small-Scale Vertical Vorticity in the Ocean" *EOS,* **68**, 1313.

Prater, M.D., M.A. Kennelly and T.B. Sanford, 1986: "Observations of Jets in the California Current" *EOS,* **67**, 1047.

UNCLASSIFIED
SECURITY CLASSIFICATION OF THIS PAGE

REPORT DOCUMENTATION PAGE

Form Approved
OMB No. 0704-0188

1a. REPORT SECURITY CLASSIFICATION Unclassified	1b. RESTRICTIVE MARKINGS
2a. SECURITY CLASSIFICATION AUTHORITY	3. DISTRIBUTION / AVAILABILITY OF REPORT NA
2b. DECLASSIFICATION / DOWNGRADING SCHEDULE	
4. PERFORMING ORGANIZATION REPORT NUMBER(S) APL-UW TR 9210	5. MONITORING ORGANIZATION REPORT NUMBER(S)
6a. NAME OF PERFORMING ORGANIZATION Applied Physics Laboratory University of Washington 6b. OFFICE SYMBOL *(If applicable)*	7a. NAME OF MONITORING ORGANIZATION
6c. ADDRESS *(City, State, and ZIP Code)* 1013 N.E. 40th Street Seattle, Washington 98105	7b. ADDRESS *(City, State, and ZIP Code)*
8a. NAME OF FUNDING / SPONSORING ORGANIZATION Office of Naval Research 8b. OFFICE SYMBOL *(If applicable)*	9. PROCUREMENT INSTRUMENT IDENTIFICATION NUMBER N00014-86-K-0690
8c. ADDRESS *(City, State, and ZIP Code)* 800 North Quincy Street Arlington, VA 22217-5000	10. SOURCE OF FUNDING NUMBERS PROGRAM ELEMENT NO. / PROJECT NO. / TASK NO. / WORK UNIT ACCESSION NO.

11. TITLE *(Include Security Classification)*
Observations and Hypothesized Generation of a Meddy in the Gulf of Cadiz

12. PERSONAL AUTHOR(S)
Mark D. Prater

13a. TYPE OF REPORT	13b. TIME COVERED	14. DATE OF REPORT *(Year, Month, Day)*	15. PAGE COUNT
Technical	FROM _____ TO _____	May 1992	143

16. SUPPLEMENTARY NOTATION
Dissertation submitted in partial fulfillment of the requirements for the degree of Doctor of Philosophy -- University of Washington, School of Oceanography

17. COSATI CODES			18. SUBJECT TERMS *(Continue on reverse if necessary and identify by block number)*
FIELD	GROUP	SUB-GROUP	

19. ABSTRACT *(Continue on reverse if necessary and identify by block number)*

The formation of Mediterranean water **eddies** and the characteristics of the Mediterranean outflow that lead to formation are investigated. In September of 1988, an expedition was made to the Gulf of Cadiz to survey a Meddy soon after formation. The objectives of this study were to i) compare a "young" Meddy with older ones found elsewhere, ii) determine the formation site for the Meddy, iii) determine the generation mechanism for the Meddy, and iv) determine the dynamical relationship between the Meddy and the Mediterranean outflow. A regional survey was done, which mapped the Mediterranean outflow and located a Meddy, which was then mapped in greater detail.

(cont.)

20. DISTRIBUTION / AVAILABILITY OF ABSTRACT ☒ UNCLASSIFIED/UNLIMITED ☒ SAME AS RPT. ☐ DTIC USERS	21. ABSTRACT SECURITY CLASSIFICATION Unclassified
22a. NAME OF RESPONSIBLE INDIVIDUAL	22b. TELEPHONE *(Include Area Code)* / 22c. OFFICE SYMBOL

DD Form 1473, JUN 86 *Previous editions are obsolete.*
S/N 0102-LF-014-6603

SECURITY CLASSIFICATION OF THIS PAGE
UNCLASSIFIED

19, cont.

The observed Meddy had a radius to maximum velocity of 9 km, a vertical extent of 650 m, and a central anticyclonic vorticity of $-0.85f$. The Meddy consisted of two vertically aligned cores, both of which were in cyclogeostrophic balance. The Meddy contained a large potential vorticity (Q) anomaly, with levels an order of magnitude lower than ambient. The Meddy had a more negative Rossby number and a higher Burger number than previously observed Meddies. The formation site of the Meddy was found through analysis of Gulf of Cadiz water properties to be near a canyon region south of Portugal. The Meddy was shown not to have been generated solely by geostrophic adjustment, which requires vortex squashing to produce strong negative vorticity. Instead, the most likely candidate mechanism was baroclinic instability of the outflow. This hypothesis is supported by strong vertical shear in the outflow, a radial scale of the Meddy consistent with a baroclinic disturbance, and the existence of a cyclonic partner of the Meddy. Topography, however, may trigger the instability. The Q in the formation region was similar to that in the Meddy. However, the Q anomaly in the Meddy was dominated by negative relative vorticity, while in the outflow the nonlinear effect due to vertical shear dominated. The conversion from the vertical shear to the lateral shear component of the Q anomaly during Meddy formation is consistent with a meandering outflow constrained by potential vorticity conservation. The flux of potential vorticity was markedly less in the formation region than further upstream, indicating that the outflow Q was recently modified.